European Commission

JRC TECHNICAL REPORTS

Guidelines for stress-test design for non-nuclear critical infrastructures and systems: Applications

STREST Reference Report 5

Editor: Pitilakis K
Contributors: Akkar S, Argyroudis S, Babič A, Basco A, Basili R, Brizuela B, Cheng Y, Courage W, Crowley H, Dolšek M, Erdik M, Esposito S, Fotopoulou S, Giardini D, Iqbal S, Karafagka S, Lorito S, Matos JP, Piatanesi A, Reinders J, Rodrigues D, Romano F, Salzano E, Schleiss AJ, Selva J, Stojadinovic B, Tonini R, Uckan E, Volpe M
Reviewer: Mignan A
Publishing editor: Tsionis G

2016

EUR 28341 EN

JRC Science Hub
https://ec.europa.eu/jrc

JRC104658

EUR 28341 EN

PDF	ISBN 978-92-79-64600-3	ISSN 1831-9424	doi:10.2788/85094
Print	ISBN 978-92-79-64601-0	ISSN 1018-5593	doi:10.2788/11979

Luxembourg: Publications Office of the European Union, 2016

How to cite this report: Pitilakis K, Akkar S, Argyroudis S, Babič A, Basco A, Basili R, Brizuela B, Cheng Y, Courage W, Crowley H, Dolšek M, Erdik M, Esposito S, Fotopoulou S, Giardini D, Iqbal S, Karafagka S, Lorito S, Matos JP, Mignan A, Piatanesi A, Reinders J, Rodrigues D, Romano F, Salzano E, Schleiss AJ, Selva J, Stojadinovic B, Tonini R, Tsionis G, Uckan E, Volpe M, *Guidelines for stress-test design for non-nuclear critical infrastructures and systems: Applications*, EUR 28341 EN, doi:10.2788/85094

STREST

D 7.6.5

DELIVERABLE

PROJECT INFORMATION

Project Title:	Harmonized approach to stress tests for critical infrastructures against natural hazards
Acronym:	STREST
Project N°:	603389
Call N°:	FP7-ENV-2013-two-stage
Project start:	01 October 2013
Duration:	36 months

DELIVERABLE INFORMATION

Deliverable Title:	Guidelines for stress-test design for non-nuclear critical infrastructures and systems: Applications
Date of issue:	31 July 2016
Work Package:	WP7 – Dissemination and stakeholder interaction
Editor/Author:	Kyriazis Pitilakis (Aristotle University of Thessaloniki)
Reviewer:	Arnaud Mignan (ETH Zürich)

REVISION: Final

SEVENTH FRAMEWORK PROGRAMME

Project Coordinator:	Prof. Domenico Giardini
Institution:	ETH Zürich
e-mail:	giardini@sed.ethz.ch
fax:	+ 41 446331065
telephone:	+ 41 446332610

Table of contents

Abstract iii

Acknowledgments v

Deliverable contributors vii

1. Introduction 1

2. ST@STREST methodology for stress testing of critical non-nuclear infrastructures .. 3

   2.1 Multiple-expert integration 3

   2.2 ST@STREST workflow 4

      2.2.1 Phase 1: Pre-assessment phase 4

      2.2.2 Phase 2: Assessment phase 5

      2.2.3 Phase 3: Decision phase 5

      2.2.4 Phase 4: Report phase 6

   2.3 Stress test levels 6

   2.4 Proposed grading system 8

      2.4.1 Grading of the components 10

3. Application of stress test concepts to ENI/Kuwait oil refinery and petrochemical plant, Milazzo, Italy 13

   3.1 Phase 1: Pre-assessment phase 13

      3.1.1 Data collection 13

   3.2 Phase 2: Assessment phase 13

      3.2.1 Component level assessment (ST-L1a) 13

      3.2.2 System level assessment for single hazard (ST-L2b / L2d) 15

   3.3 Phase 3: Decision phase 17

      3.3.1 Single risk analysis 17

      3.3.2 Combined risk analysis 19

      3.3.3 Guidelines and critical events 19

   3.4 Phase 4: Report phase 23

4. Application of stress test concepts to large dams in the Valais region of Switzerland 25

   4.1 Introduction 25

   4.2 Phase 1: Pre-assessment phase 26

   4.3 Phase 2: Assessment phase (ST-L3c / L3d) 27

   4.4 Phase 3: Decision phase 29

   4.5 Phase 4: Report phase 30

   4.6 Final notes 32

5. Application of stress test concepts to major hydrocarbon pipelines, Turkey 33

   5.1 Phase 1: Pre-assessment phase 33

   5.2 Phase 2: Assessment phase 34

5.3 Phase 3: Decision phase 35
5.4 Phase 4: Report phase 36
6. Application of stress test concepts to Gasunie national gas storage and distribution network, Holland 37
6.1 Introduction 37
6.2 Phase 1: Pre-assessment phase 37
6.2.1 Data collection 37
6.2.2 Risk measures and objectives 40
6.2.3 Set-up of the stress test 41
6.3 Phase 2: Assessment phase 42
6.3.1 Component level assessment (ST-L1a) 42
6.3.2 System level assessment for single hazard (ST-L2a) 42
6.4 Phase 3: Decision phase 46
6.4.1 Risk objectives check 46
6.4.2 Disaggregation/sensitivity analysis 48
6.4.3 Guidelines and critical events 48
6.5 Phase 4: Report phase 49
7. Application of stress test concepts to port infrastructures of Thessaloniki, Greece 51
7.1 Phase 1: Pre-assessment phase 51
7.1.1 Data collection 51
7.1.2 Risk measures and objectives 53
7.2 Phase 2: Assessment phase 54
7.2.1 Component level assessment (ST-L1a) 54
7.2.2 System level assessment (ST-L2b / L2d / L3d) 55
7.3 Phase 3: Decision phase 62
7.3.1 Risk objectives check 62
7.4 Phase 4: Report phase 63
8. Application of stress test concepts to industrial district, Italy 65
8.1 Phase 1: Pre-assessment phase 65
8.2 Phase 2: Assessment phase (ST-L1a / ST-L2b) 67
8.3 Phase 3: Decision phase 69
8.4 Phase 4: Report phase 71
9. Conclusions and recommendations 73
References 75
List of abbreviations and definitions 81
List of figures 83
List of tables 87

Abstract

In the context of the STREST project, an engineering multi-level risk-based methodology to stress test critical non-nuclear infrastructures, named ST@STREST, has been developed. This reference report summarizes ST@STREST framework and its exploratory application to six key representative Critical Infrastructures (CIs) in Europe, exposed to variant hazards, namely: a petrochemical plant in Milazzo, Italy, large dams of the Valais region in Switzerland, hydrocarbon pipelines in Turkey, the Gasunie national gas storage and distribution network in Holland, the port infrastructure of Thessaloniki, Greece and an industrial district in the region of Tuscany, Italy. According to the characteristics of each case study, different stress test levels were applied.

The application to the selected CIs is presented following the workflow of ST@STREST, comprised of four phases: Pre-Assessment phase; Assessment phase; Decision phase; and Report phase. First the goals, the method, the time frame, and the appropriate stress test level to apply are defined. Then, the stress test is performed at component and system levels and the outcomes are checked and compared to the acceptance criteria. A stress test grade is assigned and the global outcome is determined by employing a grading system. Finally, critical events and risk mitigation strategies are formulated and reported to stakeholders and authorities.

Acknowledgments

The research leading to these results has received funding from the European Community's Seventh Framework Programme [FP7/2007-2013] under grant agreement n° 603389.

Deliverable contributors

AUTH	Kyriazis Pitilakis
	Sotiris Argyroudis
	Stavroula Fotopoulou
	Stella Karafagka
ETH Zurich	Simona Esposito
	Bozidar Stojadinovic
	Domenico Giardini
	Arnaud Mignan
UL	Matjaž Dolšek
	Anže Babič
INGV	Jacopo Selva
	Sarfraz Iqbal
	Manuela Volpe
	Roberto Tonini
	Fabrizio Romano
	Beatriz Brizuela
	Alessio Piatanesi
	Roberto Basili
	Stefano Lorito
AMRA	Ernesto Salzano
	Anna Basco
EUCENTRE	Helen Crowley
	Daniela Rodrigues
EPFL	José P. Matos
	Anton J. Schleiss
TNO	Wim Courage
	Johan Reinders
BU	Sinan Akkar
	Yin Cheng
	Eren Uckan
	Mustafa Erdik

1. Introduction

Critical infrastructures (CIs) are of essential importance for the modern society. Extreme natural events can interrupt services, cause damage, or even destroy such CI systems, which consequently trigger disruption of vital socio-economic activities, extensive property damage, and/or human injuries or loss of lives. Recent catastrophic events showed that the CI systems rarely recover their functionality back to the pre-disaster state, significantly increasing the concerns of the public.

In the context of the STREST project, a harmonized approach for stress testing critical non-nuclear infrastructures, ST@STREST, has been developed. The aims of the ST@STREST methodology and framework are to quantify the safety and the risk of individual components as well as of whole CI system with respect to extreme events and to compare the expected behaviour of the CI to acceptable values. In particular, a multi-level stress test methodology has been proposed. Each level is characterized by a different scope (component or system) and by a different level of risk analysis complexity (starting from design codes and ending with state-of-the-art probabilistic risk analyses, such as cascade modelling). This allows flexibility and application to a broad range of infrastructures. The framework is composed of four main phases and nine steps. First the goals, the method, the time frame, and the total costs of the stress test are defined. Then, the stress test is performed at component and system level; additionally, the outcomes are checked and analysed. Finally, the results are reported and communicated to stakeholders and authorities. The ST@STREST methodology (ST@STREST) is summarized in Chapter 2 of this report, with the details presented in the companion European Reference Report 4 (Esposito et al 2016).

In the following chapters, the application of ST@STREST to six CIs in Europe is presented in detail: the ENI/Kuwait oil refinery and petrochemical plant in Milazzo, Italy when impacted by earthquakes and tsunamis (Chapter 3); the large dams in the Valais region of Switzerland under multi-hazard effects, considering earthquakes, floods, internal erosion, bottom outlet malfunctions, and hydropower system malfunction (Chapter 4); the major hydrocarbon pipelines in Turkey, focusing to seismic threats at pipe-fault crossing locations (Chapter 5); the Gasunie national gas storage and distribution network in Holland, exposed to earthquake and liquefaction effects (Chapter 6); the port infrastructures of Thessaloniki in Greece, subjected to earthquake, tsunami and liquefaction hazards (Chapter 7); and the industrial district in the region of Tuscany, Italy, exposed to seismic hazard (Chapter 8). These case studies are representative of the CIs categories identified in STREST: 1) individual, single-site infrastructures with high risk and potential for high local impact and regional or global consequences; 2) distributed and/or geographically-extended infrastructures with potentially high economic and environmental impact, 3) distributed, multiple-site infrastructures with low individual impact but large collective impact or dependencies. The successful application of the proposed ST@STREST methodology to the six different CIs demonstrates its viability and shows there areas where additional developments are needed.

2. ST@STREST methodology for stress testing of critical non-nuclear infrastructures

The aims of the proposed methodology are to assess the performance of individual components as well as of whole CI systems with respect to extreme events, and to compare this response to acceptable values (performance objectives) that are specified at the beginning of the stress test. ST@STREST is based on probabilistic and quantitative methods for best-possible characterization of extreme scenarios and consequences.

The proposed ST@STREST methodology makes it possible to conduct stress test different levels, to accommodate the large diversity of CIs. Each Stress Test Level (ST-L) is characterized by different focus (component or system) and by different levels of risk analysis complexity (starting from design codes and ending with state-of-the-art probabilistic risk analyses). The selection of the appropriate Stress Test Level depends on regulatory requirements, based on the different importance of the CI, and the available human/financial resources to perform the stress test.

The proposed ST@STREST process is transparent: a description of the assumptions made to identify the hazard and to model the risk (consequences) and the associated frequencies is required. The data, models and methods adopted for the risk assessment and the associated uncertainties are clearly documented and managed by different experts involved in the stress test process, following a pre-defined process for managing the multiple-expert integration (Selva et al 2015). This allows defining how reliable the results of the stress test are in terms of Accuracy (i.e. level of detail and sophistication) of the test.

The workflow of ST@STREST comprises four phases: Pre-Assessment phase; Assessment phase; Decision phase; and Report phase. In the Pre-Assessment phase the data available on the CI (risk context) and on the phenomena of interest (hazard context) is collected. Then, the goal, the time frame, the total costs of the stress test, and the most appropriate Stress Test Level to apply to test the CI are defined. In the Assessment phase, the stress test is performed at Component and System Levels. In the Decision phase, the stress test outcomes are checked, i.e. the results of risk assessment are compared to the objectives defined in Pre-Assessment phase. Then critical events, i.e. events that most likely cause a given level of loss, are identified and risk mitigation strategies and guidelines are formulated based on the identified critical events and presented in the Report phase.

2.1 Multiple-expert integration

The involvement of multiple experts is critical in a risk assessment when potential controversies exist and the regulatory concerns are relatively high. In order to produce robust and stable results, the integration of experts plays indeed a fundamental role in managing subjective decisions and in quantifying the epistemic uncertainty capturing *'the center, the body, and the range of technical interpretations that the larger technical community would have if they were to conduct the study'* (SSHAC, 1997). To this end, the experts' diverse range of views and opinions, their active involvement, and their formal feedbacks need to be organized into a structured process ensuring transparency, accountability and independency.

EU@STREST, a formalized multiple expert integration process has been developed within STREST (Selva et al 2015) and integrated into the ST@STREST Workflow. This process guarantees the robustness of stress test results, considering the differences among different CIs. With respect to the different levels in the SSHAC process developed for nuclear critical infrastructures (SSHAC, 1997), the proposed process is located between SSHAC levels 2 and 3 in terms of expert interaction, but it also makes an extensive use of classical Expert Elicitations, and is extended to single risk and multi-risk analyses. The core actors in EU@STREST are the Project Manager (PM), the Technical Integrator (TI),

the Evaluation Team (ET), the Pool of Experts (PoE), and the Internal Reviewers (IR). The roles of these actors and the interactions among them are described below.

The PM is a stakeholder who owns the problem and is responsible and accountable for the successful development of the project and the communication with the authorities and public. The TI is an analyst responsible and accountable for the scientific management of the project, responsible for capturing the views of the informed technical community in the form of a community knowledge, to be implemented in the hazard and risk calculations. The ET is a group of analysts that actually perform the risk assessment required under the guidelines provided by the TI. The team is selected by the TI and the PM, and it may include internal CI resources and/or external experts. The ET also represents the interface between the project and the CI authorities, and guarantees the successful and reciprocal acknowledgement of choices and results. The PoE represents the larger technical community within the process. Individual experts of the PoE may also act as proponents and advocates a particular hypothesis or technical position, in individual communications with the TI. They participate in the interviewing processes lead by the TI, providing the TI with their opinions on critical choices/issues. The IR is one expert or a group of experts on subject matter under review that independently peer reviews and evaluates the work done by the TI and the ET. This group provides constructive comments and recommendations during the implementation of the project. In particular, IR reviews the coherence between TI choices and PM requests, the TI selection of the PoE in terms expertise coverage and scientific independence, the fairness of TI integration of PoE feedbacks, and the coherence between TI requests and ET implementations. The participation of the different actors varies along the different phases of the stress test (Fig. 2.1).

2.2 ST@STREST workflow

The ST@STREST workflow represents a systematic sequence of steps (processes), which have to be carried out in a stress test. The ST@STREST workflow shown in Fig. 2.1, comprises four phases and each phase is subdivided in a number of specific steps, with a total of 9 steps. In the following a detailed description of the four phases is provided together with a specification of the involvement of the different experts in process.

2.2.1 Phase 1: Pre-assessment phase

The Pre-Assessment phase comprises three steps. First, the data available on the CI and on the phenomena of interest (hazard context) is collected in STEP 1 (Data collection). Also data coming from Stress Tests performed on other similar CI and other CIs in the same location is collected. In this step, the stress test participants are selected: the PM selects the TI and the IR; the TI and the PM jointly select the ET. Then, the TI, with the technical assistance of the ET, collects data and relevant information about hazards and the CI, and about previous stress tests. The TI pre-selects the potential target hazards and the relevant CI components. In STEP 2 (Risk Measures and Objectives), the goal of the project is defined. In particular, one or more risk measures (e.g. fatalities, economic losses) and objectives (e.g. expected loss, annual probability etc.) are defined by the PM, based on regulatory requirements and previous stress tests. Then in STEP 3 (Set-up of the Stress Test), the time frame, the total costs of the stress test, the most appropriate Stress Test Level (ST-L) and the stress test accuracy level to apply are defined. The selection of the ST-L is made by the PM with the assistance of the TI, based on regulatory requirements. The conclusion of STEP 3 may take time and may differ in case the PoE is in place or not.

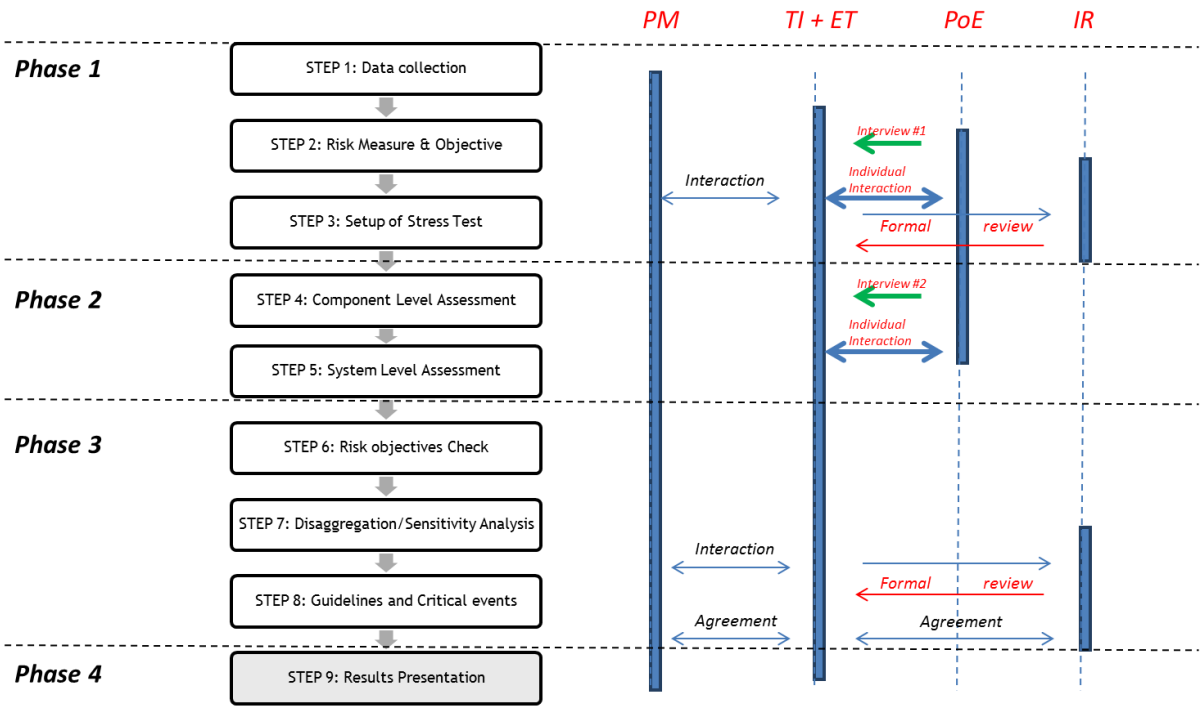

Fig. 2.1 Workflow of ST@STREST methodology and interaction among the main actors during the multiple-expert process EU@STREST

2.2.2 Phase 2: Assessment phase

The Assessment phase is characterized by two steps in which the stress test is performed at the Component (STEP 4: Component Level Assessment) and the System (STEP 5: System Level Assessment) levels according to the Stress Test Level selected in Phase 1. At Component level, the performance of each component of the CI is checked by the hazard-based assessment, design-based assessment or risk-based assessment approach (see Section 2.3). This check is performed by the TI or by one expert of the ET selected by the TI. At System level, first, the TI finalizes the required models. In particular, if the PoE is in place (sub-levels c), the TI organizes the classical Expert Elicitations i) to fill potential methodological gaps, ii) to quantify the potential scenario and iii) to rank/score the alternative models to enable the quantification of the epistemic uncertainty. The members of the PoE perform the elicitation separately. Open discussions among the PoE members (moderated by the TI) are foreseen only if significant disagreements emerge in the elicitation results. If the PoE is not in place but EU assessment is required (sub-level b), the TI directly assigns scores/ranks the selected models. Then, the TI actually implements all the required models and performs the assessment, with the technical assistance of the ET. If specific technical problems emerge during the implementation and application, the TI may solve them through individual interactions with members of the PoE (if foreseen at the ST-Level, see Section 2.3).

2.2.3 Phase 3: Decision phase

In the Decision Phase, the stress test outcomes are determined i.e. the results of risk assessment are compared with the risk objectives defined in Phase 1 (STEP 6: Risk Objectives Check). This task is performed by the TI, with the technical assistance of the ET. Depending on the type of risk measures and objectives defined by the PM (e.g. F-N curve, expected mean) and on the methods adopted, the comparison between results from probabilistic risk assessment with these goals may differ. One possibility to assess the outcome of the stress test is by using grading system (AA – negligible risk, A – as

low as reasonably practicable (ALARP) risk, B – possibly unjustifiable risk, C – intolerable risk) detailed in Section 2.4. Then critical events, i.e. events that most likely cause the exceedance of the considered loss value are identified through a disaggregation analysis in STEP 7 (Disaggregation/Sensitivity Analysis). Finally, risk mitigation strategies and guidelines are formulated based on the identified critical events in STEP 8 (Guidelines and Critical events). This task is performed by the TI with the technical assistance of the ET. All the results in all the steps of PHASE 2 and PHASE 3 are specifically documented by the TI. The IR reviews the activities performed in assessments from STEP 4 to STEP 8. The TI, with the technical assistance of the ET, updates the final assessments accounting for the review. Final assessments and decisions are documented by the TI. Based on such documents, The PM, TI and IR make the final agreement.

2.2.4 Phase 4: Report phase

The Report phase comprises one step (STEP 9: Results Presentation) where the results are presented to CI authorities and regulators. This presentation is organized and performed by PM and TI. The presentation includes the outcome of the stress test in terms of the grade, the critical events, the guidelines for risk mitigation, and the accuracy of the methods adopted in the stress test. Note that the time for this presentation is set in PHASE 1, and it cannot be changed during PHASES 2 and 3.

2.3 Stress test levels

Due to the diversity of types of CIs and the potential consequence of failure of the CIs, the types of hazards and the available resources for conducting the stress tests, it is not optimal to require the most general form of the stress test for all possible situations. Therefore, three stress test variants, termed Stress Test Levels (ST-Ls) are proposed:

- Level 1 (ST-L1): single-hazard component check;
- Level 2 (ST-L2): single-hazard system-wide risk assessment;
- Level 3 (ST-L3): multi-hazard system-wide risk assessment.

Each ST-L is characterized by a different scope (component or system) and by a different complexity of the risk analysis (e.g. the consideration of multi hazard and multi risk events) as shown in Fig. 2.2.

The aim of the ST-L1 (Component Level Assessment) is to check each component of a CI independently in order to show whether the component passes or fails the minimum requirements for its performance, which are defined in current design codes. The performance of each component of the CI is checked for the hazards selected as the most important (e.g. earthquake or flood, etc.). At component-level there are three methods to perform the single-hazard component check. These methods differ for the complexity and the data needed for the computation. The possible approaches are: the hazard-based assessment, design-based assessment, and the risk-based assessment approach.

In the hazard-based assessment, the performance of the component is checked by comparing the design value of intensity of the hazard which was actually used in the design of the component (building, pipeline, storage tank, etc.), to the design value of intensity of the hazard prescribed in current regulatory documents or to the value of intensity according to the best possible knowledge. In the design-based assessment the expert compares the demand, with the capacity, (expressed in terms of forces, stresses, deformations or displacements). The assessment can be based on factoring the results from the existing design documentation or by performing design (assessment) of the component according to current state-of-practice. In the risk-based assessment, the hazard function at the location of the component and the fragility function of the component are required to evaluate the probability of meeting the risk acceptance

criteria. Design-based assessment is recommended when only ST-L1 is performed. In the case, when ST-L1 is followed by ST-L2, in which component-specific fragility functions are used, it makes sense to perform risk-based assessment of the components since fragility functions are anyway required in ST-L2. More details on the possible approaches for ST-L1 assessment can be found in STREST D5.1 (Esposito et al 2016).

Since a CI is a system of interacting components, ST-L1 is inherently not adequate. Nevertheless, ST-L1 is obligatory because design of (most) CI components is regulated by design codes, and the data and the expertise are available. Further, for some CIs, the computation of system-level analysis (single and multi-risk) could be overly demanding in terms of available knowledge and resources. The outcome of the ST-L1 is most often qualitative, e.g. component is compliant with the current regulation, component is not compliant with current regulation, or the regulation does not yet exist for this type of component or type of hazard.

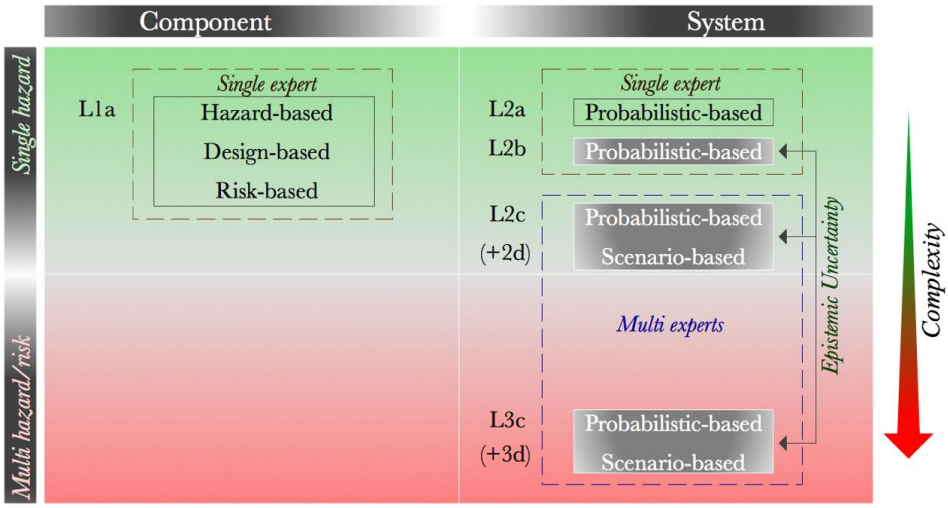

Fig. 2.2 ST-Levels in the ST@STREST methodology

The stress test assessment at the system level of the CI is foreseen at ST-L2 or ST-L3 where the probabilistic risk analysis of the entire CI (system) is performed. The system level assessment is highly recommended, since it is the only way of revealing the majority of the mechanisms leading to potential unwanted consequences. However, note that it requires more knowledge and resources (financial, staff) for conducting the stress test, thus it is not made obligatory (if not required by regulations). At these levels, potentially different implementations are possible. The quantification of epistemic uncertainty may not be performed (sub-level a). If performed, it may be based either on the evaluations of a single expert (sub-level b) or on the evaluations of multiple-experts (sub-level c). Indeed, a more accurate quantification of the technical community knowledge distribution (describing the epistemic uncertainty) can be reached if more experts are involved in the analysis and, in particular, when dealing with all critical choices. A description of possible methods to threat epistemic uncertainty in each ST-Level and sub-level can be found in STREST D5.1 (Esposito et al 2016) and SSHAC (1997).

Further, in case specific needs have been identified in the Pre-assessment phase (e.g. important methodological/modelling gaps) and such requirements cannot be included into the risk assessment for whatever reason, scenario-based analysis should be also performed as complementary to the system ST-L selected (sub-level d). Levels 2d and 3d are complementary to L2c and L3c, respectively. In this case, multiple experts define and evaluate possible scenarios that, for whatever reason, cannot be included into probabilistic risk analysis. In this case, the choice of performing a scenario-based assessment should be justified and documented by the TI, and reviewed by the IR. If

scenario-based assessment is finally selected, the choice of the scenarios should be based on ad hoc expert elicitation experiments of the PoE (SSHAC 1997). These additional scenarios are meant to further investigate the epistemic uncertainty by including events otherwise neglected only for technical reasons. Indeed, L2d and L3d are performed to evaluate the potential impact of epistemic gaps identified by experts, eventually increasing the capability of exploring the effective epistemic uncertainty. Thus, it is foreseen only as complementary to a full quantification of epistemic uncertainty in a multiple-expert framework.

The system level analysis is thus performed according to: 1) the degree of complexity of the analysis (single vs. multi hazards), and 2) the degree of involvement of the technical community in taking critical decisions and in the quantification of the epistemic uncertainty for the computation of risk. According to these two aspects a subdivision for ST levels has been introduced (Table 2.1, Fig. 2.2). The selection of the actual procedure to be implemented (row and column in Table 2.1) is performed in the Pre-Assessment (Phase 1). These two choices essentially depend on regulatory requirements, on the different importance of the CI, and on the available human/financial resources to perform the stress test. A criticality assessment of the CIs, aimed at identifying and ranking CIs, may represent a practical tool to support the choice of the appropriate ST level (Esposito et al 2016).

Table 2.1 ST-Levels

		Number of Experts		
		Single-expert		**Multiple-expert**
	Epistemic Uncertainty	**No**	**Yes**	**Yes**
ST-L	1	1a	-	-
	2	2a	2b	2c (+2d)
	3	-	-	3c (+3d)

2.4 Proposed grading system

The first outcome of the stress test, obtained in the STEP 6 (Risk Objectives Check), is described using a grading system, proposed herein, and is based on the comparison of results of risk assessment with the risk objectives (i.e. acceptance criteria) defined at the beginning of the test (STEP 2: Risk Measures and Objectives).

The proposed grading system (Fig. 2.3) is composed of three different outcomes: Pass, Partly Pass, and Fail. The CI passes the stress test if it attains grade AA or A. The former grade corresponds to negligible risk and is expected to be the goal for new CIs, whereas the latter grade corresponds to risk being as low as reasonably practicable (ALARP; Jonkman et al 2003) and is expected to be the goal for existing CIs. Further, the CI partly passes the stress test if it receives grade B, which corresponds to possibly unjustifiable risk. Finally, the CI fails the stress test if it is given grade C, which corresponds to intolerable risk.

The project manager (PM) of the stress test defines the boundaries between grades (i.e. the risk objectives) by following requirements of the regulators. The boundaries can be expressed as scalar (Fig. 2.3 and Fig. 2.4, top) or continuous (Fig. 2.4, bottom) measures. Examples of the former include the annual probability of the risk measure (e.g. loss of life) and the expected value of the risk measure (e.g. expected number of fatalities per year), whereas the latter is often represented by an F-N curve, where F represents the cumulative frequency of the risk measure N per given period of time. In several countries, an F-N curve is defined as a straight line on a log-log plot. However, the parameters of these curves, as well as parameters of scalar risk objectives (i.e. regulatory boundaries in general) may differ between countries and industries (Bowles et

al 1999; Health & Safety Executive (HSE) 1989; MHLUPE 1988; Paté-Cornell 1994; Whitman 1984).

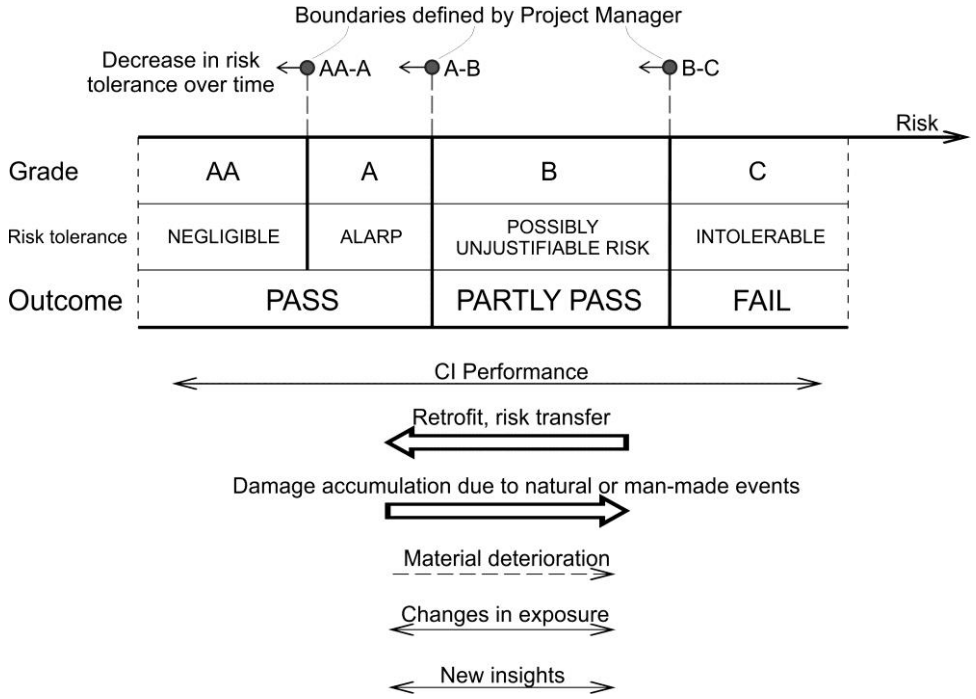

Fig. 2.3 Grading system for the global outcome of stress test

In general, the CI performance can be understood as time-variant. It may change due to several reasons, such as ageing long-term degradation process (e.g. corrosion), man-made events (e.g. terrorist attacks), changes in exposure (e.g. population growth) that may increase the probability of failure or loss of functionality or exacerbate the consequences of failure during their lifetime (Fig. 2.3). In the proposed grading system, it is foreseen that the performance of the CI or the performance objectives can change over time. Consequently, the outcome of the stress test is also time-variant. For this reason, stress tests are periodic, which is also accounted for by the grading system. If the CI passes a stress test (grade AA or A), the risk objectives for the next stress test do not change until the next stress test. The longest time between successive stress tests should be defined by the regulator considering the cumulative risk. However, most of existing CIs will probably obtain grade B or even C, which means that the risk is possibly unjustifiable or intolerable, respectively. In these cases, the grading system has to stimulate the stakeholders to upgrade the existing CI or to start planning a new CI in the following stress test cycle. It is proposed that stricter risk objectives are used or that the time between the successive stress tests is reduced in order to make it possible that stakeholders adequately upgrade their CIs in few repetitions of stress tests, which means that the CI will eventually obtain grade A or the regulator will require that the operation of the CI be terminated.

The basis for redefinition of risk objectives in the next evaluation of stress tests is the so-called characteristic point of risk. In the case when scalar risk measures are used, the characteristic point of risk is represented directly by the results of risk assessment (Fig. 2.4, top). In the case when the result of risk assessment is expressed by an F-N curve, the characteristic point is defined by one point of the F-N curve. It is recommended that the point associated with the greatest risk above the ALARP region be selected. In this case the characteristic point is defined as the point of the F-N curve which is the farthest from the limit F-N curve that represents the boundary between grades A and B (A-B boundary) (see blue line in Fig. 2.4a).

Once the characteristic point is determined, the grading system parameters for the next evaluation of stress test can be defined. If the CI obtains grade B in the first evaluation of stress test (ST1, blue dot in Fig. 2.4a), the grading system foresees the reduction of the distance between grades B and C (B-C boundary) in the next stress test (ST2, Fig. 2.4b). This reduction should be equal to the amount of cumulative risk beyond the ALARP region assessed in ST1. This ensures risk equity over two cycles, which may be expressed by the following expression:

$$R_{evaluated,\,ST1} - R_{(A\text{-}B)} = R_{(B\text{-}C),\,ST1} - R_{(B\text{-}C),\,ST2} \tag{2.1}$$

where $R_{(A\text{-}B)}$ is the A-B boundary, $R_{(B\text{-}C),ST1}$ and $R_{(B\text{-}C),ST2}$ are the B-C boundary in ST1 and ST2, respectively, and $R_{evaluated,ST1}$ is the value of risk measure assessed in the ST1. Note that the left side of the Eq. 3.7 is equal to the amount of risk beyond the ALARP region assessed in ST1. Furthermore, if grade C (red dot in Fig. 2.4a) is given in ST1, both the B-C boundary and the period until ST2 are reduced (Fig. 2.4c). In this case, the B-C boundary is set equal to the A-B boundary, since this is the maximum possible reduction of the region of possibly unjustifiable risk. Moreover, the reduced period until ST2 ($t_{cycle,redefined}$) is determined on the basis of equity of risk above the ALARP region over two cycles and can be calculated using the following expression:

$$t_{cycle,redefined} = t_{cycle,initial} \cdot \frac{R_{evaluated,\,ST1} - R_{(A\text{-}B)}}{R_{(B\text{-}C),\,ST1} - R_{(A\text{-}B)}} \tag{2.2}$$

where $t_{cycle,initial}$ is the initial amount of time between two stress tests.

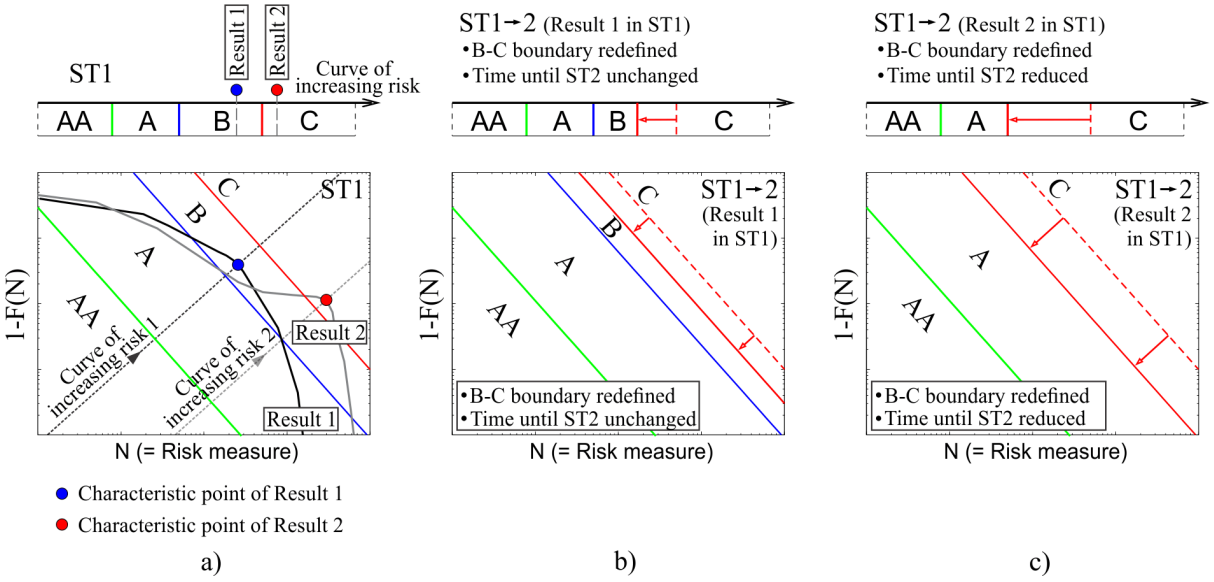

Fig. 2.4 Grading system in time domain using scalar risk objectives (top) and limit F-N curves (bottom): a) two different results of the first evaluation of stress test (ST1), b) redefinition of the parameters of the grading system due to Result 1 in ST1, and c) redefinition of the parameters of the grading system due to Result 2 in ST1

2.4.1 Grading of the components

Similar to the case of system level assessment, three thresholds need to be defined (between grades AA and A, between grades A and B and between grades B and C) in order to consistently evaluate the components of a CI.

For the Component-Level Assessment (STEP 4), there are three methods to perform the single-hazard component check: the hazard-based assessment, design-based

assessment and the risk-based assessment approach. These methods differ for the complexity and the data needed for the computation.

If the result of a hazard-based assessment or a design-based assessment is that the component is in compliance with the requirements, a grade A is assigned to the component. If these types of assessment result in the component not being in compliance with the requirements, a grade C is assigned to the component or a higher accuracy level assessment is required. However, the grading system at the component level is equal to that proposed in the case of system-level assessment if risk-based assessment is used.

If a component is assigned grade C, mitigation actions need to be taken. The time in which the grade needs to be improved depends on the type of assessment. If a hazard-based or a design-based assessment is used, the mitigation has to be made immediately, as the component is not in compliance with the requirements. If a risk-based assessment is used, the time in which the grade has to be improved is determined on the basis of the amount of risk corresponding to the component reaching the designated limit state (see ERR4, Esposito et al 2016 for more details).

3. Application of stress test concepts to ENI/Kuwait oil refinery and petrochemical plant, Milazzo, Italy

3.1 Phase 1: Pre-assessment phase

3.1.1 Data collection

The refinery of Milazzo (Raffineria di Milazzo) is located in the north part of the island of Siciliy, in Italy. It is an industrial complex, which transforms crude oil into a series of oil products currently available on the market (LPG, gasoline, jet fuel, diesel and fuel oil) and comprises a number of auxiliary services. Total production currently stands at circa 9.3 million tons. The refinery has many storage tanks containing a large variety of hydrocarbons, such as LPG, gasoline, gasoil, crude oil and atmospheric and vacuum residues. The capacities of the tanks vary from 100 m^3 (fuel oil, gasoil, gasoline, kerosene) to 160 000 m^3 (crude oil). All tanks are located in catch basins (bunds) with concrete surfaces. Only the LPG is stored in pressurised spheres, all other substances are stored in single containment tanks. A filling degree of 80 % is assumed.

In a QRA the societal risk is determined. In order to do so, the (actual) presence of persons in the surroundings needs to be taken into account (Fig. 3.1), since the numbers of persons present influences the societal risk. Only persons within the impact area of the site need to be taken into account. Persons on-site are not considered for the external risk.

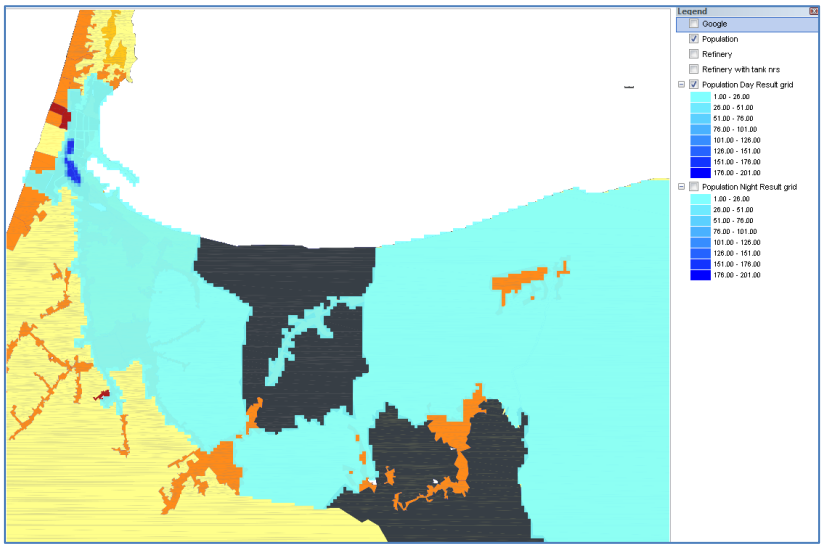

Fig. 3.1 Overview of population density as used in QRA

3.2 Phase 2: Assessment phase

Natural events may dramatically interact with industrial equipment with different intensity and hazards (Krausmann et al 2011; Salzano et al 2013).

3.2.1 Component level assessment (ST-L1a)

When NaTech risks should be considered, the natural hazards should be evaluated for the site under analysis, following the methodologies detailed in previous work-packages and deliverables of the STREST project.

Earthquake hazard

The probabilistic seismic hazard analysis (PSHA) presented in this section concerns the Italian port of Milazzo, situated in northern Sicily. For the purposes of this study, the area around Milazzo was discretized into a grid of forty-eight points (potential seismic event epicentres) with a grid spacing of approximately 25 km, as shown in the following Fig. 3.2.

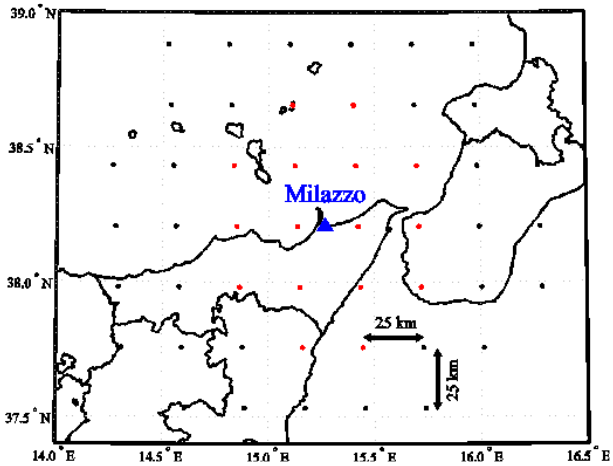

Fig. 3.2 Grid of potential epicentres around Milazzo considered in the PSHA analysis. Grid points within a 50 km radius from Milazzo are displayed as red dots

For each single point on this grid, the Italian National Institute of Geophysics and Volcanology (Istituto Nazionale di Geofisica e Vulcanologia - INGV) provided the joint probability mass of strike, dip and rake, for a total of around three thousand four hundred "rupture scenarios" of probability. This information forms the basis of the elaboration, as it allows the probabilistic assignment of finite-fault geometries to all scenarios that enter the PSHA calculations. The hazard curve for Milazzo in terms of peak ground acceleration (PGA), can be found in Fig. 3.3.

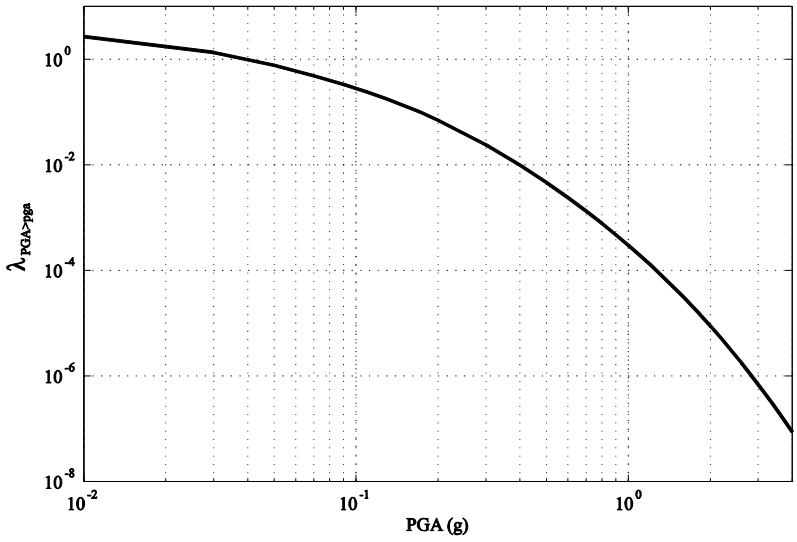

Fig. 3.3 Hazard curve for Milazzo in terms of MAF of exceedance of PGA, calculated according to the methodology presented

Tsunami hazard

Probabilistic Tsunami Hazard Analysis (PTHA) is a methodology to assess the exceedance probability of different thresholds of hazard intensity, at a specific site or region in a given time period, due to any given source. Different potential tsunamigenic sources should be considered, such as earthquakes, landslides, meteorite impacts or atmospheric phenomena. Here, we focus only on tsunami of seismic origin, which is the dominant component of PTHA in most of the areas of the world, both in terms of occurrence and in terms of effects (Parsons & Geist 2009). Following the definition proposed in Lorito et al (2015), we deal with Seismic PTHA (SPTHA), that is, tsunamis generated by co-seismic sea floor displacements due to earthquakes.

3.2.2 System level assessment for single hazard (ST-L2b / L2d)

Probabilistic risk assessment

The impact of natural hazards on the accident or release scenarios and frequencies is discussed. The release frequencies are given in Table 3.1. These frequencies have been calculated by taking into account the methodology described in STREST D4.1 (Salzano et al 2015), where equipment vulnerability with respect to the intensity of the natural events has been assessed by taking into account the construction characteristics of equipment and, more important, the new limit states based on the release of content.

Scenario based assessment

Flammable substances can be ignited upon release. Direct ignition will lead to a pool fire (liquids) or jet fire (gases). If a liquid is not ignited immediately, it will start to evaporate and a flammable atmosphere could be formed, which will disperse with the wind. If a gas is not ignited immediately, the gas will also disperse.

Ignition of that flammable cloud will result in a flash fire, with possibly an explosion (causing overpressure effects), if the cloud is obstructed.

It has been assumed that the consequences of a delayed ignition are minor compared to the consequences of a pool fire for the flammable liquids: only pool fires have been considered.

A special phenomenon occurs upon the instantaneous release of a liquefied gas.

An instantaneous release is followed by an instantaneous evaporation and a physical explosion, called Boiling Liquid Expanding Vapour Explosion (BLEVE). Often the gas cloud is ignited resulting in a fireball.

The probability of ignition depends on the flammability of a substance and the quantity released. Table 3.2 presents the ignition probabilities according to the Purple Book (VROM 2005).

Not all substances present on site are considered individually and representative substances have been determined. Table 3.3 shows which representative substance is used for each product. Atmospheric residue, heavy vacuum gas oil and vacuum residue have not been considered in the QRA. For all flammable liquids considered, the ignition probability of K1-liquids is assumed: this is a conservative approach.

The probability of a BLEVE is given in Table 3.4.

Table 3.1 Scenarios and frequencies for stationary vessels due to natural hazards

Scenario	**Frequency (-/yr)**		
	Atmospheric vessels- single containment	*Pressurized vessels*	*Pipelines*
Earthquake			
Instantaneous release of the complete inventory	$3.70 \cdot 10^{-3}$	$1.16 \cdot 10^{-9}$	-
Continuous release of the complete inventory in 10 min at a constant rate of release	$3.70 \cdot 10^{-3}$	$1.16 \cdot 10^{-9}$	-
Continuous release from a hole with an effective diameter of 10 mm	$7.33 \cdot 10^{-2}$	0	-
Full bore rupture	-	-	$5.56 \cdot 10^{-2}$
Tsunami	*Atmospheric vessels- single containment*	*Pressurized vessels*	*Pipelines*
Instantaneous release of the complete inventory	$1.85 \cdot 10^{-5}$- $3.47 \cdot 10^{-4}$	0	-
Continuous release of the complete inventory in 10 min at a constant rate of release	$1.85 \cdot 10^{-5}$- $3.47 \cdot 10^{-4}$	0	-
Continuous release from a hole with an effective diameter of 10 mm	0	0	-
Full bore rupture	-	-	0
Earthquake + Tsunami			
Instantaneous release of the complete inventory	$3.7 \cdot 10^{-3}$- $4.05 \cdot 10^{-3}$	$1.16 \cdot 10^{-9}$	-
Continuous release of the complete inventory in 10 min at a constant rate of release	$3.7 \cdot 10^{-3}$- $4.05 \cdot 10^{-3}$	$1.16 \cdot 10^{-9}$	-
Continuous release from a hole with an effective diameter of 10 mm	$7.33 \cdot 10^{-2}$	0	-
Full bore rupture	-	-	$5.56 \cdot 10^{-2}$

Table 3.2 Ignition probabilities

Source		**Direct ignition probability (-)**				
		Substance				
Continuous	Instantaneous	K3, 4	K2	K1 liquid	K0, Gas, low reactive	K0, Gas, average/ high reactive
< 10 kg/s	< 1000 kg	0	0.01	0.065	0.02	0.2
10-100 kg/s	1000- 10 000 kg	0	0.01	0.065	0.04	0.5
> 100 kg/s	> 10 000 kg	0	0.01	0.065	0.09	0.7

Table 3.3 Representative substances

Product	Representative substance
Atm residue	NA
Crude	Pentane
Fuel oil	Nonane
Gasoil	Nonane
Gasoline	Pentane
HVGO	NA
Jet/ kerosene	Nonane
LPG	Propane
Naphtha	Pentane
Others	Pentane
VAC residue	NA

Table 3.4 BLEVE probability

	Probability BLEVE
Stationary installations	0.7

3.3 Phase 3: Decision phase

3.3.1 Single risk analysis

The calculated risk for each individual event (industrial, earthquake, or tsunami) is first compared. Fig. 3.4 presents the locational risk contours. The black crosses indicate the location of the scenarios. The industrial risks result in large contours, especially for the lower risk levels (10^{-7}, 10^{-8}/yr). These contours are dominated by the risks related to the LPG storage vessels. The location of the LPG tanks is given in Fig. 3.5 by the red squares. When only considering earthquake induced risks the 10^{-7} and 10^{-8}/yr risk contours are smaller. This is due to the lower release frequency for the LPG vessels. The higher risk levels (> 10^{-6}/yr) are dominated by the atmospheric vessels. These have a higher release frequency compared to the industrial risks, resulting in larger 10^{-5} and 10^{-4}/yr contours.

The industrial risks on the right side of the site are mainly caused by the atmospheric tanks. When comparing the industrial risks with the earthquake induced risks, one can observe that the risks on the right side of the site have increased by a factor of approx. 1000: for the earthquake induced risks the 10^{-4}/yr contour is located at almost the same location as the 10^{-7}/yr contour of the industrial risks. This is due to the failure frequency of the atmospheric tanks: failure due to earthquake is a factor 1000 higher than failure due to industrial activities.

The risks associated with tsunami-induced releases are the smallest of the three release causes. Only atmospheric vessels close to the shore will result in releases. Vessels located further away do not pose risks.

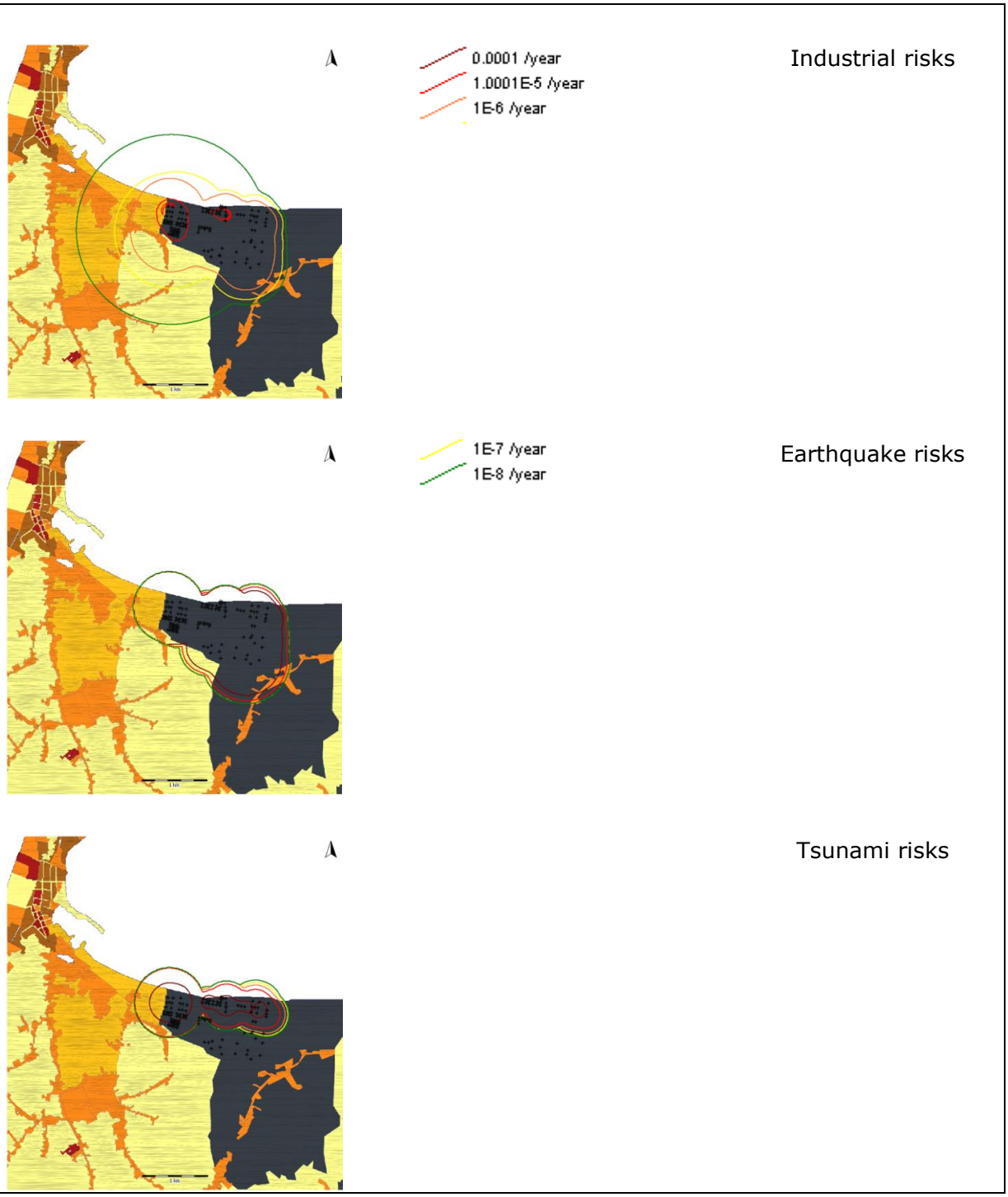

Fig. 3.4 Locational risk – Single hazard only. Larger figures are included in Appendix I

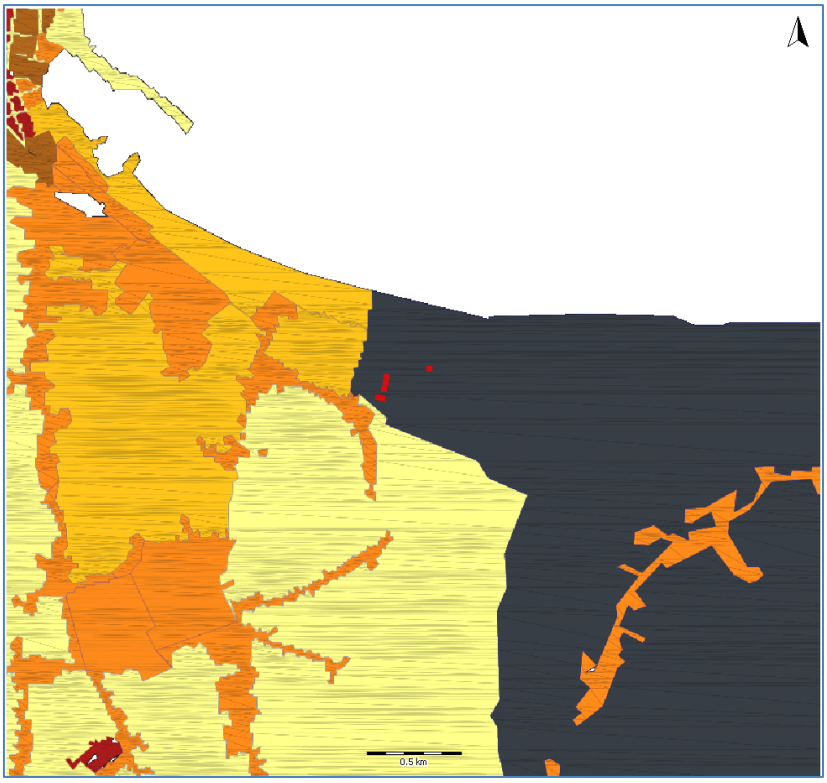

Fig. 3.5 Location of LPG Spheres (red squares)

3.3.2 Combined risk analysis

Fig. 3.6 shows the location risk when considering:

- industrial risks + earthquake induced risks;
- industrial risks + tsunami induced risks;
- industrial risks + earthquake and tsunami induced risks.

The most dominant risks are the industrial and earthquake induced risks.

3.3.3 Guidelines and critical events

For a better comparison of the locational risk, a horizontal cross-section of the locational risk is made. This line is given in Fig. 3.7.

The locational risk along the red line is given in Fig. 3.8. The distance 0 m corresponds to the left end of the red line in Fig. 3.7. The black line (industrial risks) is overlapped by the purple (industrial + tsunami), orange (industrial + earthquake + tsunami) and green (industrial + earthquake) lines between 0 and 1400 m. The red line (tsunami) starts at 1400 m and is overlapped by the purple line (industrial + tsunami). Beyond 1400 m the orange (industrial + earthquake + tsunami) line, blue line (earthquake) and green line (industrial + earthquake) overlap. Fig. 3.8 shows that for this pilot case low risks ($< 10^{-6}$ /yr) are dominated by the industrial risks as these risks are caused by failure of the LPG vessels. Earthquake and tsunami do not damage these vessels. Tsunami results in approximately 10 times higher risk along the transect line and earthquakes in approximately 1000 times higher risk.

Naturally induced hazards cause an increase in the total risks. As a tsunami only damages a limited number of the vessels along the shoreline, the risk increase is limited.

Similar results, for earthquakes only and simplified analysis for the earthquake hazard, have been found in other works (Salzano et al 2003; Campedel et al 2008; Fabbrocino et al 2005; Salzano et al 2009).

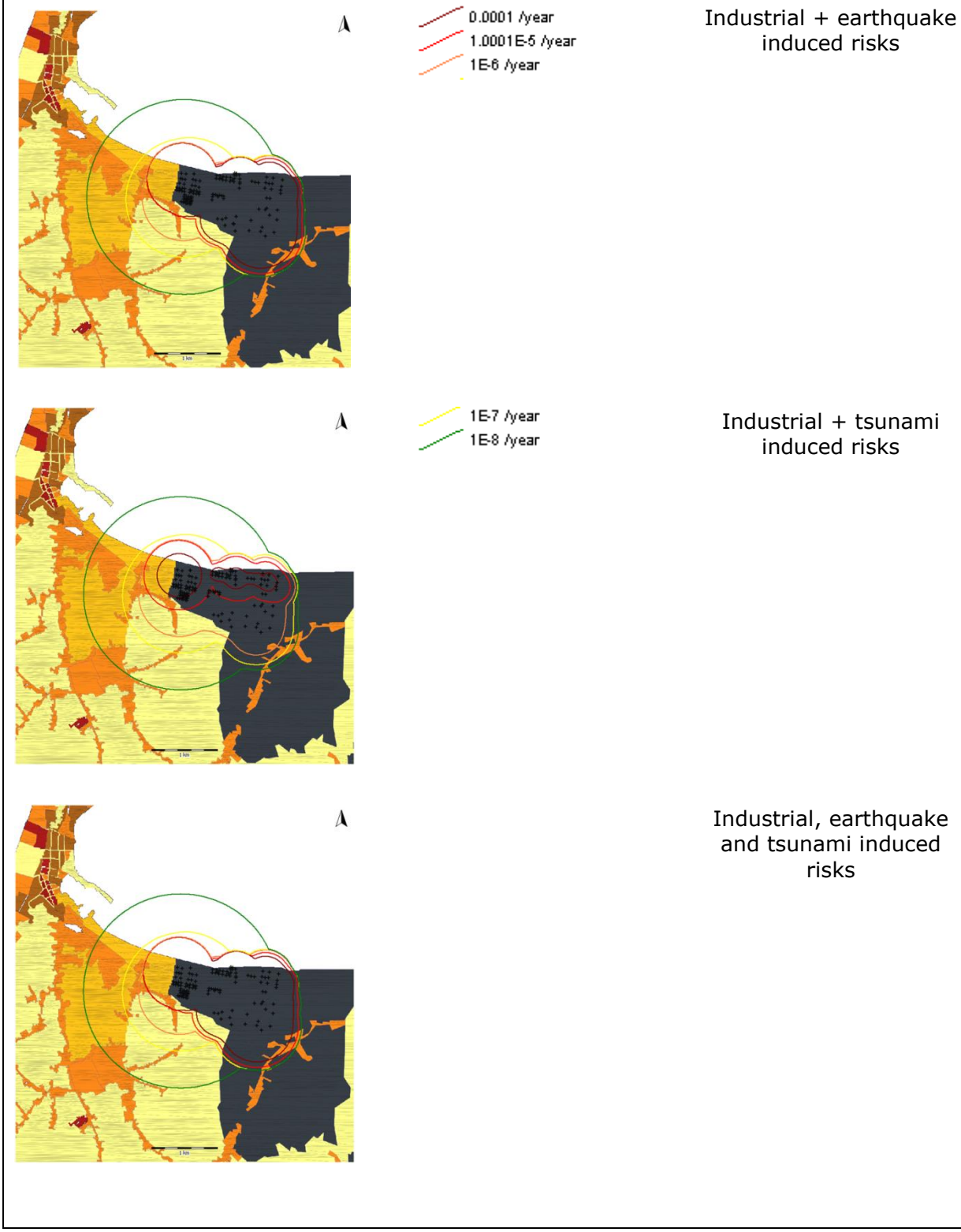

Fig. 3.6 Locational risk – Hazard combinations

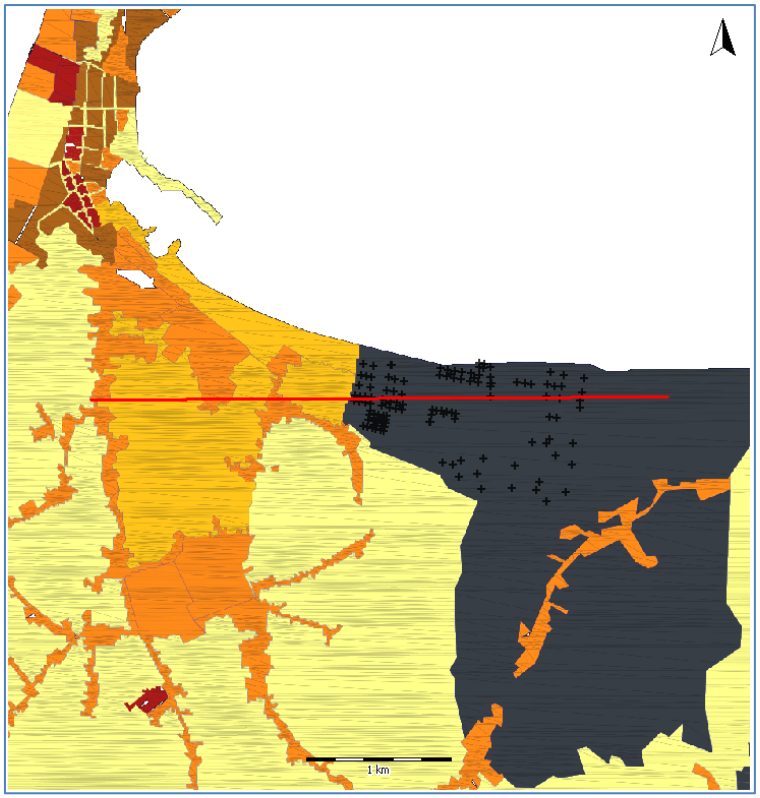

Fig. 3.7 The cross-section of the locational risk (red line) in Fig. 3.8

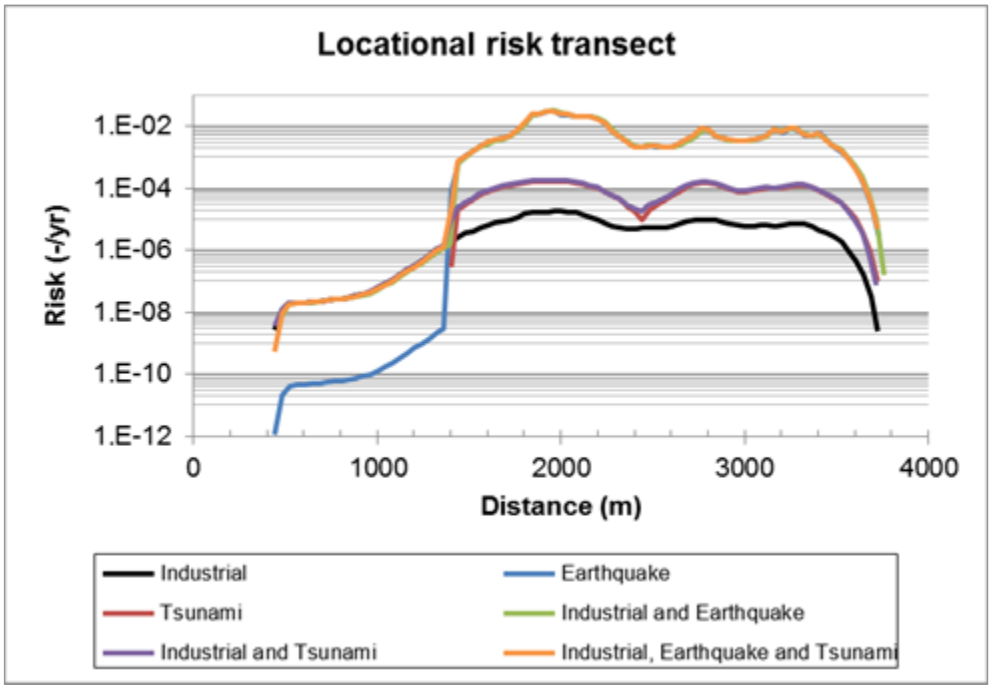

Fig. 3.8 Locational risk transect

The societal risk for the base situation (without accounting for natural hazards) is presented in Fig. 3.9.

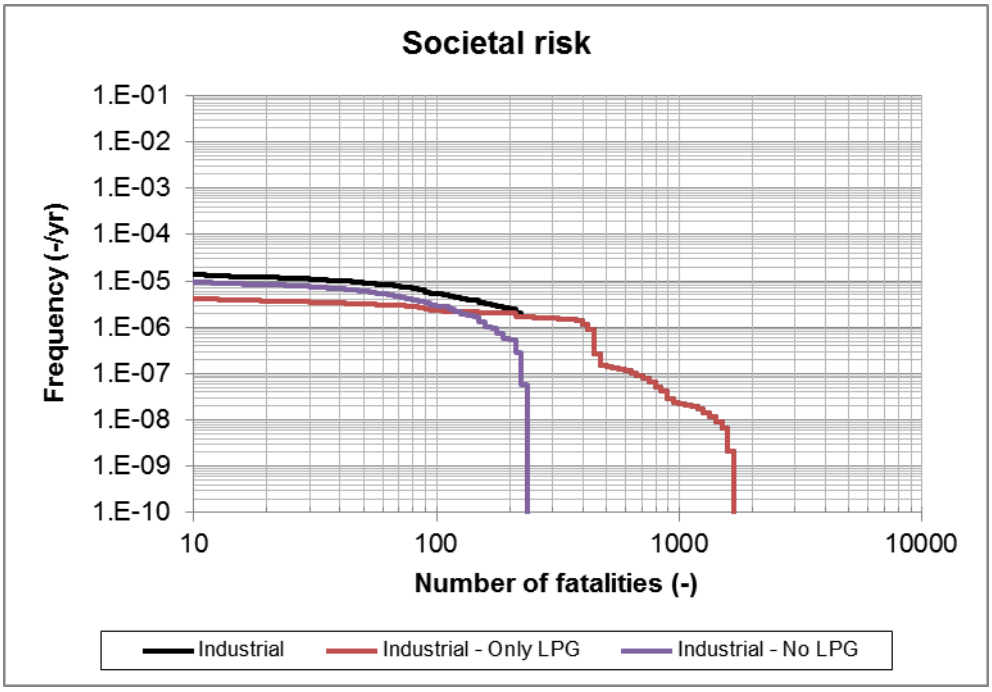

Fig. 3.9 Societal risk without accounting for natural hazards- with and without LPG tanks

The societal risk is mainly caused by the LPG tanks, as can be seen by comparing the black and red line. By not accounting for the LPG tanks (purple line), the maximum number of fatalities is reduced from 1650 to 220.

Fig. 3.10 shows the societal risk per cause. Up to approx. 200 fatalities the naturally induced hazards have a higher frequency of occurring, due to the higher failure frequency of the atmospheric vessels. Larger numbers of fatalities are only caused by industrial risks or by earthquakes - this is due to the failure of the LPG vessels.

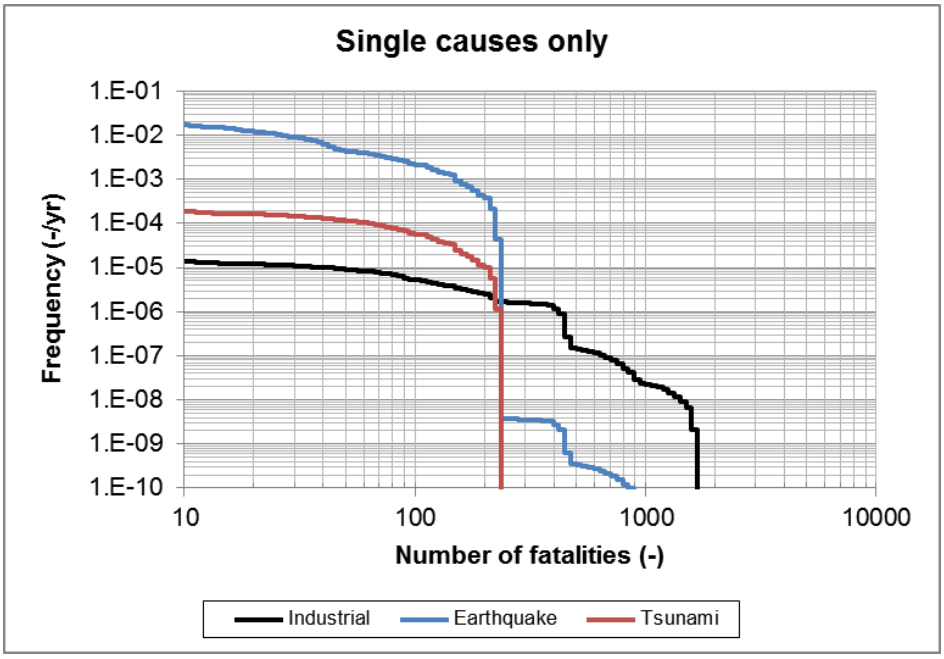

Fig. 3.10 Societal risk- industrial, earthquake or tsunami induced

The cumulated risks are given in Fig. 3.11 (the orange and green line overlap).

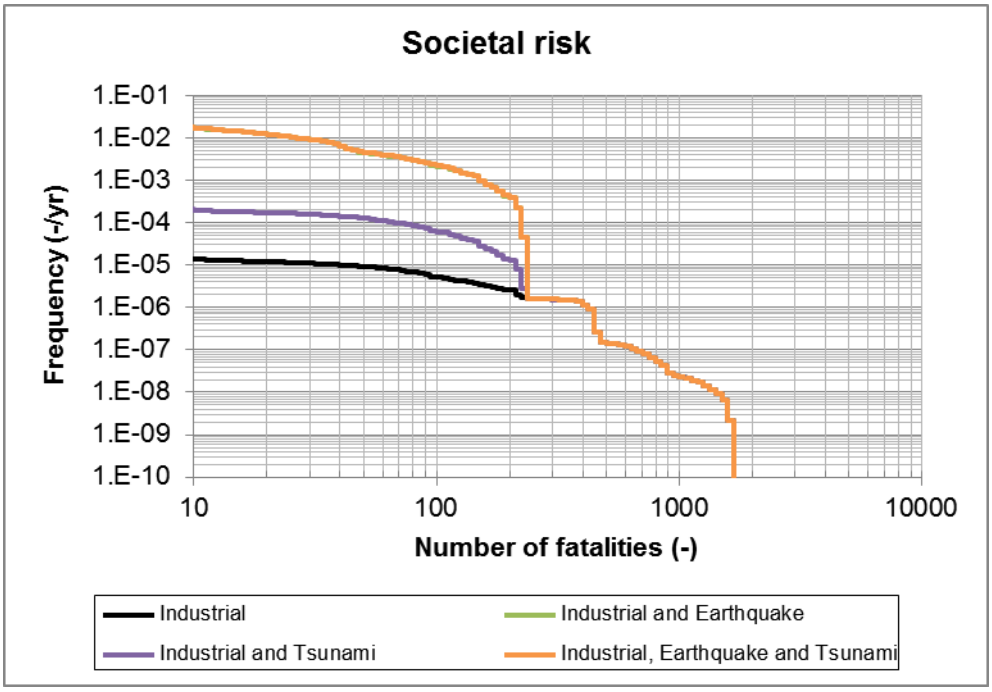

Fig. 3.11 Societal risk- cumulated risks

Fatalities up to approx. 200 are dominated by earthquakes; more than 200 fatalities are dominated by the industrial causes.

3.4 Phase 4: Report phase

Naturally induced hazards can play an important role in the total risk associated with the presence of installations with dangerous goods. In this study the effect of an increased frequency (caused by earthquakes or tsunamis) of a number of release scenarios on locational and societal risk was assessed.

The impact of natural induced hazards depends on many (location specific) factors. For the specific site analysed in this work, a tsunami only damages a limited number of the atmospheric storage vessels along the shoreline. Hence the increase on the total risk is limited. Nonetheless, the overloading of emergency response should be considered, at least for the tanks along the coastline.

Of more importance is the effect of an earthquake, which significantly increases the failure frequency of atmospheric storage tanks. Neither an earthquake nor a tsunami significantly increases the failure frequency of, and hence risk imposed by, pressurised vessels (like LPG spheres). As for the considered site, the risk is largely dominated by the LPG tanks when failing due to industrial-related causes, whereas the impact of the natural hazards is limited.

All in all though, naturally induced hazards should be considered when determining the overall risk and the risks associated with natural disaster.

This pilot case has been performed to show the impact of naturally induced hazards on the outcome of a quantitative risk assessment (QRA) of an industrial site holding dangerous substances. The aim was not to perform a detailed QRA of the pilot site (for such exercise much more detailed information would have been required) but merely to show how (the more common) scenarios are affected by an increased release frequency caused by earth quakes and tsunamis.

Other scenarios that may be relevant in cases of earthquakes or tsunamis have not been evaluated. For instance failure of multiple tanks has not been taken into account. This

may result in released volumes exceeding the catch basins capacity, and hence lead to larger pool sizes, especially in case of failure of catch basins.

Also domino effects have not been considered. For instance, if a pool of flammable material extends to an area with LPG spheres, BLEVEs may occur. Neither has the effect of debris (or large objects like ships) carried land inward with a tsunami, been taken into account. Such phenomena will result in larger effect areas, and may hence increase the number of casualties. However, it should be realised that the natural hazards we are considering here (earthquakes and tsunamis) have a large areal impact. This means many of the fatalities calculated in the QRA, would have occurred also had such an installation not been present, because of the collapse of houses and other buildings.

4. Application of stress test concepts to large dams in the Valais region of Switzerland

4.1 Introduction

Although design, maintenance, and surveillance practices depend on national legislations, the international guidelines (e.g. International Commission on Large Dams, ICOLD) that many national codes reflect aim to avoid dam failures altogether, this being true even in the face of extreme natural events (such as floods or earthquakes). Worldwide this objective has been, at least so far, very well met. Fortunately, in the last decades relatively few large dams have failed due to natural causes in countries that enforce the internationally accepted best practices in terms of dam safety.

Regardless of specific characteristics, dams operate by storing substantial volumes of water in the upstream reservoir, the release of this water to downstream areas being controlled according to operational guidelines and targets. In view of that, in order to correctly frame risk and vulnerability assessments for dams, one should consider, beyond the dam body, the foundation, the reservoir, the appurtenant structures (e.g. spillways, bottom outlets, or hydropower systems) and, most importantly, the downstream areas potentially affected by floods.

Following a dam failure or breach, typically characterized by an uncontrolled release of the reservoir, a large amount of water travels downstream in the form of a dam-break wave. While the dam-reservoir system is vulnerable to several hazards and monetary losses associated with it in the event of a failure amount to very large figures, the larger share of the losses associated with a dam failure are likely to occur downstream (Fig. 4.1). Stemming from this, and while it is important to pay close attention to the dam-reservoir system (in order to quantify the probability of failures taking place and as a means to assess which are the most likely chains of events potentially leading to those failures), evaluating the processes that may unfold downstream is paramount.

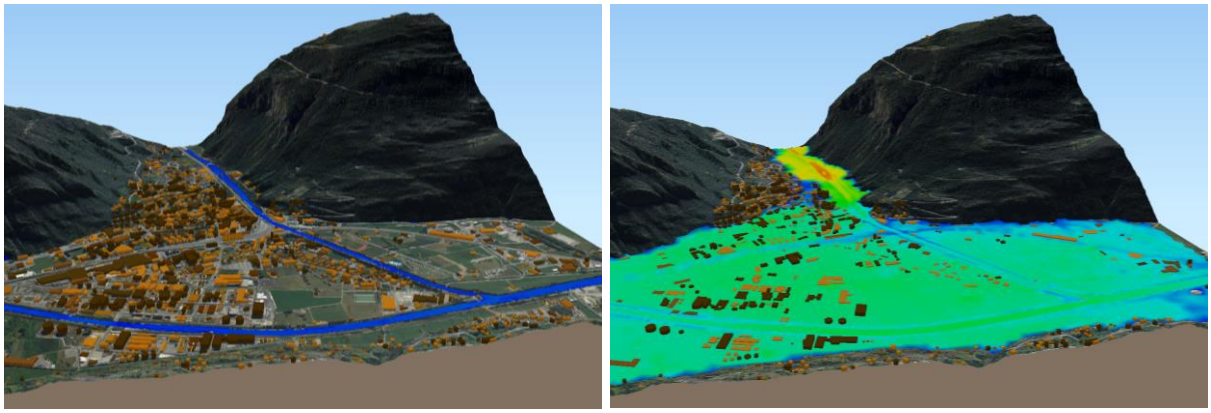

Fig. 4.1 Dam break wave spreading across a river flood plain and inundating a city. Colour characterizing water depths from dark blue (0 m) to bright red (30 m)

Safety assessments for large dams have been routinely carried out for decades. These often include geological surveys, numerical modelling of the dam structures, hydrological studies, and hydraulic evaluations of outlet structures. The engineering supporting these endeavours is well developed albeit mostly based on deterministic frameworks. National legislations, ICOLD Bulletins, and ICOLD benchmark workshops (Gunn et al 2016; Zenz and Goldgruber 2013) are a great source of information on current best practices.

How the transition to probabilistic approaches is to be made in the field of dam safety is, today, a topic of heated debate. Regardless of how that transition will unfold, it is

believed that, in the future, probabilistic approaches will gain increased relevance in relation to deterministic ones.

One of the general conclusions of the conceptual case study analysed in STREST (Pitilakis et al 2016; Salzano et al 2015) is that it is increasingly possible to address long-standing limitations of probabilistic frameworks, most notably the computational demands associated with numerical modelling of dam structural responses and dam-break wave propagation.

From a technical perspective, large dams' features change widely in order to adapt to each project's specificities and their behaviour is not easily – nor should it be – predicted without the laborious undertaking of customized numerical simulations (e.g. Gunn et al 2016; Zenz and Goldgruber 2013). One of the main challenges of applying ambitious probabilistic frameworks to dam safety is how to evaluate numerous scenarios without making hefty concessions on the numerical modelling side. It is proposed that machine learning regression models are used to "map" a reduced number of numerical model outcomes to a whole domain of possible hazards and element responses.

Conceptually, hazard inter-actions, "intra-actions", and coincidences may lead to failures that are difficult to foresee resorting to a deterministic approach. In parallel, uncertainty on hazard characterization and element responses may have an acknowledgeable impact on overall risk, which presents a further advantage of relying on probabilistic frameworks.

The work developed on large dams within STREST below is a follow-up to STREST's D4.1 (Salzano et al 2015), where the basis of the methodology is laid out, STREST's D6.1 (Pitilakis et al 2016), where it is extended. It attempted to overcome hurdles related to the practical application of probabilistic frameworks. Naturally, this section reflects lessons learnt from that experience. The Generic Multi-Risk (GenMR) framework was adopted as the computational tool to "manage" simulations. It is based on a sequential Monte Carlo method and its principles are well described in Mignan et al (2014). Obviously, when using this method – as much as any other – reliable outcomes are very much dependent on realistic inputs.

The findings reported here are based on a conceptual case study of a large alpine earthfill dam. The infrastructure is approximately 100 m high, with a reservoir capable of holding over 100 000 000 m^3 of water. It is equipped with a spillway in order to cope with excessive water levels, a bottom outlet that allows for the control of the volume of water stored, and a hydropower system through which the main purpose of the dam is fulfilled: producing energy. The modelled system includes also the valley below the dam down to a distance of roughly 30 km, where a sizable urban agglomeration is assumed to exist.

4.2 Phase 1: Pre-assessment phase

The pre-assessment is arguably the most important part of the stress test of large dams. Very relevant on its own, the response of each element of the system to hazard-induced actions is essential and an input to the Monte Carlo probabilistic framework.

This phase of the stress test will not be particularly emphasized, as the recommendations, methodologies and models required to complete it are well established among the dam engineering community. Also, checking whether each component of the system is up to par with regulations is recommended practise already.

That said, it is important to highlight that applying a probabilistic framework should not equate to a relaxation of the standards proposed for existing safety assessments based on deterministic principles. Although such a step was bypassed on the test case presented in STREST D6.1 (Pitilakis et al 2016) it is recommended that a full range of element's responses is computed through the use of detailed models prior to the application of a probabilistic framework. In the case of constraining computational

demands involved in doing so, it is recommended that a regression model be fitted from a number of computed actions/responses pairs (e.g. a catalogue of peak ground acceleration's effects on sustained damages or degrees of functionality). Regression models of this type and their regression errors would allow for n-dimensional fragility functions to be prepared for posterior employment in fast-to-compute probabilistic Monte Carlo simulations.

4.3 Phase 2: Assessment phase (ST-L3c / L3d)

Classical risk analyses for dams generally correspond to very detailed scenario-based analyses considering only a few hazard interactions. Here, ST-L3c was tested with promising results, being therefore the recommended approach. Falling into a ST-L3d level, scenarios tested according to current practice should continue to be carried out for rare events of interest which are not easily reproduced using a purely probabilistic analysis.

It is recommended that the risk study of a large dam is split into two main parts: the dam-reservoir system, whose analysis should yield failure conditions, modes, and expected frequency, and the downstream area, which focused on the development of eventual breaches, the propagation of dam-break waves, and the evaluation of losses.

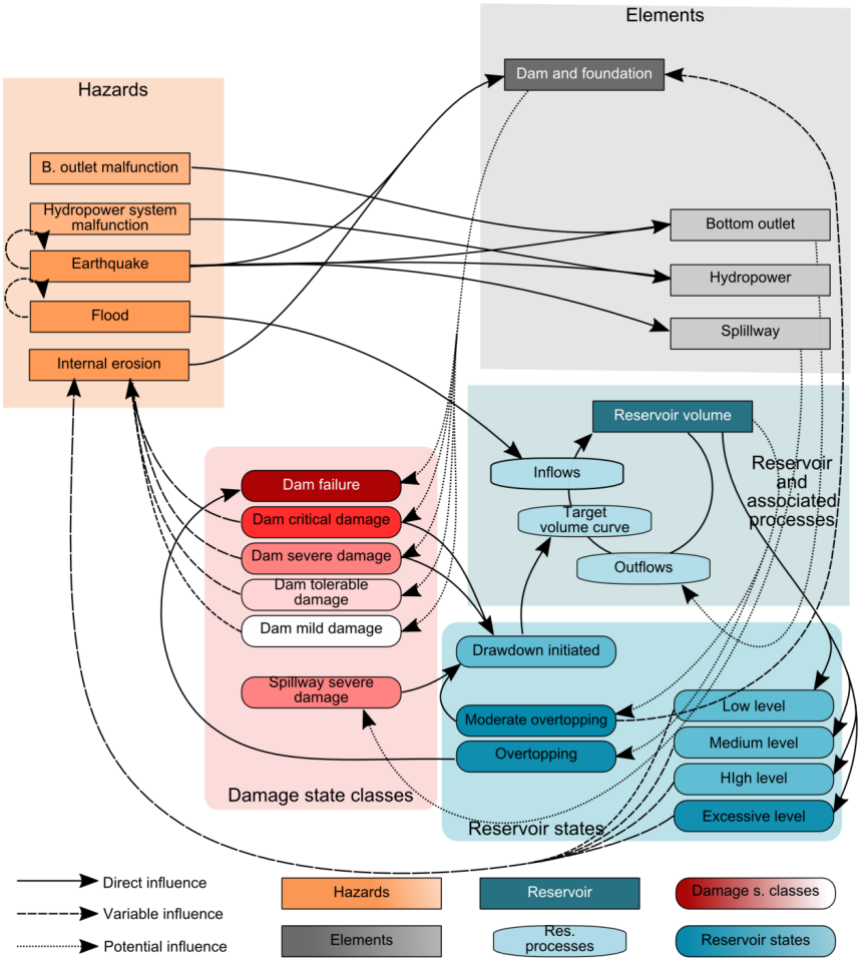

Fig. 4.2 Scheme of hazards, elements, system states, and interactions considered in the application of the GenMR framework to large dams. Case of an embankment dam. Adapted from Mignan et al (2015) and presented in Matos et al (2015)

Focusing on the dam-reservoir system, it is suggested that hazards are not studied individually, but rather that an inclusive modelling approach is implemented. As an example, STREST proposed the (simplified) scheme of hazards, elements, system states and interactions illustrated in Fig. 4.2. Such a scheme is dynamical in nature, and thus requires lengthy and full simulations of the system to yield results. Some advantages of its use are a quantitative appreciation of occurrence frequencies, the representation of inter-actions, "intra-actions" and coincidences, and the possibility of accounting for aleatoric and epistemic uncertainties.

An example of results obtainable through the proposed dynamic simulations is presented in Fig. 4.3. There, a failure by overtopping is prompted by the occurrence two related earthquakes (T=12 600 years followed by T=3 200 years). While the dam withstood both, its outlet structures did not and recovery efforts were unsuccessful in rehabilitating them before the peak of the inflow season. Without a full simulation of the dam-reservoir system such a chain of events could certainly be imagined, but its probability would be hard to guess and, therefore, so would its relevance.

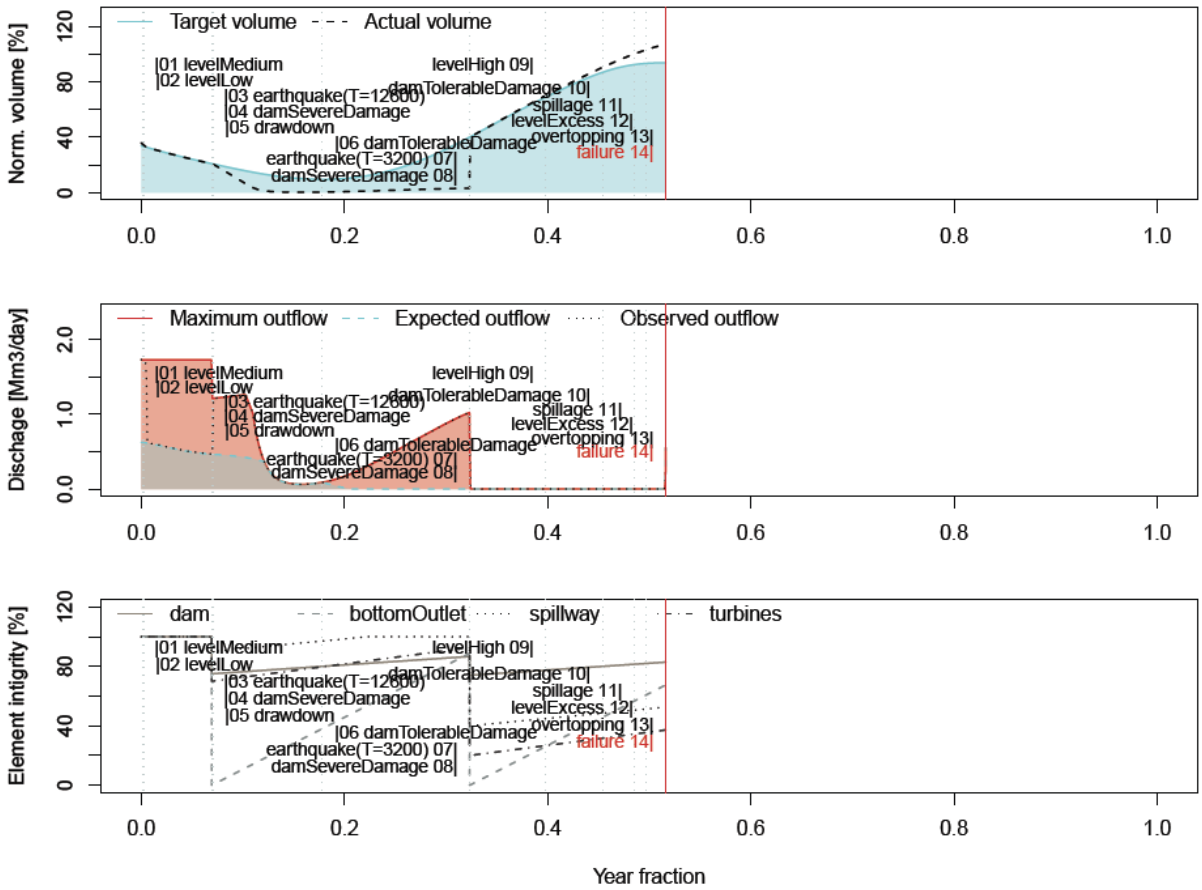

Fig. 4.3 Example of a chain of events leading to failure (Pitilakis et al 2016)

Hazard coincidences appeared to affect the risk of the system (Matos et al 2015). More relevantly still, including effects of epistemic uncertainty related to hazards and uncertainty at the level of the component's responses led to an approximate 4-fold increase in risk in comparison to that of a system evaluated based on expected values.

Moving downstream, assessing losses associated with a failure is an intricate process which is, as the former, marked by uncertainty. One can start with the hydrograph that characterized the dam-break wave near the dam; in the case of embankment dams, closely related to the development of the breach. Froehlich (2008) addressed this issue and quantified how, even under similar initial conditions, breaches can develop

differently. Naturally, these differences are relevant to loss estimation endeavours. An example of two very different (but possible) floods resulting from a failure of the conceptual dam that was studied is shown in Fig. 4.4.

It is advised that the full range of possible dam-break waves is studied. This is, however, not straightforward. Current numerical models useful for studying the propagation of dam-break waves – particularly 2D, which are the generally more accurate than 1D ones – are computationally demanding and running them for a great number of possible outflow hydrographs may be quite unpractical. As proposed in Pitilakis et al (2016) and Darcourt (2016), which used the free BASEMENT software for hydraulic modelling (Vetsch et al 2005), the problem may be overcome by resorting to non-linear regression models calibrated based on a limited but well-chosen catalogue of simulations. If well fitted, regression models can be used to estimate inundation parameters (e.g. max. water depth, max. water velocity, or wave arrival time) in any location of the computational domain for any possible dam breach event. A discussion of the challenges associated with the hydraulic modelling of sizeable areas can be found in Darcourt (2016).

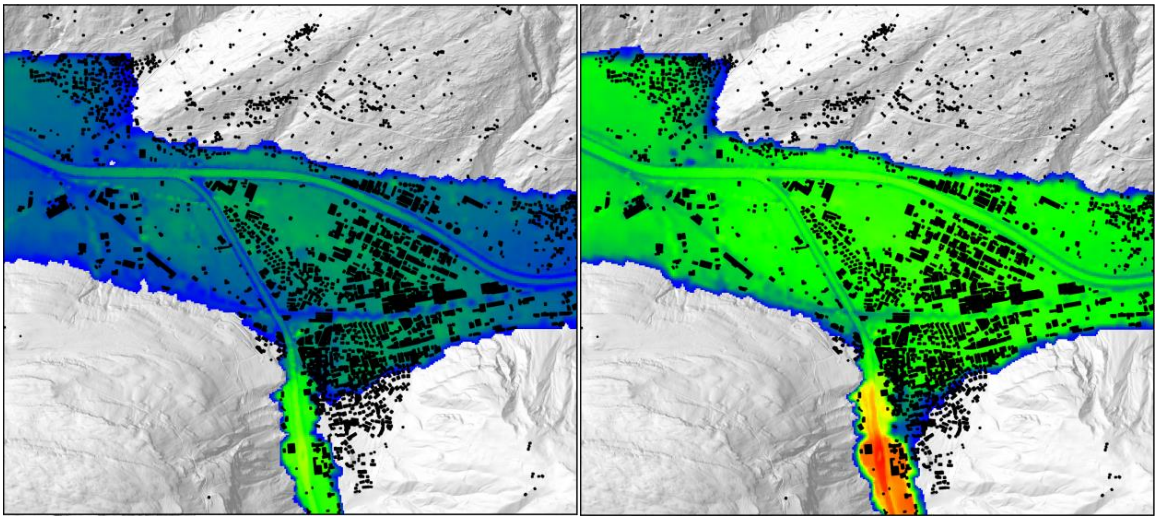

Fig. 4.4 Inundations calculated for low (left) and high (high) peak discharge/volume breach hydrographs. Adapted from Pitilakis et al (2016)

The process summarized until now allows the calculation of inundation parameters and the evaluation of their probability of occurrence, including epistemic and aleatoric uncertainties. Tangible as well as intangible losses can be computed as a function of these. In essence, the methodologies already developed to do so within deterministic frameworks can be used. Due to this, the work that focused on large dams under STREST did not go into great detail in what concerns the estimation of losses, having stopped short of estimating costs or loss of life. It did, however, estimate damages to buildings based on fragility curves which, based on a fortunate shortage of observations for dam-break events, were based on damages from tsunamis (e.g. Suppasri et al 2013).

4.4 Phase 3: Decision phase

The implementation of the previously summarized approach allows for the verification of a number of possible decision criteria. Compared to deterministic practices, it has the advantage of explicitly accounting for various sources of uncertainty and, therefore, rendering possible an effective disaggregation of risk. Also, it can go well beyond an analysis that focuses on expected values and lay out the full probability distribution of system states and consequences.

Based on 20 million full year-long simulations of the dam-reservoir system and downstream areas, an F-N curve characterizing the volume of collapsed or washed away buildings due to the failure of the conceptual dam under study exemplifies what kind of results can and should be derived from the proposed probabilistic framework (Fig. 4.5). Naturally, such a curve can be extended to loss of life or any other criterion that is considered relevant.

Detailed losses associated with deterministic scenarios are useful for decision making and will continue to be so for the foreseeable future. As such, it is not proposed that they are replaced by probabilistic approaches. Notwithstanding, in the face of the additional information that the latter can add to traditional deterministic safety assessments and their enormous potential, it is recommended that probabilistic approaches are employed and developed further.

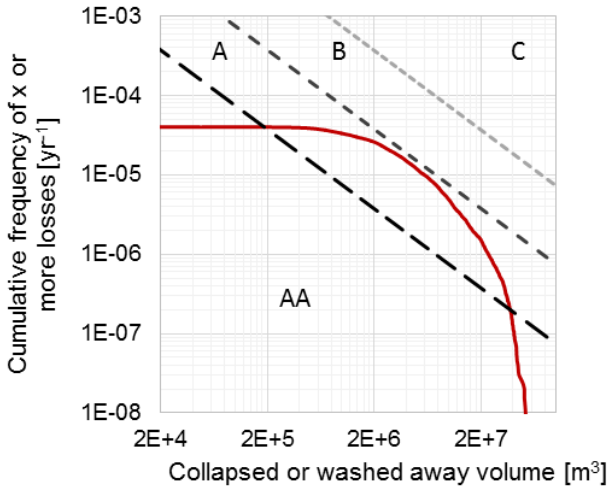

Fig. 4.5 F-N curve based on collapsed or washed away built volume following a dam failure upstream (Pitilakis et al 2016)

4.5 Phase 4: Report phase

Reporting based on analyses complemented with probabilistic frameworks such as the one tested within STREST have the advantage of being apt to attribute probability to losses and, thus, lead to formal risk estimations.

An example of formally framed risk that can be included in a report is the expected damages such as those illustrated in Fig. 4.6.

Going further than that, one can present results that draw from the full probabilistic distribution of damages. In Fig. 4.7, the probability of states of interest (buildings collapsed of washed away), not necessarily being those with greater probability of occurrence, is given. Evidently, reporting is not bound – nor should it be – limited to such damage states. Examples would be loss of life probabilities or information on flood timing (Fig. 4.8).

Perhaps most relevantly, it is recommended that reports contain objective evaluations of the uncertainty of the presented results and detailed sensitivity analyses that support them.

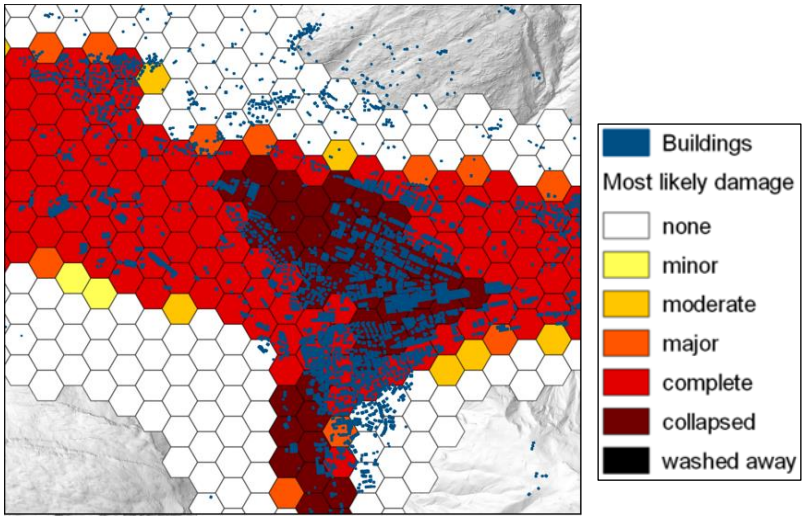

Fig. 4.6 Most likely damage to 3 or more stories reinforced concrete buildings in the event of a dam failure upstream. Adapted from Pitilakis et al (2016)

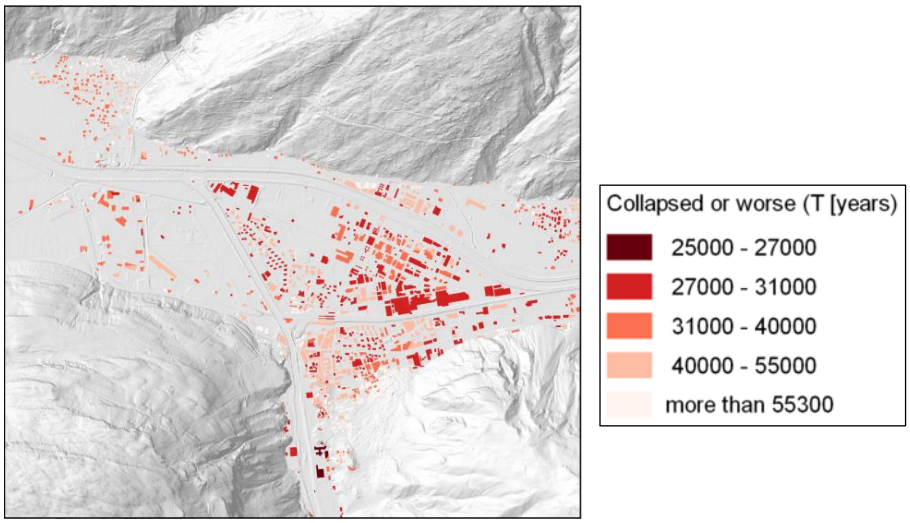

Fig. 4.7 Return period of buildings collapsing or being washed away as a consequence of dam failures. Adapted from Pitilakis et al (2016)

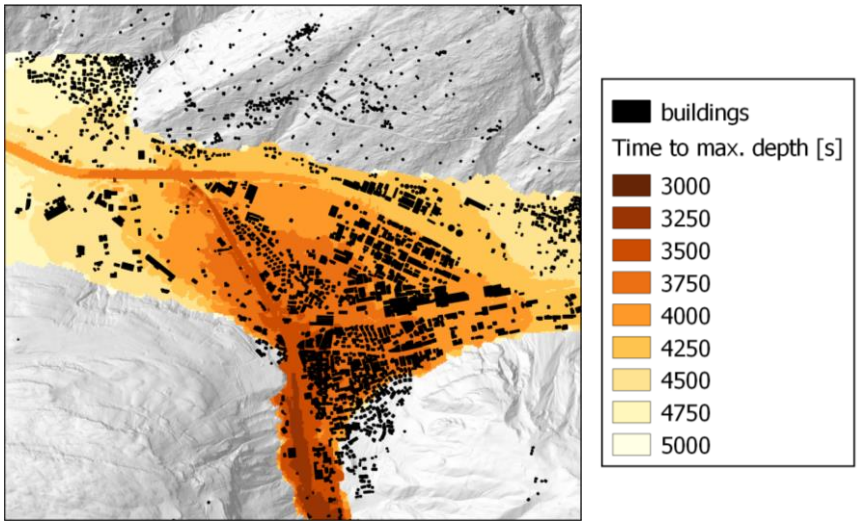

Fig. 4.8 Time to maximum depth

4.6 Final notes

The evaluation of risk for large dams is difficult due to a number of reasons: generally dam systems are complex and there are many sources of uncertainty involved in their evaluation; also, the numerical models required for adequate characterization of element's responses and dam-break wave propagations are demanding and computationally expensive; above all, the low frequency of the events leading to failure goes hand in hand with a fortunately meagre amount of empirical data to be used for validation purposes. In essence, it is hard to state with certainty that one assessment method is better than any other.

Deterministic approaches for the safety assessment of large dams have been in use for decades, with mostly satisfying results. They should by no means be put aside. Despite that, probabilistic approaches – at least conceptually – contain deterministic ones (in essence they are probabilistic approaches employing Heaviside cumulative distribution functions) and have the potential to go beyond them. In that sense, it is the unwieldy nature that ambitious probabilistic frameworks may have (both conceptual and in terms of computational requirements), the fact that they easily expose information gaps, and the reluctance to change a common practice that has mostly been proven effective that continues to justify the reliance on deterministic frameworks.

The work focusing on large dams that was undertaken under STREST has been an attempt to show how some of the unwieldiness that is associated to probabilistic frameworks can be mastered. More, it has shown that, in the presence of realistic inputs, formal estimates of risk can be produced and the probability distribution of losses characterized. Today, it is possible to account for hazard inter-actions, "intra-actions" and coincidences, as well as for not only aleatoric, but also epistemic uncertainties. Naturally, though the analysis of simulation results it is possible to pinpoint the largest contributors to risk in a large dam system and inform appropriate action.

Moving from deterministic to increasingly probabilistic frameworks in large dam safety assessments is a difficult endeavour that will most likely take time; methodologies should be adapted, computational models updated, and (the many) data gaps filled. It is believed, however, that the advantages of embracing the probabilistic view are many and, at least on the long run, its disadvantages few.

5. Application of stress test concepts to major hydrocarbon pipelines, Turkey

The proposed stress test procedure is implemented to the BTC (Baku-Tbilisi-Ceyhan) major hydrocarbon pipeline in Turkey. Following the ST@STREST main phases, that is, Pre-assessment, Assessment, Decision, and Report, the seismic risk of BTC pipeline exposed to the fault offsets in Turkey is assessed.

5.1 Phase 1: Pre-assessment phase

The pre-assessment phase includes three steps: data collection, risk measures and objectives, and set-up of the stress test. Firstly, the main participants of the risk assessment team are selected: the project manager (PM) selects the technical integrator (TI) and the internal reviewer (IR) whereas TI and PM jointly select the evaluation team (ET). The technical integrator, with the technical assistance of ET, collects data about the major seismic hazard levels that are likely to affect the pipeline as well as the mechanical properties of the BTC pipeline. The data collection also includes major mechanical properties of BTC pipeline as well as critical pipeline components that are likely to be affected from the target hazard levels.

Fig. 5.1 Overview of BTC pipeline

As the transmission pipeline, the investigated BTC pipeline (Fig. 5.1), is 1758 km long with a daily oil transportation of world's ~1% daily petroleum output (about 1 million barrels). The BTC pipeline yearly natural gas excess capacity (as of today) is 30 billion cubic meters (https://de.wikipedia.org/wiki/Baku-Tiflis-Ceyhan-Pipeline). The pipeline

diameter is 42 inches throughout most of Azerbaijan and Turkey. The pipeline diameter scales up to 46 inches in Georgia and reduces to 34 inches for the last downhill section to the Ceyhan Marine Terminal in Turkey. The BTC pipeline facilities include: 8 pump stations (2 in Azerbaijan, 2 in Georgia, 4 in Turkey), 2 intermediate pigging stations, 1 pressure reduction station and 101 small block valves.

The transmission pipeline features high quality continuous buried pipes. Unlike water pipelines, which are generally constructed as segmented pipes, the continuous steel pipelines are more likely to suffer damage due to permanent fault displacements (PFDs) rather than ground strains caused by seismic wave propagation. Therefore, the fault displacement (offset) induced by earthquakes is defined as the target hazard. Five main pipe-fault crossing locations are identified along the BTC route for PFD hazard. The hazard information (e.g. fault name, fault length, style-of-faulting, fault geometry, etc.) as well as normalized locations of pipe-fault crossings (l/L, as referred to STREST D6.1 Pitilakis et al 2016), pipe-fault crossing angles, etc. are collected at these pipe-fault intersections. The pipe cross sections at these five locations have the same pipe diameter (42 inches or 1.0688m) and the same thickness (20.62mm). The mechanical properties of the pipe and the soil conditions surrounding the pipe at the fault-pipe intersections of interest are also identified as part of data collection phase because they are essential for the calculation of pipeline strains.

The pipeline rupture or loss of pressure integrity (pipeline failure) along BTC pipeline due to fault offsets is identified as the risk measure. The risk objectives of the BTC pipeline are determined from the *Guidelines for the Seismic Evaluation and Upgrade of Water Transmission Facilities* (Eidinger and Avila 1999). In reference to the risk grading system proposed in STREST D5.1 (Esposito et al. 2016), pipeline failure at different probabilities under 2475-year PFD are defined as the risk objective.

In the test set-up phase, the STREST Level 1a (ST-L1) is selected as the component-based risk assessment. Level 2a (ST-L2a) is selected at the system level. The penalties in the stress tests (Pitilakis et al. 2016) due to modelling deficiencies of pipeline are disregarded at all levels. Modelling uncertainties (fault mapping accuracy and fault complexity) affecting the seismic hazard are accounted for during the computation of probabilistic PFD.

5.2 Phase 2: Assessment phase

The assessment phase comprises of two main steps: component level assessment (ST-L1) and system level assessment (ST-L2). The component level assessment considers hazard-based (ST-L1a) and design-based (ST-L1b) levels whereas risk-based assessment (ST-L2a) is done at the system level.

In the hazard-based assessment, the 2475-year fault displacements at five pipe-fault crossings are computed from the Monte-Carlo based probabilistic PFD hazard (Pitilakis et al 2016) and are compared with the prescribed ALA (2001, 2005) hazard requirements. The 2475-year PFD hazard level is the recommended hazard level for continuous pipelines by the pipe seismic design provisions in ALA (2001, 2005). The comparisons indicate that of the five pipe-fault crossings, the computed 2475-year PFD hazard at #2, #3 and #4 pipe-fault crossings are larger than the ALA requirements (Pitilakis et al 2016). On the other hand, the computed 2475-year PFD hazard at #1 and #5 pipe-fault crossing are in compliance with the ALA requirements.

The tensile pipe strain under the computed 2475-year PFD (design level PFD for pipeline) is compared with the allowable tensile pipeline strain provided in ALA seismic guidelines (2001, 2005). The allowable tensile pipe strain is designated as 3% in the ALA seismic pipeline design provisions (2001, 2005). The comparisons are done for all five pipe-fault crossings and the tensile strains at these pipe-fault crossings comply with the code requirements (Pitilakis et al 2016).

In the risk-based assessment at system level, the seismic risk of pipeline failure is evaluated by comparing the annual exceedance rate of pipeline failure with the suggested allowable pipeline failure rates in the literature.

The probabilistic pipeline seismic risk against fault rupture is achieved by integrating the probabilistic fault displacement hazard, mechanical response of pipe due to fault displacement and empirical pipe fragility function (Cheng and Akkar 2016). The concept is similar to the conventional probabilistic seismic risk assessment (McGuire 2004). Since both tensile and compressive strains developed along the pipe during an earthquake can cause pipe failure, the seismic risk of pipe failure should consider the aggregated effects of these two strain components. The formula to calculate the seismic risk are proposed and is given in STREST D6.1 (Pitilakis et al 2016). The annual failure probability (P_f) for pipelines at fault crossings is computed for different pipe-fault crossing angles, i.e.,α, associated with the uncertainty over α to manifest the inherent complications during the fault rupture process. The inaccuracy in fault-pipe crossing angle is modelled by a truncated normal probability with alternative standard deviations of 2.5° and 5°.

The literature is limited in addressing the expected performance of steel pipelines transmitting gas or oil under extreme events. Honegger and Wijewickreme (2013) suggest annual failure rates less than 1/24750 (4.04E-5) as the acceptable rates for pipelines under seismic loading. The same limit is also used in the current US building standards (ASCE 2010) as the target annual probability against building collapse under earthquake-induced loads. We also used the same annual failure rate for probabilistic risk-based pipeline assessment at the five designated pipe-fault crossings (STREST D6.1; Pitilakis et al 2016). The comparisons of allowable annual pipe failure rate (4.04E-5) with those calculated at each fault pipe-fault crossing indicate that pipe-fault crossings #3 and #4 are not safe as their computed failure rates are larger than the allowable annual failure rate. The hazard at these fault crossings is relatively higher with respect to the other three pipe-fault crossings that might explain the higher failure rates (STREST D6.1; Pitilakis et al 2016). The pipe-fault crossing angles are low at these pipe-fault crossings that also make the pipe segments more vulnerable to the accumulation of tensile strains.

The pipeline annual failure rates at the five pipe-fault crossings are used to compute the aggregated failure risk along the whole BTC pipeline to complete the probabilistic risk assessment at system level (ST-L2). To this end, two marginal probabilities are computed: (a) perfect correlation between pipe failures at the five pipe-fault crossings (P_{fc}) and (b) independent pipe failures at the five pipe-fault crossings (P_{fi}). The aggregated risk is defined as the annual exceedance probability of the pipeline failure (P_f).

Using the theory described in STREST D6.1 (Pitilakis et al 2016), the aggregated marginal failure probabilities of BTC pipeline (i.e., perfect correlation and independent failures) exposed to 2475-year PFD hazard are very high. The computed failure probabilities range between 40% to 50% (see details in Pitilakis et al 2016). According to the grading system in Esposito et al (2016), the pipeline risk in the project falls in to Grade B: *possibly unjustifiable risk*. These calculations conclude that there is a need of retrofitting the pipes at pipe-fault crossings.

5.3 Phase 3: Decision phase

The probabilistic pipe failure risk assessment yield higher probabilities of pipe failure at #3 and #4 pipe-fault crossings. Therefore, the pipeline segments at #3 and #4 pipe-fault crossings are identified as critical components to the aggregated BTC pipeline failure risk. Thus, these pipe segments are selected to be retrofitted. We also decided to reconsider the pipe-fault crossing angle uncertainty at pipe-fault intersection #5. Pipeline under compression would result in larger damage when pipe-fault crossing angle is

larger than 90°, which might be the case under the consideration of pipe-fault crossing angle uncertainty at intersection #5.

The effective retrofitting of the pipeline segments at these three pipe-fault crossings is to change the pipe-fault intersection angle. Therefore, in the risk mitigation strategies, we change the intersection angles of all these three pipe-fault intersection angles to around 80°. The resulting aggregated risk probability of the BTC pipeline failure due to fault displacement is given in Table 5.1. The reduction in pipeline failure risk is evident when compared to the current pipe failure probability that is around 40% to 50%. Considering the marginal correlations of the pipe failure risk at each fault crossing, the probability of BTC pipeline failure due to fault offset is at the most ~2% under 2475-year PFD. According to the grading system proposed in the stress test, the BTC pipeline risk after the proposed mitigation strategy is Grade AA: negligible.

Table 5.1 Aggregated failure probability of BTC pipeline under 2475-year PFD hazard before and after the risk mitigation strategies

	P_{fc} (perfectly correlated case)	**P_{fi} (statistically independent case)**
Before retrofit	38.56%	51%
After retrofit	0.775%	2.206%

5.4 Phase 4: Report phase

The outcomes of the stress test for BTC pipeline are presented to the CI authorities and the regulator. The presentation is organized and performed by the Project Manager (PM) and Technical Integrator (TI). The followings brief the main contents of the presentation.

The seismic risk of BTC pipeline at the fault crossings is graded as B at the system level assessment, according to the grading system for the global outcome of the stress test (as shown in Fig. 2.3). Grade B is defined as "possibly unjustifiable risk". All five fault crossings contribute to this risk but the #3 and #4 fault crossings that are located on the North Anatolian fault zone and Deliler fault zone are identified as the critical components. As pipe-fault crossing angle is an important parameter in pipeline risk mitigation imposed by permanent fault offsets, the proposed plan is to change the pipe-fault intersection angle at the most critical pipe-fault crossings. In essence, the pipe segments at the fault crossings #3, #4 and #5 are decided to be retrofitted by changing their pipe-fault intersection angles from 30°, 40°, and 90° to 80°. Note that the pipe segment at the intersection #5 with the design pipe-fault crossing angle (α) of 90° is changed to 80° to consider the uncertainty in α due to fault mapping inaccuracy. A small deviation in α arising from the modelling deficiency of mapped faults may result in pipe-fault crossings larger than 90° that would yield critical compressive strains at the pipe cross-section. The change in α at the fault crossings #3, #4 and #5 marks the risk grade as AA that corresponds to "negligible" risk in the BTC pipeline.

6. Application of stress test concepts to Gasunie national gas storage and distribution network, Holland

6.1 Introduction

The Groningen field is a large natural gas field located in the northern Netherlands, contributing to approximately half of the natural gas production in the Netherlands. On- and offshore natural gas production and distribution is the key component of the national energy supply in the Netherlands. The gas distribution relies on a major gas pipeline infrastructure, with a total length of over 12000 km of installed pipes in. The production from the Groningen field and other natural gas fields mostly located in the north east part of the country supply the Dutch economy and major export across Europe, via cross-border long distance gas pipelines (European Natural Gas Round-About).

Located in an area of very low tectonic seismicity, gas extraction in the region has led to an increase in seismicity since the early 1990s and in particular after 2003. Initially, this increase, including the 2006 earthquake near Westeremden with a magnitude M_L = 3.4 was considered to be a statistical variation within the uncertainty range of the measurements. A renewed focus on the issue of seismicity induced by gas production in Groningen started in 2012 triggered by the earthquake near Huizinge (16th August 2012) with magnitude M_L=3.6. It was felt as more intense and with a longer duration than previous earthquakes in that area and significantly more building damage was reported as a result of this earthquake. It materialized into the realization that over the past few years seismicity in the Groningen area had increased beyond statistical variation. It was realized that the earthquakes could pose a potential safety risk (WINN_TA-NAM 2016).

The current chapter describes the application of the stress test methodology to part of the main gas distribution network of Gasunie Gas Transport Services (Gasunie-GTS). The case consists of a distributed and geographically extended infrastructure with potentially high economic and environmental impact.

6.2 Phase 1: Pre-assessment phase

6.2.1 Data collection

For the case study, a sub-network is selected located in the induced earthquake prone area, directly above the main gas field (Fig. 6.1). The sub-network selected covers an area of approximately 3360 km^2. It contains 4 MPa (40 bar) to 8 MPa (80 bar) main gas transmission pipes, with a total length in the order of 1000 km. Different pipe diameters are present within this sub-network ranging from 114 millimetres (4 in) to 1219 mm (48 in). Apart from 426 valve stations, it contains compressor stations, measure and regulations stations, reducing stations and a mixing station (11 in total). With respect to the end nodes of the sub-network: 15 feeding stations and 91 receiving stations are accounted for, the latter being sub-divided into approximately 40 industrial, 50 municipal and 1 export.

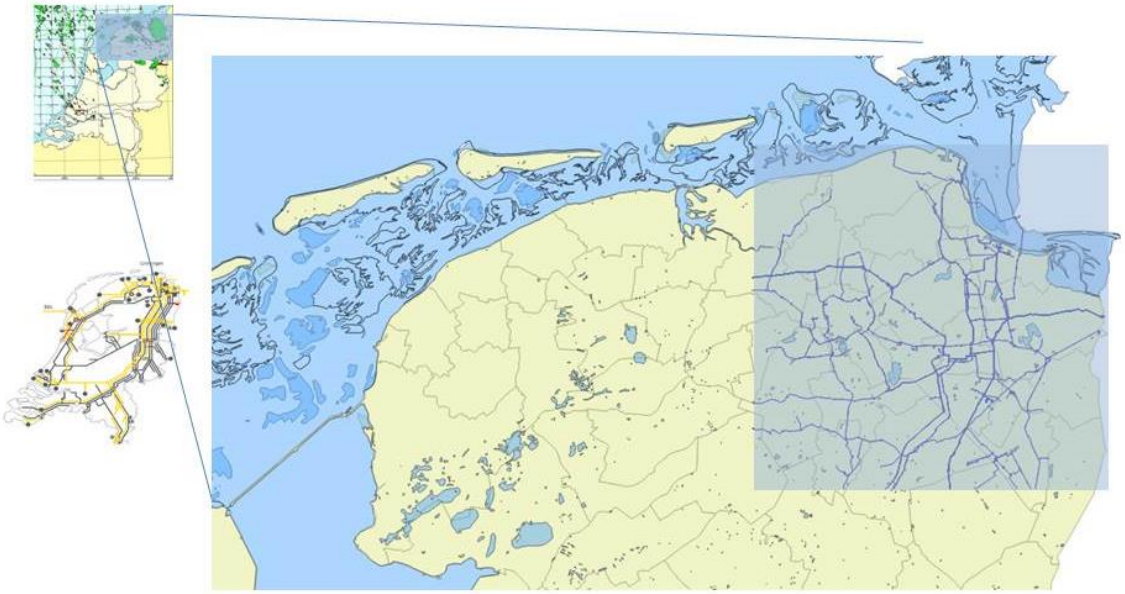

Fig. 6.1 Selected sub system of the gas distribution network (right) located above main natural gas field (top left)

GIS databases were obtained from Gasunie-GTS with properties of the pipeline system: coordinates, diameter, wall-thickness, material, yield stress, maximum operational pressure and depth of soil cover. As the database originally contained 6378 unique valued combinations of diameter, wall-thickness, yield stress and pressure, these properties were first classified into groups in order to reduce the number of unique sets. This resulted in 136 different pipe configurations composed out of the following values:

- 12 diameter values: from 114 to 1219 mm;
- 39 wall thicknesses: from 4 to 31.5 mm;
- 5 yield strength values: from 241 to 483 MPa;
- 3 operational pressures: 40, 66 and 80 bar.

An example of the modelled network layout, showing different pipe diameters is presented in Fig. 6.2.

Fig. 6.3 shows the locations and types of stations that are included in the network modelled. Apart from source and demand stations as end nodes, in between nodes are shown and labelled as M&R (measure and regulation stations). Although labelled only as M&R, they in fact stand for compressor stations, measure and regulations stations, reducing stations or a mixing station. Values next to these stations indicate the number of pipes that are connected to the site of the station.

The target hazard is the seismic hazard as a result of the gas extraction from the Groningen gas field. Numerous studies have been performed over the past several years and are still on-going leading to more and more refined models dedicated to the Groningen area. In the current stress test one of the earlier versions is being adopted. The seismic model adopted consists of the following:

Seismic zonation: The so-called Z1 model from Dost et al (2013) dividing the area in 4 zones.

Ground motion prediction equation (GMPE): The Akkar et al (2014) modified GMPE model (Bommer 2013).

Magnitude distribution: The classical Gutenberg-Richter (GR) relation.

Maximum magnitude: In the context of the stress test analysis, a value of 6.0 is applied, although ongoing studies indicate a value of 5.

Annual event rate: The annual event rate for events with M≥1.5 is set to 30 events per year (Dost et al 2013), although current studies tend to a value of 23.

The zonation and corresponding values for the magnitude and frequency distributions are shown in Fig. 6.4 and Table 6.1.

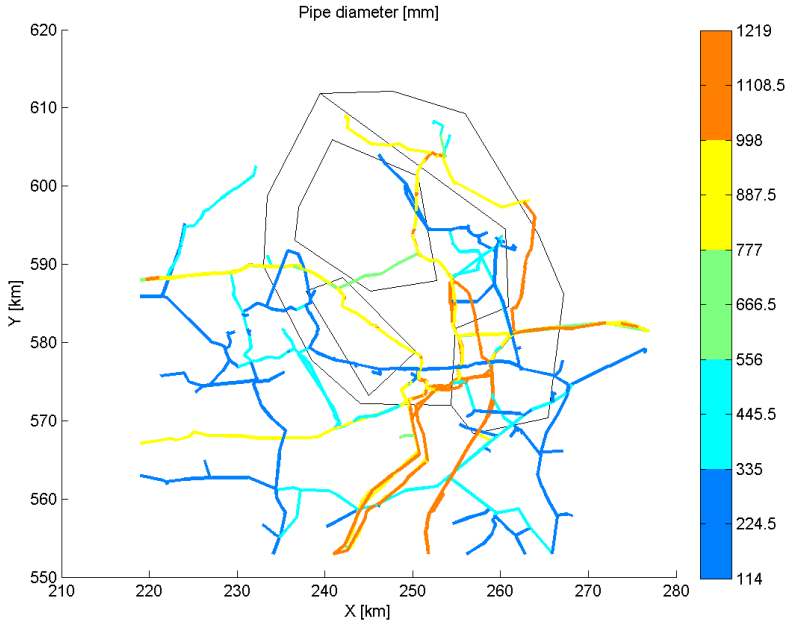

Fig. 6.2 Distribution of pipe diameters (mm) present in the modelled sub network (black lines on background indicate the earthquake zones)

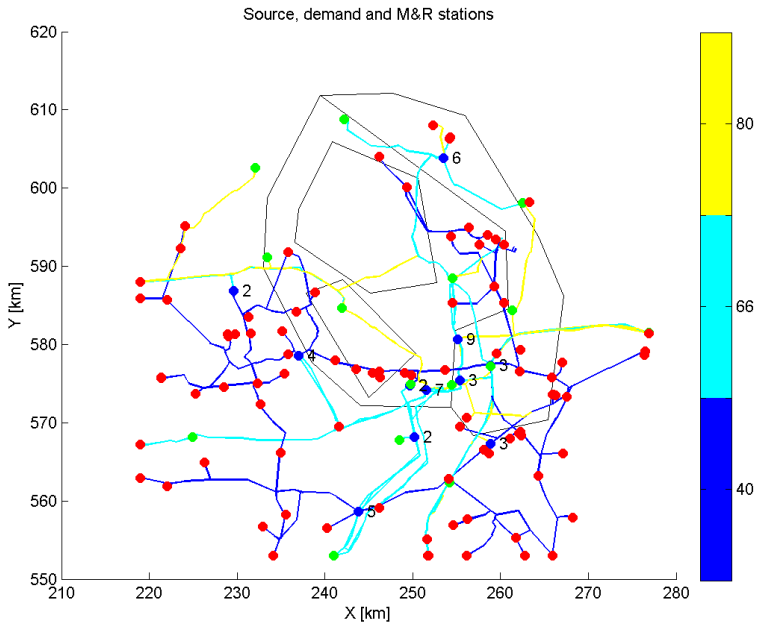

Fig. 6.3 Locations of stations in the modelled sub network: source stations (green) demand stations (red) and M&R stations (blue). Pipeline colours and colour bar refer to the pressures ([bar]) in the pipe sections

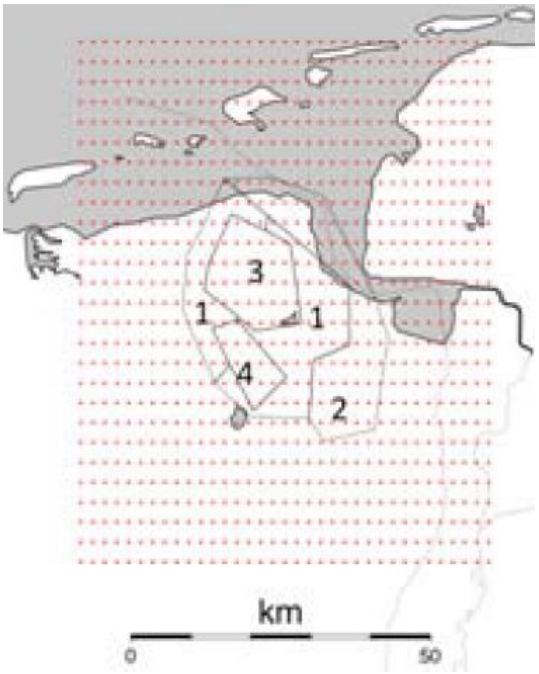

Fig. 6.4 Division of Groningen area in seismic zones (Dost et al 2013)

Table 6.1 Gutenberg-Richter parameters (Dost et al 2013)

Zone Number	Description	a	b	M_{min}-M_{max}
1	Background	0.364	1	1.5-6
2	Eastern block	0.017	1	1.5-6
3	Central North	0.498	0.8	1.5-6
4	Central South	0.121	1	1.5-6

6.2.2 Risk measures and objectives

Serviceability Ratio (*SR*) and Connectivity Loss (*CL*) are used as risk measures (Esposito 2011).

The Serviceability Ratio (*SR*) is directly related to the number of demand nodes (*n*) in the utility network, which remain accessible from at least one source node following an earthquake. It is computed according to Eq. 6.1:

$$SR = \frac{\sum_{i=1}^{n} w_i X_i}{\sum_{i=1}^{n} w_i} \tag{6.1}$$

In which X_i represents the functionality of facility (demand node) i, which is modelled as the outcome of a Bernoulli trial (X_i = 1 if the facility is accessible from at least one supply facility or source node), and w_i is a weighting factor assigned to demand node i.

Connectivity Loss (*CL*) measures the average reduction in the ability of endpoints to receive flow from sources counting the number of the sources connected to the *i*-th demand node in the original (undamaged) network ($N^i_{source,orig}$) and then in the possible damaged network ($N^i_{source,dam}$) after an earthquake event. It is expressed by the following equation:

$$CL = 1 - \left\langle \frac{N^i_{source,dam}}{N^i_{source,orig}} \right\rangle \tag{6.2}$$

where () denotes averaging over all demand nodes.

An as low as reasonable practicable (ALARP) grade of the risk measures is targeted for the existing gas transport network to pass the stress test (Jonkman et al 2003).

In the Netherlands a standard for quantified risk assessment (QRA) exists, known as "the coloured books". They were issued by the national "Committee for the Prevention of Disasters" (CPR) and describe the methods to be used for modelling and quantifying the risks associated with dangerous materials (CPR 18E, 1999). Installations, types and frequencies of loss of containment (LOC), calculation methods, risk acceptance criteria and even the computer program to use are prescribed.

Currently the computer program CAROLA (CAROLA, 2010) is used for these calculations in the Netherlands, which is based on PIPESAFE (Acton et al, 2002).

In the current application of the stress test methodology to the Gasunie-GTS case, no full QRA was performed for the 1000 km sub-network. However, values for the annual failure rates originally prescribed in the purple book (CPR 18E, 1999) and adjusted values nowadays used for the Gasunie network in CAROLA are selected to define grade boundaries (Table 6.2).

Table 6.2 Grading boundaries (failure frequencies) for stations and pipe sections

Boundary	Pipe [$yr^{-1}km^{-1}$]	Station [yr^{-1}]
AA-A	8 10-6	8 10-6
A-B	6 10-5	6 10-5
B-C	1.4 10-4	1.4 10-4

Using these boundary values for the grading system enables the asset owner Gasunie-GST to relate the outcome of the stress test to his own QRA's as performed with CAROLA with non-earthquake related failure frequencies.

For illustrative purposes only, indicative grading boundaries are attributed to the values of the performance parameter connectivity loss (CL). The boundaries used are taken from Esposito et al (2016b). No actual calibrations for these bounds with respect to economic loss or fatalities exist yet for the sub-network at hand and the grading is indicative and provisional.

6.2.3 Set-up of the stress test

In the Gasunie case the Stress Test has been performed up till level ST-L2a with the earthquakes as single hazard.

ST-L1 considers individual components. A risk based approach is applied for individual stations and pipe segments making use of the ST-L2a results.

For Level ST-L2a a full Probabilistic Risk Analysis using Monte Carlo simulations is performed for the network analysis.

No scenario-based assessments are performed on component or network level.

Accuracy levels targeted are classified as Advanced. Detailed information and advanced methods are being used in the stress test. The method adopted for the component level assessment is risk-based while the System level is performed according to the performance-based earthquake engineering (PBEE) framework (Weatherill et al 2014). Site specific hazard analyses are being performed and structure specific fragility functions being used. Although the team performing the Stress test did not actively participate themselves in the on-going research into the man induced seismicity in the Groningen area, use is made of the outcomes of these studies by, among others, the NAM, KNMI, TNO and Deltares as well as by an international community of experts (WINN_TA-NAM 2016).

6.3 Phase 2: Assessment phase

6.3.1 Component level assessment (ST-L1a)

Sampled results (failure, no failure) per component from the Mont Carlo analysis of the network analysis are used to calculate annual failure frequencies for pipes and stations.

For the pipe sections the resulting values are presented as a contour plot in Fig. 6.5 whereas corresponding values for the stations are shown in Fig. 6.6.

6.3.2 System level assessment for single hazard (ST-L2a)

The methodology for the evaluation of seismic performance of the network under study consists of five major steps:

- Seismic hazard assessment of the region considering gas depletion as source of the seismic activities.
- Evaluation of the PGA, PGV and displacement (liquefaction) hazard, in order to estimate the seismic demand.
- Seismic demand evaluation at each facility and the pipe sections within the network to obtain the failure probability using appropriate fragility curves.
- Vulnerability analysis through the use of a connectivity algorithm to integrate the damage of facilities and pipe sections into the damage of the system.
- Probabilistic risk assessment of the case study using Monte Carlo simulation in terms of mean functionality and annual exceedance curve.

OOFIMS software was used as a basis, kindly provided by the Sapienza - University of Rome, Dept. of Structural & Geotechnical Engineering (Franchin et al 2011). A new class for modelling the gas network was added for this study.

Fragility functions

The probabilities of soil liquefaction as a function of PGA values

The probability of soil liquefaction was investigated for soil conditions in the Groningen Area. The study is based on the Idriss-Boulanger model (Idriss and Boulanger 2008) and is described in more detail in (Miraglia et al 2015). Two soil profiles based on CPT tests were analysed by describing the soil properties as stochastic parameters and sampling the liquefaction response of the layers with earthquake events. The sampling results eventually were summarized as a fragility curve as a function of PGA values (see Fig. 6.7).

The probability of pipe failure, given soil liquefaction occurred (permanent seismic load effects)

Soil liquefaction can cause permanent displacements, expressing themselves in lateral displacements and or settlements. Besides that, depending on the weight of the pipe segments relative to the volumetric weight of the liquefied soil, pipe segments will start floating or sinking due to gravity. From these three aspects only the latter is considered: substantial lateral spread is not expected in the flat Groningen area, settlements are assumed to be confined to dozens of centimetres, whereas uplift due to buoyancy can reach the value of the soil cover depth.

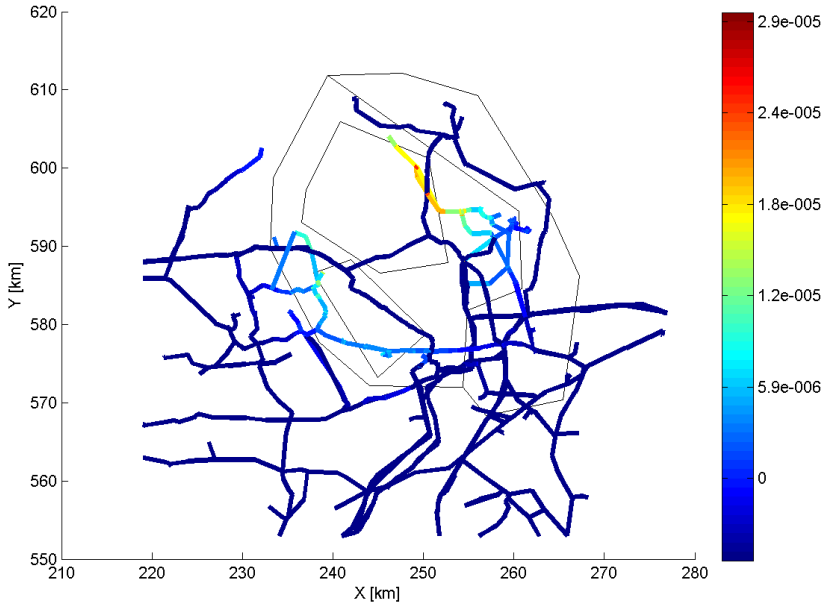

Fig. 6.5 ST-L1a: annual failure frequencies (per km) for the pipe sections

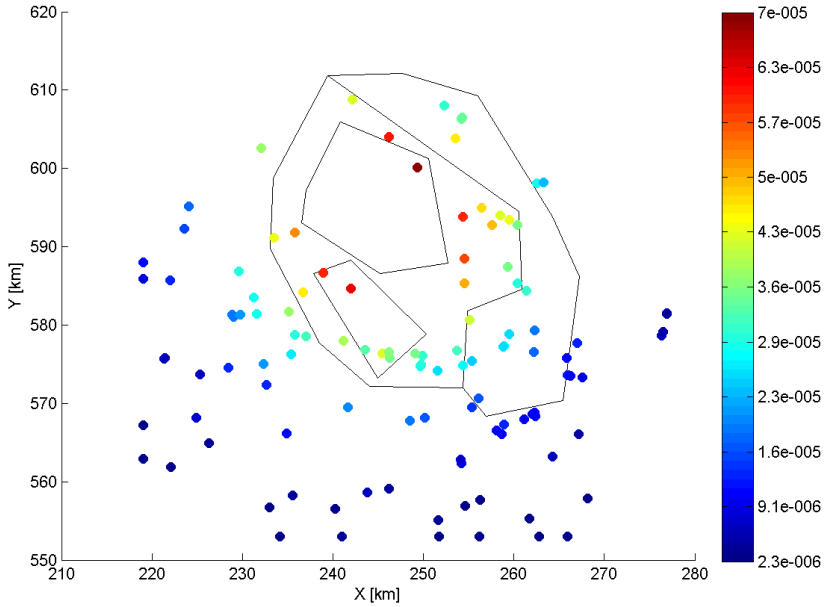

Fig. 6.6 ST-L1a: annual failure frequencies for the stations

Structural reliability calculations are performed for each of the 136 pipe configurations (distinct sets of values for diameter, wall thickness, yield stress and gas pressure). In these calculations the pipe properties are treated as stochastic variables. The limit state function is formulated as the von Mises stress due to gas pressure as well as bending due to uplift against the yield stress. The bending stress due to uplift was calculated in a mechanical model in which the pipe is embedded in stiff soil at its endings and is allowed to uplift towards ground level. The length of the pipe in liquefied soil is adjusted during the limit state evaluations such that this maximum value (cover depth) is reached. Gas pressure is modelled as a normal distribution with a 10% coefficient of variation. Diameter, wall thickness and yield stress are log-normally distributed with variation

coefficients of respectively 3, 3 and 7 %. Finally, also the soil cover depth is modelled stochastically: normal distributed with a mean value of 1.5 m and 20% coefficient of variation. FORM analyses were performed for each situation (pipe configuration) and reliability indices (β) are calculated as a proxy for the probability of failure given liquefied soil. Fig. 6.8 graphically depicts the distribution of the different values found for the different pipe sections.

Length effects of liquefaction-related pipe failure will, in the OOFIMS tool, be taken into account by assuming a correlation length of 200 m along the pipe.

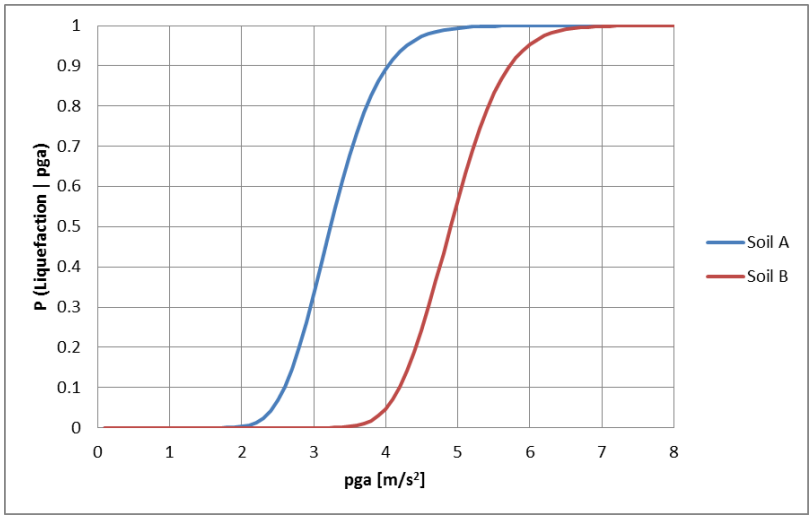

Fig. 6.7 Soil liquefaction fragilities of two soil profiles in the Groningen area (Miraglia et al 2015)

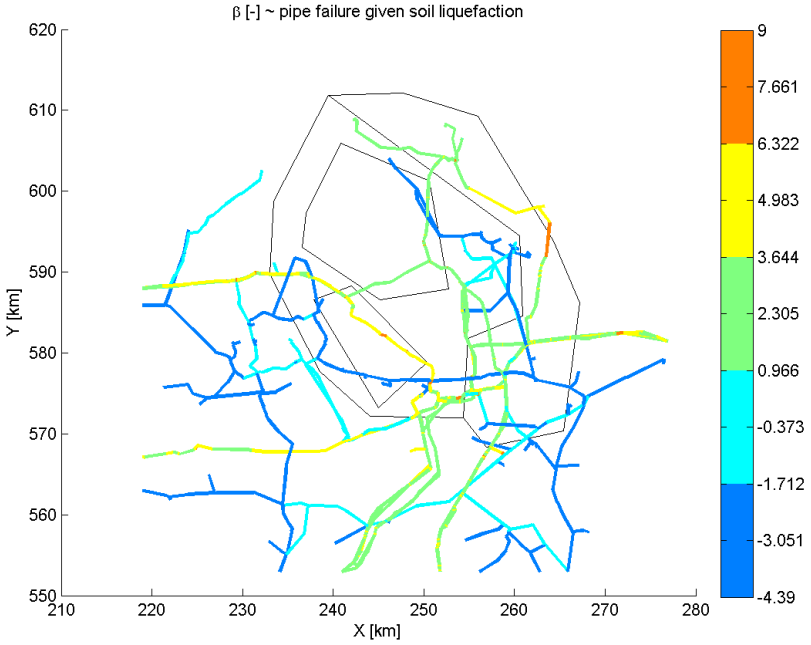

Fig. 6.8 Distribution of reliability indices for failure due to soil liquefaction for different pipe sections

The probability of pipe failure as a function of PGV values (transient seismic load effects)

For transient load effects structural reliability calculations are performed for different pipe geometries with a limit state based on Newmark's shear wave formulae of seismic strain for buried pipelines. In addition stresses due to gas pressure and due to initial curvatures in the pipeline stretches are accounted for. The same stochastic parameters as above are used for diameter, wall thickness, pressure and yield stress are used. The curvature is modelled as a lognormal distribution with mean 2000 m and 100 m standard deviation. In addition the shear wave velocity V_{s30} is modelled as a lognormal stochastic variable having a mean of 200 m/s and a standard deviation 20 m/s.

Again, FORM analyses were performed for each situation (pipe configuration) with different values of seismic load PGV. Thus fragility curves are derived which are presented in Fig. 6.9. In this figure also a fragility curve from Lanzano et al (2013) is presented for reference. It shows the current fragility curves to be on the conservative side.

Length effects of transient loading related pipe failure are modelled by implementing a repair rate model according to ALA (2001):

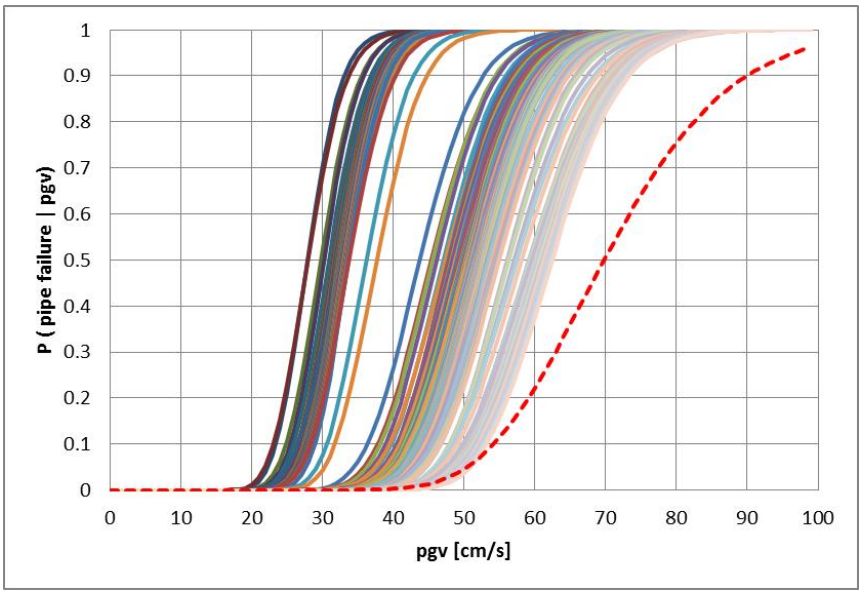

Fig. 6.9 Calculated pipe fragilities with respect to transient seismic load effects. Different solid lines correspond to different pipe properties. The red dotted line is taken from Lanzano et al (2013)

The probability of station failure as a function of PGA values

For the stations existing fragility curves have been selected (NIBS, 2004). The one selected corresponds to a moderate damage state and is described as a lognormal cumulative distribution with a mean of 2.4 m/s2 and a coefficient of variation of 60%. The moderate damage state is selected as it is the first damage state with such malfunctioning that it leads to connectivity loss and a decrease in serviceability ratio. Besides this, the station types vary between compressor stations, measure and regulations stations, reducing stations or a mixing station. All with different mechanical and or electrical components and some sheltered in one story masonry buildings and others in open air. Choosing the moderate damage state is partly motivated by selecting a conservative envelope for all types.

Probabilistic risk assessment

Seismicity, network, and network properties are modelled with the OOFIMS tool and Monte Carlo simulations are performed. Network performance in terms of connectivity loss (CL) and serviceability ratio (SR) were defined as the primary indicators in the stress test.

Fig. 6.10 (top graph) shows the performance of the network in terms of the annual probability of exceedance for the connectivity loss (CL). The results show a good performance with respect to CL: the annual probability of having a connectively loss of e.g. 50% or more is 3.6 10^{-5}.

Annual exceedance frequencies for the serviceability ratio (SR) are presented in the bottom graph of Fig. 6.10. It shows very high exceedance frequencies for all values of the serviceability ratio, with only a drop at the very end of the horizontal axis near SR reaching one. Hence it shows a high robustness of the network, indicating a vast redundancy in possible paths between demand and source nodes.

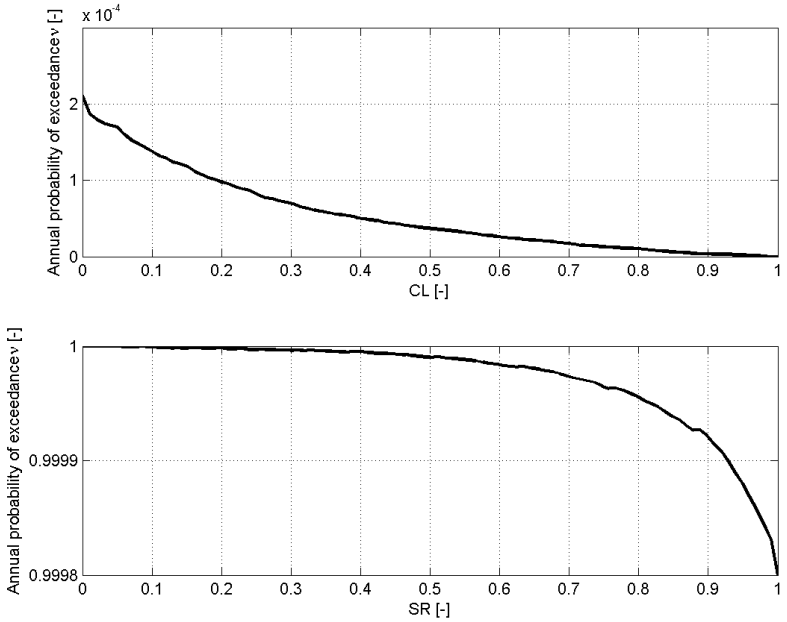

Fig. 6.10 Annual probability of exceedance for network connectivity loss *CL* (top) and network serviceability rate *SR* (bottom)

6.4 Phase 3: Decision phase

6.4.1 Risk objectives check

An "as low as reasonable practicable (ALARP)" grade of the risk was targeted for the gas transport network to pass the stress test.

With the component results from section 6.3.1 and the grading boundaries from section 6.2.2, the following results are obtained for the pipe sections and the stations:

- Pipe sections: Most pipe sections obtain grade AA, some obtain grade A. The pipe sections pass the stress test.
- Stations: Most stations are classified with grade AA or A. Some, near or within the seismic zone, obtain grade B. The stations partly pass the stress test.

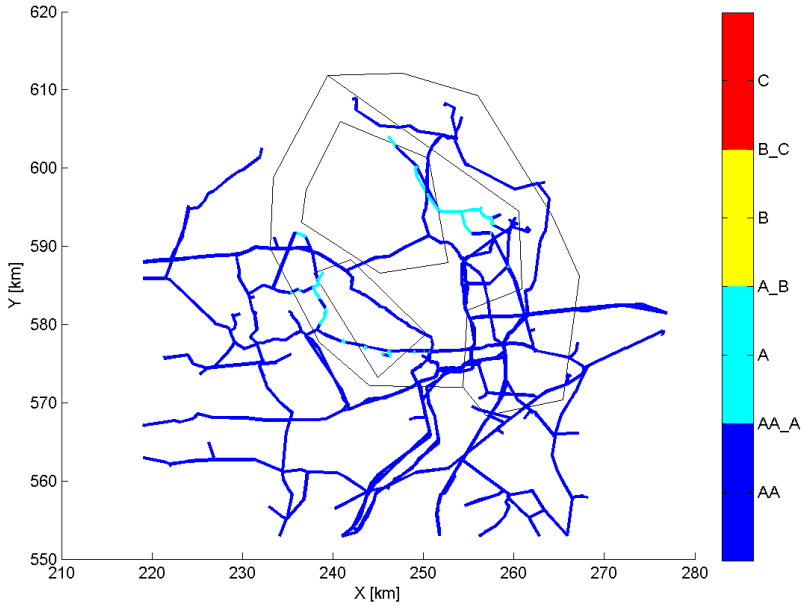

Fig. 6.11 Obtained grading for the individual pipelines (M_{max} = 6; annual rate =30)

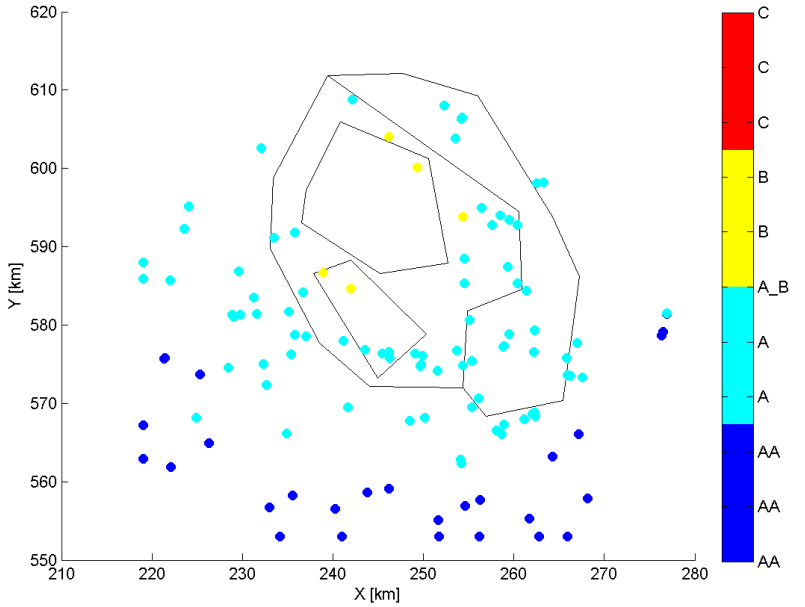

Fig. 6.12 Obtained grading for the stations (M_{max} = 6; annual rate =30)

The grading results for pip segments and stations are presented in Fig. 6.11 and Fig. 6.12.

Fig. 6.13 presents the values for the connectivity loss relative to the indicative grading boundaries. The network performance complies with grade AA and passes the stress test.

These findings are obtained despite a number of conservative assumptions made with respect to fragilities. Also the seismic demand was modelled in a conservative way with a maximum magnitude of 6 and a b-value of 0.8 for seismic zone 3 in the Gutenberg-Richter model.

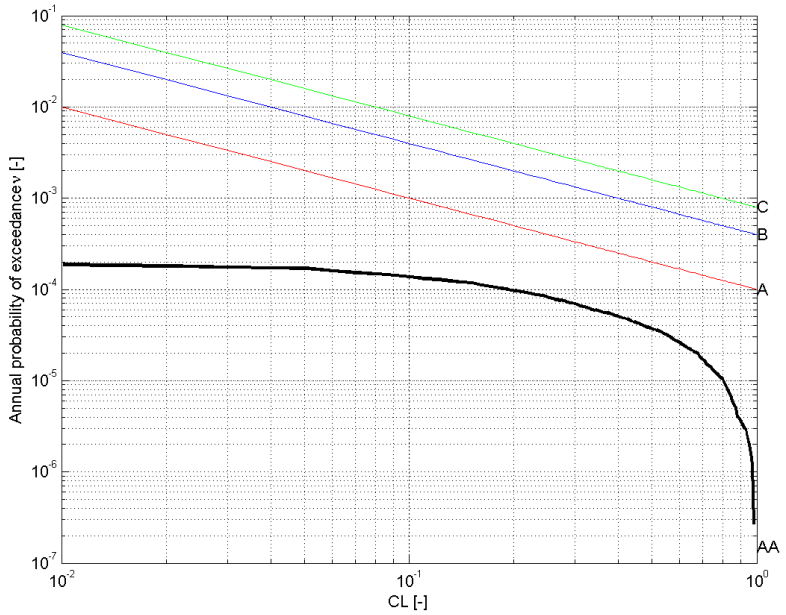

Fig. 6.13 Exceedance frequencies for connectivity loss relative to (indicative) grading boundaries.

6.4.2 Disaggregation/sensitivity analysis

Disaggregation analyses were performed with respect to seismic events (magnitudes and zones), pipe components and stations.

First network performance losses (CL>0.1) are found from M>3.5 onwards and for extreme values of performance losses (CL>0.9) a substantial contribution from seismic zone 4 is observed.

Pipe sections, which have a major contribution to performance loss, were identified by selecting events with a low performance loss (CL<=0.1). Specific pipe sections to the South-West and North-East of seismic zone 3 were localized.

As all stations are modelled with the same fragility functions the only discriminate factor in selecting the most vulnerable ones would be their distance with respect to possible seismic sources, see Fig. 6.6. Combined with the number of pipe connections at the corresponding interconnecting stations as shown in Fig. 6.3 their possible contribution to the network performance loss can be identified.

With respect to sensitivity analysis the impact on network performance of the maximum event magnitude as well as the impact of the value for the annual event rate was investigated.

With respect to the component grading it holds that confining the maximum events to M=5 leads to all stations being in either grade A or AA. Likewise, when the annual rate is set to 23 per year, no more stations being in state are found.

6.4.3 Guidelines and critical events

With respect to the network as a whole, a strong redundancy in the paths from demand to source nodes is taken into account. This is a strong feature for obtaining the stress test results.

With respect to components, both types (pipe sections and stations) are found to contribute evenly to the network performance indicators as can also be concluded from the component level assessments. From these:

- Specific pipe sections can to some extend be identified as being a weakest link in the network. These sections should be checked on their current actual state assessing the need for upgrading.
- For the stations a rather strong assumption is made with respect to the fragility curve adopted. These should be quantified in more detail and depending to findings retrofitting of stations might be necessary.

In the current analysis soil liquefaction is the dominant failure mechanism. As much uncertainty still exists in the liquefaction fragilities for the Groningen area, further studies into these fragilities and their geographical distribution is recommended.

6.5 Phase 4: Report phase

The stress test is performed as being initiated by the asset owner, the Gasunie-GTS.

Reporting, in terms of the grade, the critical events, the guidelines for risk mitigation, and the accuracy of the methods adopted in the stress test is accomplished by the current report.

In summary the stress test results are presented in Table 6.3.

Table 6.3 Stress test results for Gasunie-GTS sub-network

Item	M_{max}	$N_{M>1.6}$	Grading	Result
Pipes sections	6	30	AA, A	Pass
	6	30	AA, A, B	Partly pass
Stations	*5*	30	AA, A	Pass
	6	*23*	AA, A	Pass
Network *CL*	6	30	AA	Pass

In addition to this report, a presentation will be given at the Gasunie-GTS.

Hence, no formal presentation of the outcome of the stress test to (other) CI authorities and/or regulators is foreseen.

7. Application of stress test concepts to port infrastructures of Thessaloniki, Greece

ST@STREST is applied and tested in the port of Thessaloniki, one of the most important ports in Southeast Europe and the largest transit-trade port in Greece, a characteristic example of distributed and/or geographically extended infrastructures with potentially high economic and environmental impact. The port occupies a total space of 1.5 million m2, includes 6 piers spreading on a 6200 m long quay and a sea depth down to 12 m, with open and indoors storage areas, suitable for servicing all types of cargo and passenger traffic. The port also has installations for liquid fuel storage, while is located in proximity to the international natural-gas pipeline and is linked to the national and international road and railway network (www.thpa.gr). The goal of this study is to apply the ST@STREST framework to the port infrastructures exposed to different seismic hazards i.e. ground shaking, liquefaction and tsunami. The framework consists of four phases: Pre-Assessment, Assessment, Decision and Report phase, which are performed in sequence. Each phase is subdivided in a number of specific steps (Fig. 7.1).

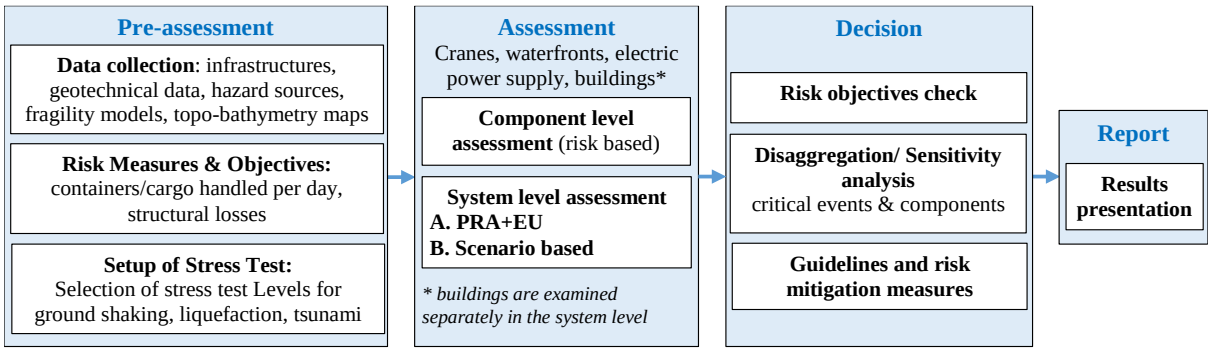

Fig. 7.1 Flowchart of the ST@STREST framework for the stress test application in the port of Thessaloniki

7.1 Phase 1: Pre-assessment phase

7.1.1 Data collection

A GIS database for the port facilities was developed by the Research Unit of Soil Dynamics and Geotechnical Earthquake Engineering (SDGEE, sdgee.civil.auth.gr) at Aristotle University of Thessaloniki in collaboration with the port Authority in the framework of previous national and European projects and it is further updated in STREST project (www.strest-eu.org). Waterfront structures, cargo handling equipment, buildings (offices, sheds, warehouses etc.) and the electric power supply system are examined (Fig. 7.2). The SYNER-G (www.syner-g.eu, Pitilakis et al 2014a) taxonomy is used to describe the different typologies. Waterfront structures include concrete gravity block type quay walls with simple surface foundation and non-anchored components. Cargo handling equipment has non-anchored components without backup power supply. Four gantry cranes are used for container loading-unloading services located in the western part of the 6th pier. The electric power supply to the cranes is assumed to be provided through non-vulnerable lines from the distribution substations that are present inside the port facilities. They are classified as low-voltage substations, with non-anchored components. In total, 85 building and storage facilities are considered in the analyses. The majority is reinforced concrete (RC) buildings comprising principally of low- and mid-rise infilled frame and dual systems with low or no seismic design. The steel buildings are basically warehouses with one or two floors while the unreinforced masonry (URM) buildings are old low-rise and mid-rise structures.

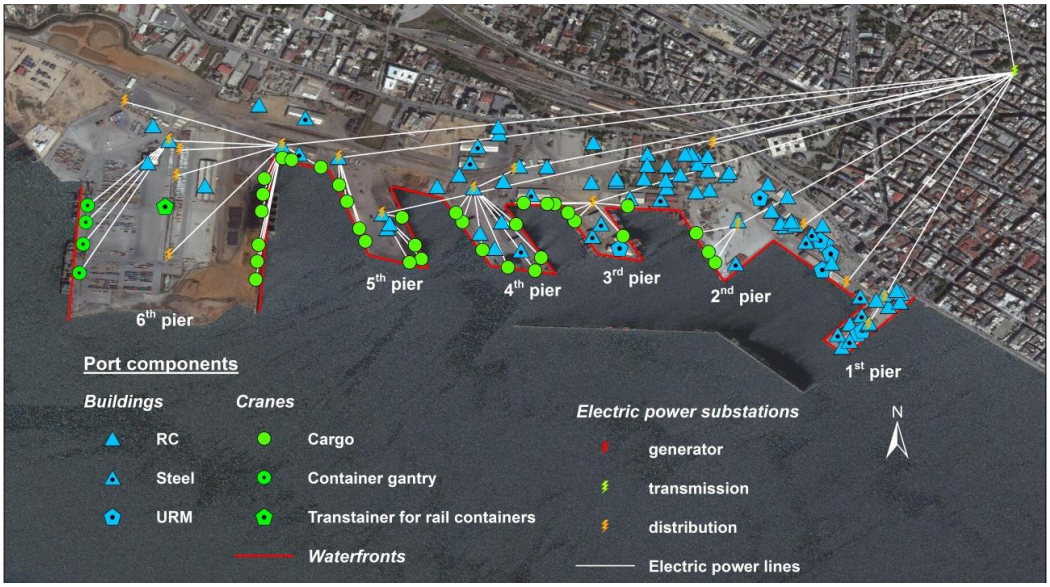

Fig. 7.2 Geographical representation of Thessaloniki's port infrastructures

Soft alluvial deposits, sometimes susceptible to liquefaction, characterize the Port subsoil conditions. The thickness of these deposits close to the sea may reach 150 m to 180 m. A comprehensive set of in-situ geotechnical tests (e.g. drillings, sampling, SPT and CPT tests), detailed laboratory tests and measurements, as well as geophysical surveys (cross-hole, down-hole, array microtremor measurements) at the port broader area provide all necessary information to perform any kind of site specific ground response analyses (Anastasiadis et al 2001). Complementary geophysical tests including array microtremor measurements have been conducted in the frame of STREST project at four different sites inside the port (Pitilakis et al 2016) using the SPatial Autocorrelation Coefficient–SPAC method (Aki 1957). All available data (Fig. 7.3) are properly archived. A topobathymetric model was also produced for the tsunami simulations, based on nautical and topographic maps and satellite images. The elevation data includes also the buildings and other structures that affect the waves while propagating inland. The resolution of the model is higher in the area of the Port.

Fig. 7.3 Location of geotechnical tests and geophysical field measurements in port area

Fragility models

The vulnerability of the Port facilities at component level (i.e. buildings, waterfront structures, cranes etc.) is assessed through fragility functions (Pitilakis et al 2014a), which describe the probability of exceeding predefined damage states (DS) for given levels of peak ground acceleration (PGA), permanent ground displacement (PGD) and inundation depth for the ground shaking, liquefaction and tsunami hazards respectively (Table 7.1). The fragility functions used to assess the damages due to liquefaction are generic (NIBS 2004), while the models used for ground shaking are either case specific (UPGRADE 2015; Kappos et al 2003, 2006; SRM-LIFE 2007, present work) or generic (NIBS 2004). New seismic fragility curves have been developed for typical quay walls and gantry cranes of the port subjected to ground shaking based on dynamic numerical analyses in collaboration with the National Technical University of Athens (NTUA) (UPGRADE 2015). Analytical tsunami fragility curves as a function of inundation depth have been developed for representative typologies of the Port RC buildings, warehouses and gantry cranes (Karafagka et al 2016; Salzano et al 2015) while, for simplicity reasons, the waterfront structures are considered as non-vulnerable to tsunami forces.

The damage states are correlated with component functionality in order to perform the risk assessments in the system level. The following assumptions are set: (i) the waterfront-pier (berth) is functional if damage is lower than moderate, (ii) the crane is functional if damage is lower than moderate and there is electric power supply (i.e. the physical damages of the substations are lower than moderate) (iii) the berth is functional if the waterfront and at least one crane is functional.

Table 7.1 Fragility functions used in the risk analyses

Hazard	Component	Intensity measure	Reference
Ground shaking	RC and URM buildings	PGA	Kappos et al (2003, 2006)
	Steel buildings		HAZUS (NIBS, 2004)
	Waterfront structures		UPGRADE (2015)
	Cranes/cargo handling equipment		
	Electric power substations (distribution, transmission)		HAZUS (NIBS, 2004), SRM-LIFE (2003-2007)
Liquefaction	Buildings/ Housed electric power substations (all considered typologies)	PGD	HAZUS (NIBS, 2004)
	Waterfront structures		
	Cranes/cargo handling equipment		
Tsunami	RC Buildings/ Electric power substations	Inundation depth	Karafagka et al (2016) Salzano et al (2015)
	Warehouses (Steel and URM buildings)		
	Cranes/cargo handling equipment		

7.1.2 Risk measures and objectives

In the Pre-Assessment phase, specific risk measures and objectives are defined related to the functionality of the port at system level and the structural losses at component

level. Since two terminals (container, bulk cargo) are assumed herein, the system performance is measured through the total number of containers handled (loaded and unloaded) per day (TCoH), in Twenty-foot Equivalent Units (TEU), and the total cargo handled (loaded and unloaded) per day (TCaH), in tones. Risk measures related to structural and economic losses of the buildings are also set for the tsunami case and the scenario based assessment. The risk objectives correspond to the boundaries of the grading system proposed in ST@STREST (Esposito et al 2017). The CI passes the stress test if is classified into grade AA (negligible risk) or A (risk being as low as reasonably practicable, ALARP). The CI partly passes the stress test if it receives grade B (possibly unjustifiable risk), while it fails the stress test if it is classified into grade C (intolerable risk). Since no regulatory boundaries exist for the moment for port facilities, continuous (i.e. straight lines on the logarithmic performance curve, see Fig. 7.5 and Fig. 7.6) and scalar (i.e. expected performance loss, see Table 7.2) boundaries were defined based on general judgment criteria for the probabilistic and scenario based system-wide risk assessment respectively in order to demonstrate the application of the ST@STREST. The stress test levels are defined and outlined in the following section.

7.2 Phase 2: Assessment phase

7.2.1 Component level assessment (ST-L1a)

The aim is to check each component of the port independently for earthquake and tsunami hazards in order to show whether the component passes or fails the pre-defined minimum requirements for its performance implied by the current codes. A risk-based assessment is performed using the hazard function at the location of the component and the fragility function of the component. These two functions are convolved in risk integral in order to obtain probability of exceedance of a designated limit state in a period of time (P_f). This probability is estimated on the basis of closed form risk equation (Fajfar and Dolšek 2012) as follows:

$$P_f = \mathrm{H}(\overline{IM})\,\exp(0.5\,\mathrm{k}^2\beta^2) \tag{7.1}$$

where $\overline{IM}$ and β are the median and log-standard deviation values respectively of the fragility function, H(IM) is the hazard function and k is the logarithmic slope of the hazard function idealized in the following form:

$$\mathrm{H(IM)} = k_o \cdot \mathrm{IM}^{-k} \tag{7.2}$$

where k_o is a constant that depends on the seismicity of the site. Proper k and k_o can be obtained by fitting the actual hazard curve provided that the entire hazard function or at least two points from the hazard function are available. For the seismic case (i.e. ground shaking), k and k_o were computed from the hazard curve corresponding to return periods equal to 475 and 4975 years for the normal and the extreme event respectively based on the site specific response analyses carried out for three representative soil profiles (scenario-based assessment) (e.g. Fig. 7.4- left). For the tsunami case, at least two points of the mean hazard function estimated from probabilistic tsunami hazard assessment at various locations in the port area were used to estimate these parameters (e.g. Fig. 7.4- right). The target (acceptable) probability of exceedance of a designated limit state for a period of time implied by the code, stakeholders and decision makers (P_t) also has to be defined for each component and different limit states. In this application the target probability of exceedance of the collapse damage state is only provided. This probability was set to $1.0 \cdot 10^{-5}$ based on the existing practice (e.g. Lazar and Dolšek 2013; Silva et al 2014) corresponding to an acceptable probability equal to 0.05% in 50 years and was properly modified based on EC8 prescriptions to account for the importance factor γ_I of the structure. To check whether or not the component is safe

against collapse, the target probability (P_t) is compared with the corresponding probability of exceeding the ultimate damage state (P_f).

As an example the proposed performance assessment approach is applied here to a strategic building of the Port, the passenger terminal, which is a low-rise infilled dual system (γ_I =1.2). The probability of exceeding the ultimate damage state (P_f), which in this study corresponds to the collapse damage state, is computed and compared with the target probability of collapse (P_t) for both earthquake and tsunami hazards. The hazard function at the location of the structure is estimated as 10^{-5} and $1.7 \cdot 10^{-4}$ for the seismic (see Fig. 7.4- left and Eq. (7.2)) and tsunami (see Fig. 7.4- right and Eq. (7.2)) case respectively, while the corresponding probabilities of collapse (P_f) are finally computed equal to $1.4 \cdot 10^{-3}$ and $2.0 \cdot 10^{-4}$. These probabilities are higher than the target (acceptable) probability of collapse (P_t) estimated equal to $4.7 \cdot 10^{-6}$ and $7.9 \cdot 10^{-6}$ for the seismic and tsunami case respectively, indicating that the structure is not safe against exceedance of the collapse limit state due to the considered hazards. Similar results are generally derived for all buildings and infrastructures providing a general assessment of the performance and resilience of the Port.

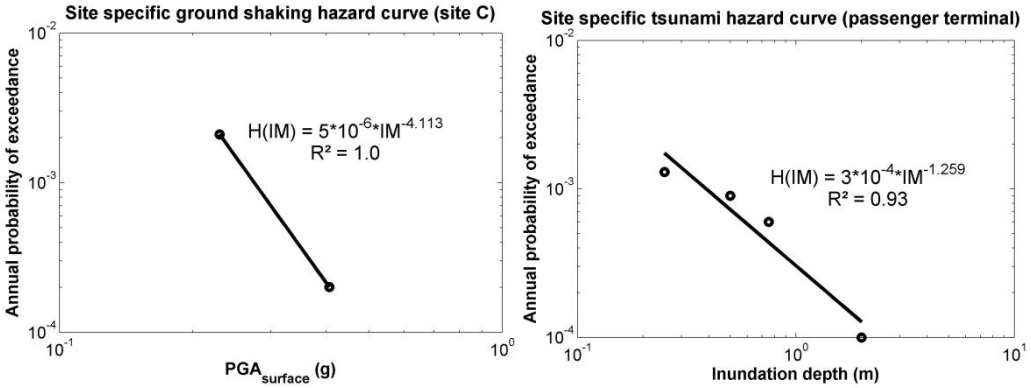

Fig. 7.4 Site specific hazard curves for ground shaking and tsunami

7.2.2 System level assessment (ST-L2b / L2d / L3d)

Probabilistic risk assessment (ST-L2b)

The system wide probabilistic risk assessment (PRA) is made separately for ground shaking, including liquefaction, and tsunami hazard, according to the methodology developed in SYNER-G (Pitilakis et al 2014b) and extended in STREST D4.2 (Kakderi et al 2015). The objective is to evaluate the probability or mean annual frequency (MAF) of events with the corresponding loss in the performance of the port operations. The analysis is based on an object-oriented paradigm where the system is described through a set of classes, characterized in terms of attributes and methods, interacting with each other. The physical model starts from a pre-defined taxonomy and requires: a) a description of the functioning of the system (intra-dependencies) under undisturbed and disturbed conditions (i.e., in the damaged state following an event); b) a model for the physical and functional damageability of each component (fragility functions); c) identification of all dependencies between systems (inter-dependencies); and d) definition of adequate Performance Indicators (PIs) for components and the system as a whole which represent the previously defined risk metrics. The computational modules include the modelling of: hazard events and intensity parameters (hazard class), physical damages of components and performance of the system (network class), and specific interactions among systems (interdependency models). A Monte Carlo simulation is carried out sampling events and corresponding damages for the given hazard. The exceedance probability of different levels of performance loss is assessed for the system

under the effect of any possible event, and the performance curve is produced, which is equivalent of risk curves for non-systemic probabilistic assessments in single (e.g. PEER formula; Cornell and Krawinkler 2000) and/or multi-risk (e.g. Selva 2013; Mignan et al 2014) analysis.

In the present application the systemic analysis concerns the container and bulk cargo movements affected by the performance of the piers, berths, waterfront and container/cargo handling equipment (cranes) while the interdependency considered here is between the cargo handling equipment and the Electric Power Network (EPN) supplying to cranes. The capacity of berths is related to the capacity of cranes (lifts per hour/tons per hour). The functionality state of each component and the whole port system is assessed based on the computed physical damages, taking also into account system inter- and intra-dependencies. Regarding the analysis of the interdependencies we assume that if a crane node is not fed by the reference EPN node (i.e. electric supply station) with power and the crane does not have a back-up supply, then the crane itself is considered out of service. The functionality of the demand node is based on EPN connectivity analysis (Pitilakis et al 2014b).

Risk assessment for ground shaking

The seismic hazard model provides the means for: (i) sampling events in terms of location (epicentre), magnitude and faulting type according to the seismicity of the study region and (ii) maps of sampled correlated seismic intensities at the sites of the vulnerable components in the infrastructure ("shakefields" method, Weatherill et al 2014). When the fragility of components is expressed with different IMs, the model assesses them consistently. Five seismic zones with M_{min}=5.5 and M_{max}=7.5 are selected based on the results of SHARE European research project (Giardini et al 2013, www.share-eu.org) and the ground motion prediction equation (GMPE) of Akkar and Bommer (2010) to estimate the outcrop ground motion parameters. Seismic events are sampled for the seismic zones affecting the port area through a Monte Carlo simulation (10,000 runs). The spatial variability is modelled using the correlation models provided by Jayaram and Baker (2009). For each site of a regular grid of points discretizing the study area, the averages of primary IM (PGA) from the specified GMPE were calculated, and the residual was sampled from a random field of spatially correlated Gaussian variables according to the spatial correlation model. The primary IM is then retrieved at vulnerable sites by distance-based interpolation and finally the local IM is sampled conditionally on primary IM. To scale the hazard to the site condition the amplification factors proposed in EC8 (EN 1998-1, 2004) are used in accordance with the site classes that were defined in the study area. HAZUS (NIBS, 2004) and the modeling procedure by Weatherill et al (2014) are applied to estimate the permanent ground displacements (PGDs) due to liquefaction.

The PIs of the port system for both the container and cargo terminal are evaluated for each simulation of the Monte Carlo analysis based on the damages and corresponding functionality states of each component and considering the interdependencies between components. The final computed PIs are normalized to the value referring to normal (non-seismic) conditions assuming that all cranes are working at their full capacity 24 hours per day. Fig. 7.5 shows the MAF of exceedance curves ("performance curve") for TCoH and TCaH. For performance loss values below 40% TCaH yields higher values of exceedance frequency, while for performance loss over 40% TCoH yields higher values of exceedance frequency.

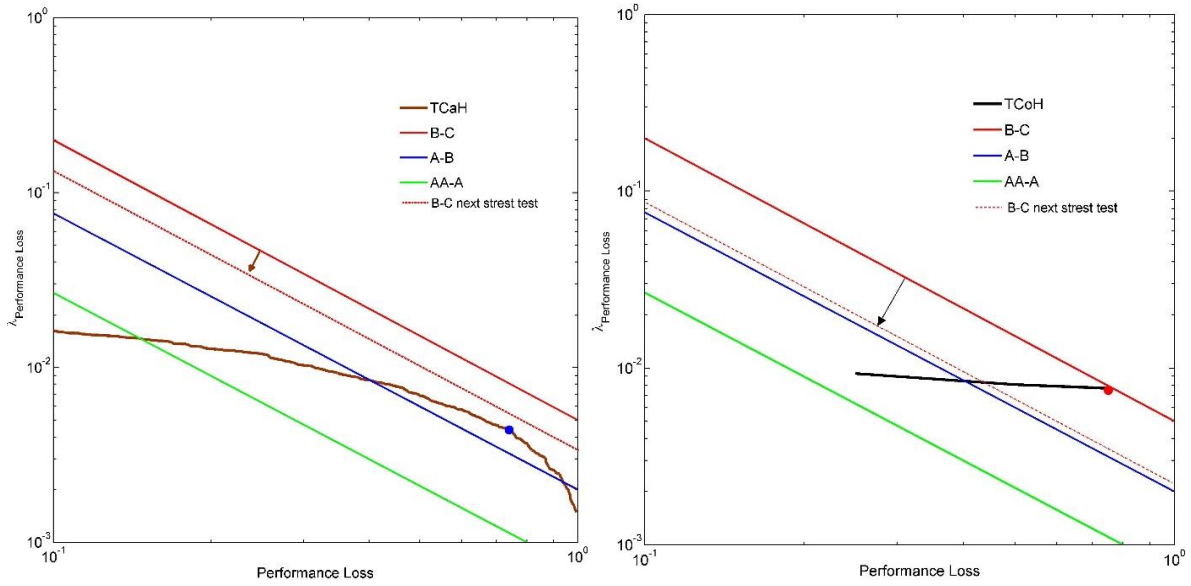

Fig. 7.5 Mean annual frequency (MAF) of exceedance values for the normalized performance loss of the container terminal (TCoH, right) and the bulk cargo terminal (TCaH, left) for the seismic hazard case. The green, blue and red continuous lines correspond to the boundaries between risk grades AA (negligible), A (ALARP), B (possibly unjustifiable risk), and C (intolerable)

Risk assessment for tsunami

A full SPTHA (Seismic Probability Tsunami Hazard Analysis) for tsunami of seismic origin, following Lorito et al (2015) has been developed, based on inundation simulation of the Thessaloniki area (Volpe et al in prep). Different potential tsunamigenic sources should be considered, such as earthquakes, landslides, meteorite impacts or atmospheric phenomena. Here, we focus only on tsunami of seismic origin, which is in most of cases the dominant component (Parsons and Geist 2009). A very large number of numerical simulations of tsunami generation, propagation and inundation on high-resolution topo-bathymetric models are in principle required, in order to give a robust evaluation of SPTHA at a local site. To reduce the computational cost, while keeping results stable and consistent with respect to explore the full variability of the sources, a method has been developed to approach the uncertainty in SPTHA (Volpe et al in prep; Selva et al 2016a, 2016b), based on four steps: 1) a full exploration of the aleatory uncertainty through an Event Tree (ET, Lorito et al 2015; Selva et al 2016a) that accounts for all available sources of information (e.g. Basili et al 2013); 2) the propagation of all potential sources till offshore (Molinari et al submitted); 3) a 2-stage filtering procedure based on Cluster Analysis on the results offshore in order to define a subset of "representative" events which approximate the hazard in the target area, in order to enable the inundation modelling (Lorito et al 2015); 4) the quantification of the epistemic uncertainty through Ensemble modelling based on (weighted) alternative implementations of steps 1 to 3 (Marzocchi et al 2015; Selva et al 2016a).

For Thessaloniki port (Selva et al 2016b; Volpe et al in prep), at steps 1 and 2, we considered a regional SPTHA which accounts for all the potential seismic sources from the Mediterranean Sea (>107 sources), implementing a large number of alternative models to explore the epistemic uncertainty (>105). Then, the 2-layer filtering procedure has been applied, obtaining 253 representative scenarios, which may be modelled to approximate the total hazard (Lorito et al 2015; Volpe et al, in prep). The numerical simulations were performed using a non-linear shallow-water multi-GPU code (HySEA, Gonzalez Vida et al 2015), using 4-level nested bathymetric grids with refinement ratio equal to 4 and increasing resolution from 0.4 arc-min (~740 m) to 0.1 arc-min (~185 m) to 0.025 arc-min (~46 m) to 0.00625 arc-min (~11 m). The results

have been input to an Ensemble model, in order to quantify in each point of the finest grid hazard curves, along with epistemic uncertainty, for two intensity measures: maximum flow depth and maximum momentum flux.

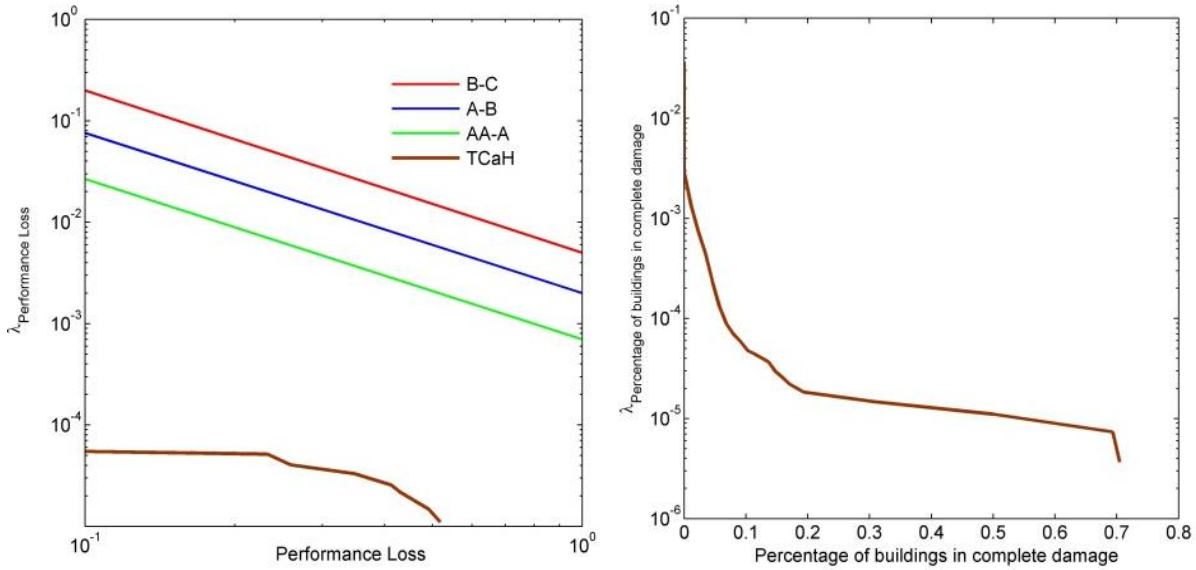

Fig. 7.6 Mean annual frequency (MAF) of exceedance values for the normalized performance loss of the bulk cargo terminal (TCaH, left) and for the buildings in complete damage state (right) for the tsunami hazard case. The green, blue and red continuous lines correspond to the boundaries between risk grades AA (negligible), A (ALARP), B (possibly unjustifiable risk), and C (intolerable)

To assess the tsunami risk a hazard module has been developed in order to enable sampling among the 253 representative scenarios, considering the probability of occurrence of the cluster of sources that each scenario represents (Lorito et al 2015). This procedure is possible for any preselected alternative model of input to the SPTHA ensemble, enabling the propagation of hazard epistemic uncertainty into risk analysis. The inundation simulation results for each sampled scenario are then loaded, in order to retrieve the tsunami intensity for any selected location. Note that, since the SPTHA analysis is based on an explicit simulation of each scenario, spatial correlations of the tsunami intensity are automatically accounted for. Given that the inundation simulation does not integrate potential collapses, tsunami intensity should be retrieved in proximity of each component's perimeter and outside the structure. In order to avoid any unwanted biases (e.g. retrieve the tsunami intensity over the roof of buildings, where the modelled tsunami flow depth is subtracted the height of the building), a characteristic radius has been assigned to each component, and the largest intensity value within the defined circle is obtained. Damages and non-functionalities are then sampled from the respective fragility curves (Table 7.1) and the retrieved tsunami intensities. The analysis has been implemented for the port infrastructures (cranes, electric power network components and individual buildings) and the PIs for the analysed system are evaluated. In Fig. 7.6 we show an indicative example for one of the alternative models (i.e. the epistemic uncertainty is not considered here). The container terminal is not expected to experience any loss (TCoH), while the loss in the cargo terminal (TCoH) is negligible. This is due to the non-vulnerable condition of waterfront structures, the high damage thresholds for the cranes (i.e. high inundation values that are not expected in the study area) as described in the fragility curves used in the application and the distance of the electric power substations from the shoreline. The annual probabilities for buildings collapses are also low. As an example 10% of the total buildings in the Port (~9 structures) will be completed damaged under tsunami forces with annual probability equal to $5 \cdot 10^{-5}$.

Scenario-based risk assessment (ST-L2d / L3d)

A scenario-based system-wide seismic risk analysis is performed complementary to the classical PRA approach described previously, to identify as accurately as possible the local site response at the port area and to reduce the corresponding uncertainties. Two different seismic scenarios were defined in collaboration with a pool of experts: the standard seismic design scenario and an extreme scenario corresponding to return periods of T_m=475 years and T_m=4975 years respectively. To perform the site response analyses a target spectrum for seismic bedrock conditions (V_s=700-800 m/s) and a suite of acceleration time histories are needed. For the 475 years scenario, the target spectrum is defined based on the disaggregation of the probabilistic seismic hazard analysis (SRM-LIFE 2007; Papaioannou 2004). This study has shown that the most significant contribution to seismic hazard for Thessaloniki port is associated with the Anthemountas fault system (i.e. a normal fault) regardless of the return period. In particular, for the 475 years scenario, the maximum annual exceedance probability for a certain PGA value with a moment magnitude M_w of 5.7 and an epicentral distance R_{epi} of 14.6 km was provided. For the 4975 years scenario, an extreme rupture scenario breaking along the whole Anthemountas fault zone with a characteristic magnitude M_w of 7.0, close to the maximum magnitude of the seismic source, was assumed. The GMPE proposed by Akkar and Bommer (2010) is applied, similarly to the probabilistic assessment. In addition to magnitude and distance, both hazard scenarios include an error term ε (which measures the number of standard deviations of logarithmic residuals σ to be accounted for in GMPE) responsible for an appreciable proportion of spectral ordinates and the contribution from ε grows with the return period (Bommer and Acavedo 2004). Thus, the median spectral values plus 0.5 standard deviations and 1 standard deviation are considered for the 475 years and the 4975 years scenarios respectively. A set of 15 accelerograms is selected for the 475 years scenario referring to rock or very stiff soils that on average fit the target spectrum. For the extreme scenario, 10 synthetic accelerograms are computed to fit the target spectrum (4975 years scenario I) and broadband ground motions are generated using 3D physics-based "source-to-site" numerical simulations (4975 years scenario II, Smerzini et al submitted).

Three representative soil profiles (denoted as A, B and C) are considered for the site response analyses (see Fig. 7.3) with fundamental periods T_o equal to 1.58s, 1.60s and 1.24s respectively. The soil profiles have been defined based on previous studies and new measurements. 1D equivalent-linear (EQL) and nonlinear (NL) site response analyses including also the potential for liquefaction are carried out for the three soil profiles using as input motions at the seismic bedrock the ones estimated for the 475 years and 4975 years seismic scenarios (I and II). The numerical codes Strata (Kottke and Rathje 2008) and Cyclic1D (Elgamal et al 2015) are used. To investigate the impact of the uncertainty in the shear wave velocity (V_s) profiles, the analyses are performed for the basic geotechnical models, considering a standard deviation of the natural logarithm of the V_s equal to 0.2. In particular, 100 realizations of the Vs profiles are considered in Strata using Monte Carlo simulations and the calculated response from each realization is then used to estimate statistical properties of the seismic response. In total 1500 and 1200 simulations are performed for the 475 and 4975 (I and II) scenarios respectively. The randomization of the Vs and the incorporation in Monte Carlo simulations is performed through the model proposed by Toro (1995). The corresponding site response variability was assessed in Cyclic1D considering expect for the basic Vs model, upper-range and lower-range models utilizing a logarithmic standard deviation for the Vs profile equal to 0.2 consistently with the Strata simulations. For the EQL approach the results are presented in terms of PGA with depth, acceleration response spectra and spectral and Fourier ratios. For the NL approach, the variation of horizontal and vertical PGD, maximum shear strain and stress, effective confinement and excess pore water pressure with depth were also computed for each analysis. Comparative plots between the EQL and NL approaches are shown in Fig. 7.7 for the 475 years and 4975 years I scenarios

for profile A while Fig. 7.8 depicts indicative results of the NL analysis for the selected input motions for the same soil profile.

The spectral values and shapes are generally comparable between the two approaches for the 475 year scenario while the response is very different for the extreme scenario that is associated with increasing shear strain accumulation. For both scenarios, the EQL spectral shapes are flatter and have less period-to-period fluctuations than the NL ones. The lower spectral values predicted by the NL approach for the extreme seismic scenario could be attributed to the liquefaction that may also result in large permanent ground deformations, which cannot be simulated by the EQL analysis. The results of the NL approach indicate (although not fully presented herein) that liquefaction is evident for all soil profiles and scenarios. However, for the extreme scenario the liquefiable layers are larger and extended to greater depths (up to 35m, e.g. see Fig. 7.8- left). Among the three representative soil profiles, liquefaction effects are shown to be more pronounced in profile A. Large variability in the computed permanent displacements is shown for the different seismic input motions (e.g. see Fig. 7.8- right). Generally low-frequency input motions increase the accumulation of lateral deformations and settlements. The computed maximum horizontal displacement values when considering the basic geotechnical models are 4.5 cm and 18.6 cm for the 475 and 4975 years seismic scenarios respectively, while the corresponding values for the vertical displacements (settlements) are 4.8 cm and 11.0 cm.

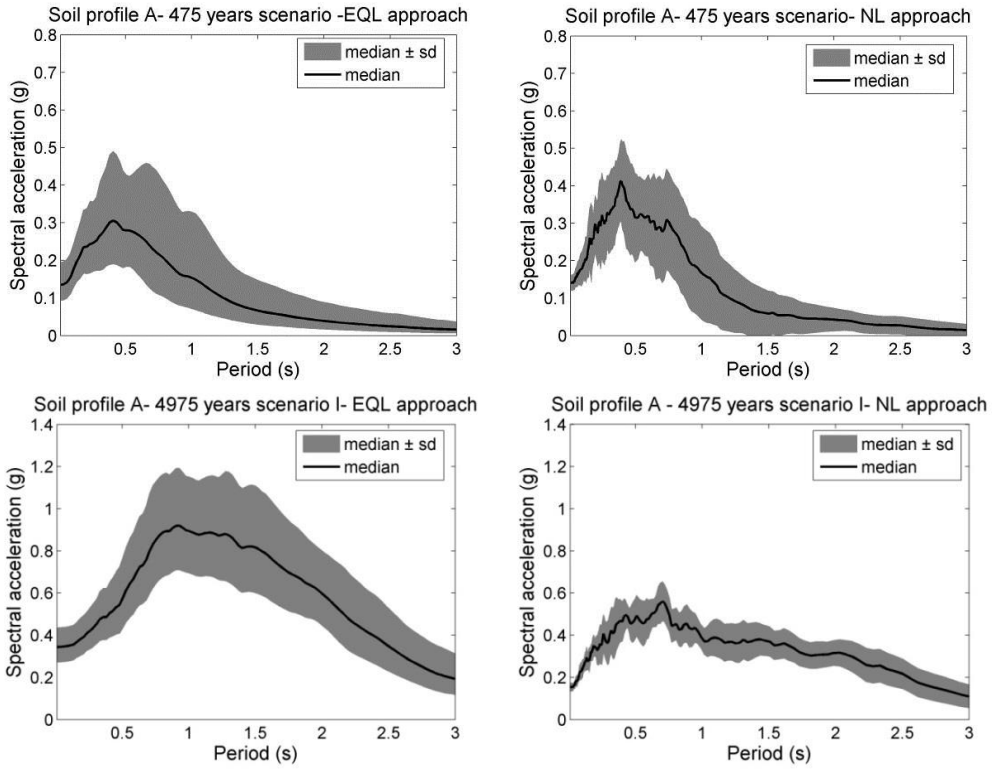

Fig. 7.7 Median ± standard deviation elastic 5% response spectra at the ground surface for soil profile A using the EQL (left) and NL (right) approaches for the 475 years scenario (top) and the 4975 years scenario I (bottom)

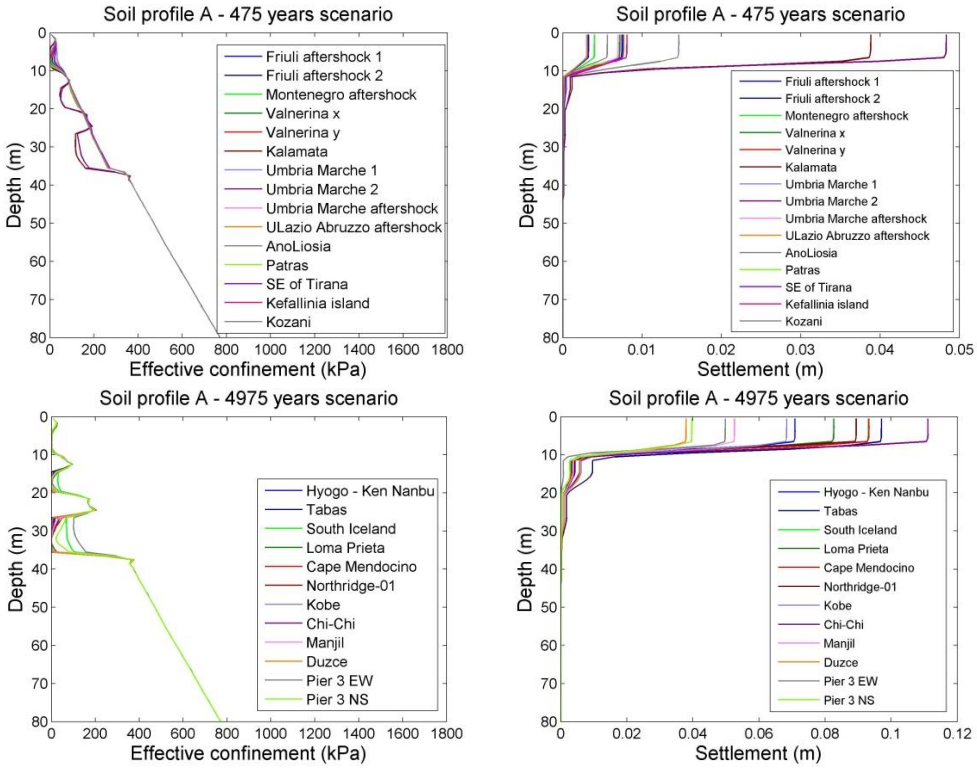

Fig. 7.8 Variation of effective confinement (left) and settlement with depth (right) for soil profile A for the 475 years scenario (top) and the 4975 years scenario (bottom)

The scenario-based risk assessment of the port buildings and infrastructures is initially performed taking into account the potential physical damages and corresponding losses of the different components of the port. Buildings, waterfront structures, cargo handling equipment and the power supply system are examined using the fragility models for ground shaking and liquefaction (Table 7.1). In particular, the vulnerability assessment is performed for the 475 and 4975 years scenarios (I and II) based on the EQL and NL site-response analyses. The results from soil profile A, B or C were considered in the fragility analysis, depending on the proximity of each component to the location of the three soil profiles. In particular, for the EQL approach, the calculated PGA values at the ground surface from the total analysis cases (i.e. 2200 analyses) for each soil profile were taken into account for the vulnerability assessment due to ground shaking. For the NL approach, except for the PGA values, the PGD (horizontal and vertical) values at the ground surface were also considered to evaluate the potential damages to buildings and infrastructures due to liquefaction effects. Finally, the combined damages are estimated by combining the damage state probabilities due to the liquefaction (PL) and ground shaking (PGS), based on the assumption that damage due to ground shaking is independent and not affect the damage due to liquefaction (NIBS, 2004). Once the probabilities of exceeding the specified DS are estimated, a median ±1 standard deviation damage index d_m is evaluated, to quantify the structural losses as the ratio of cost of repair to cost of replacement taking values from 0: no damage (cost of repair equals 0) to 1: complete damage (cost of repair equals the cost of replacement).

The spatial distribution of the estimated losses for buildings indicates that a non-negligible percentage of the port buildings is expected to suffer significant losses (higher than moderate). The median values of this percentage range from 7% for the design scenario (NL approach) to 37% for the 4975 years scenario I (EQL approach). This is to be expected taking into account that all buildings were constructed with low or no seismic code provisions. Among the considered building typologies, the RC structures appear to be less vulnerable compared to the steel and URM systems. The estimated losses are also significantly dependent on the analysis approach. In particular, the EQL

approach is associated with higher damages and losses even for the design scenario, while for the NL approach the losses to the cranes, waterfronts and electric power substations are expected solely for the 4975 scenario I.

The systemic risk is assessed following the methodology presented in the previous section (PRA approach) taking again into account the interdependencies of specific components. It is observed that the EQL approach is associated with higher number of non-functional components for all considered seismic scenarios whereas for the NL approach non-functional components are present only for the 4975 years scenario I. The estimated PIs of the port are normalized to the respective value referring to non-seismic conditions (Table 7.2). As also evidenced by the estimated functionality state of each component, the port system is non-functional both in terms of TCaH and TCoH for the 4975 years scenario I. A 100% and 67% performance loss is estimated for the TCoH and TCaH respectively when considering the EQL approach for the 475 years and 4975 years II scenarios, while the port is fully functional when considering the NL approach both in terms of TCaH and TCoH for the latter scenarios. Thus, it is observed that among the four different outcomes determined for the extreme scenario for both PIs, the CI passes the stress test in the 4975 years scenario II and NL method, which could be judged as the most reliable. It is noted that the estimated PIs do not change when considering the median+1standard deviation damage indices in the computation of the components' functionality. However, when the median-1standard deviation damage indices are taken into account in the calculations, a 100% performance loss is estimated only for the 4975 years scenario I while the port is fully functional for all the other analysis cases both in terms of TCaH and TCoH.

Table 7.2 Estimated normalized performance loss of the port system for TCaH and TCoH and comparison with risk objectives for the scenario based assessment

Scenario	Analysis type	Performance loss (1-PI/PImax)		Risk objectives			Stress test outcome	
		TCaH	TCoH	AA-A	A-B	B-C	TCaH	TCoH
475 years	EQL	0.67	1.00	0.10	0.30	0.50	Fail	Fail
	NL	0.00	0.00				Pass	Pass
4975 years I	EQL	1.00	1.00	0.30	0.50	0.70	Fail	Fail
	NL	1.00	1.00				Fail	Fail
4975 years II	EQL	0.67	1.00	0.30	0.50	0.70	Partly pass	Fail
	NL	0.00	0.00				Pass	Pass

7.3 Phase 3: Decision phase

The Decision phase comprises different steps including (i) the comparison of the assessment results with the pre-defined risk objectives, (ii) disaggregation and/or sensitivity analysis to identify critical events and components and (iii) recommendation of risk mitigation measures to improve the performance of the port.

7.3.1 Risk objectives check

In the first step of the decision phase, the risk assessment results are compared with the defined risk objectives to check whether the port system passes, partially passes or fails the stress test and to define the grading system parameters for the next evaluation of the stress test since the performance of the CI or performance objectives can change over time (Esposito et al 2017).

In Fig. 7.5 risk boundaries are plotted together with the MAF curves of the assessed performance loss. With reference to both bulk cargo and container terminals (TCaH, TCoH curves) the port obtains grade B, meaning that the risk is possibly unjustifiable and the CI partly passes this evaluation. The basis for redefinition of risk objectives in the next stress test evaluation is the characteristic point of risk, which is defined as the point associated with the greatest risk above the ALARP region (blue and red dots for TCaH and TCoH curves respectively). These points are the farthest from the A-B boundary (blue line). The proposed grading system foresees the reduction of the boundary between grades B and C (red line) in the next stress test, which is equal to the amount of risk beyond the ALARP region assessed, represented in this application by the corresponding red dashed lines in case of the bulk cargo and cargo terminals. The plot in Fig. 7.6 (left panel) indicates that the CI receives grade AA (negligible risk), and as expected in this example application, passes the stress test for the tsunami hazard. Indicative scalar performance boundaries in terms of the normalized performance loss are shown in Table 3 together with the corresponding results of the scenario based assessment. It is seen that the CI may pass, partly pass or fail for the specific evaluation of the stress test (receiving grades AA, B and C respectively) depending on the selected seismic scenario, the analysis approach and the considered risk metric (TCaH, TCoH). Based on the proposed grading system, for the case which the port obtains grade B and partly passes the stress test, the BC boundary in the next stress test is reduced (i.e. BC: 53% performance loss) while the other boundaries remain unchanged. It is noted that different grades can be derived from the probabilistic and scenario-based assessments varying between AA (for the scenario based and the probabilistic tsunami risk assessments) and C (for the scenario-based and probabilistic seismic risk assessments). It is also worth noting that the risk objectives and the time between successive stress tests should be defined by the CI authority and regulator. Since regulatory requirements do not yet exist for the port infrastructures, the boundaries need to rely on judgments.

7.4 Phase 4: Report phase

The final stage of the test involves reporting the findings, which are summarized in Table 7.3.

Table 7.3 Summary report of the stress test outcomes

Level 1	**Component level – Seismic Hazard**			
	Buildings	Cranes	Quay walls	Electric power stations
Number of components	85	35	25	17
Target probability of collapse*	$4.7\text{x}10^{-6}$ - $6.3\text{x}10^{-6}$	$4.9\text{x}10^{-6}$ - $6.3\text{x}10^{-6}$	$4.7\text{x}10^{-6}$ - $6.3\text{x}10^{-6}$	$4.7\text{x}10^{-6}$ - $6.3\text{x}10^{-6}$
Outcome	0% pass 100% fail	0% pass 100% fail	0% pass 100% fail	0% pass 100% fail
Level 1	**Component level – Tsunami Hazard**			
	Buildings	Cranes		Electric power stations
Number of components	85	35		17
Target probability of collapse*	$5.8\text{x}10^{-6}$ - $9.3\text{x}10^{-6}$	$6.6\text{x}10^{-6}$ - $8.8\text{x}10^{-6}$		$5.8\text{x}10^{-6}$ - $7.9\text{x}10^{-6}$
Outcome	0% pass 100% fail	83% pass 17% fail		0% pass 100% fail
Level 2b	**System level – Seismic Hazard (PRA)**			

Risk measure	TCoH	TCaH
Objectives boundaries (annual probability for 100% loss, logarithmic slope = 1)	B-C: $4.5x10^{-3}$ A-B: $2.0x10^{-3}$, AA-A: $7.5x10^{-4}$	B-C: $4.5x10^{-3}$ A-B: $2.0x10^{-3}$, AA-A: $7.5x10^{-4}$
Grade	B	B
Outcome	partially pass	partially pass
Next stress test objectives	B-C: $2.5x10^{-3}$ A-B: unchanged, AA-A: unchanged	B-C: $3.5x10^{-3}$ A-B: unchanged, AA-A: unchanged
Level 2b	**System level – Tsunami Hazard (PRA)**	
Risk measure	TCoH	TCaH
Objectives boundaries (annual probability for 100% loss, logarithmic slope = 1)	B-C: $4.5x10^{-3}$ A-B: $2.0x10^{-3}$, AA-A: $7.5x10^{-4}$	B-C: $4.5x10^{-3}$ A-B: $2.0x10^{-3}$, AA-A: $7.5x10^{-4}$
Grade	AA	AA
Outcome	pass	pass
Next stress test objectives	unchanged	unchanged
Level 2d/3d	**System level – Seismic Hazard (Scenario based)**	
Risk measure	TCoH	TCaH
Objectives-475 years scenario (% loss)	B-C: 50, A-B: 30, AA-A: 10	
Objectives-4975 years scenario (% loss)	B-C: 70, A-B: 50, AA-A: 30	
Grade		
475 EQL	C	C
475 NL	AA	AA
4975 years I EQL	C	C
4975 years I NL	C	C
4975 years II EQL	C	B
4975 years II NL	A	A
Outcome		
475 EQL	fail	fail
475 NL	pass	pass
4975 years I EQL	fail	fail
4975 years I NL	fail	fail
4975 years II EQL	fail	partially pass
4975 years II NL	pass	pass
Next stress test objectives		
Objectives-4975 years scenario (% loss)	B-C: 53, A-B: unchanged, AA-A: unchanged	

8. Application of stress test concepts to industrial district, Italy

This application of the STREST methodology focused on an industrial district in the province of Arezzo, in the Tuscany Region of northern Italy. This application was chosen to demonstrate the performance and consequences assessment of multiple-site, low-risk, high-impact, non-nuclear CIs. Economic loss-based risk measures and objectives have been used, given the large economic losses that were experienced in Italy following the Emilia-Romagna earthquakes in May 2012 (see STREST D2.3 Krausmann et al 2014). The economic loss has been estimated considering the loss due to structural damage, non-structural damage, contents damage and associated direct business interruption. Indirect business interruption is inferred from the customer base of the facilities contributing most to the loss. A summary is provided below on the main features of each phase of this Stress Test application.

8.1 Phase 1: Pre-assessment phase

In this phase of the stress test, all exposure, hazard and cost/loss data required to carry out a probabilistic risk assessment was sought, as well as data useful for the assessment of indirect losses (such as the customer base of each industrial facility).

The exposure data for this case study has been provided by the industrial partner in this case study: the Sezione Sismica, Regione Toscana. A database of 425 pre-cast reinforced concrete industrial facilities in the whole of Tuscany was provided, and a smaller database covering the 300 assets in the province of Arezzo was produced. The available exposure data included coordinates, year of construction, floor area, structural type, non-structural elements, and other data useful for identifying value of contents, type of business, and extent of customer base. The data on the structural and non-structural features of the structures allowed each building to be assigned to one of 8 sub-classes, as shown in Fig. 8.1, where Type 1 refers to buildings with long saddle roof beams, Type 2 to buildings with shorter rectangular beams and larger distance between the portals, V1 is vertical cladding, H1 is horizontal cladding and M1 is masonry infill.

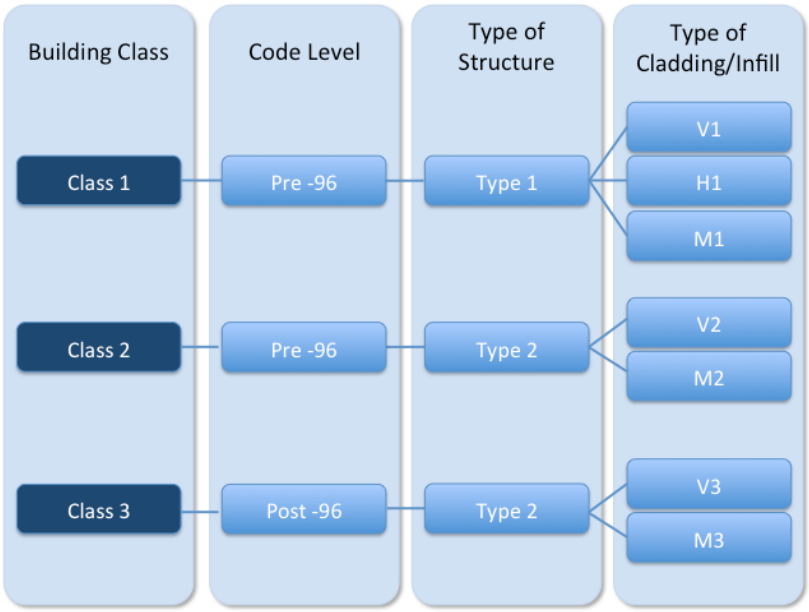

Fig. 8.1 Sub-classes of buildings in terms of structural and non-structural elements

Only seismic hazard has been considered in this case study, as it is the predominant hazard to which the industrial building stock in Tuscany is exposed. In order to generate a large set of ground motion fields characterizing the seismicity of a given region, a probabilistic seismic hazard model comprised of the following three components is required: a seismological/source model that describes the location, geometry, and seismic activity of the sources; a ground-motion model that describes the probability of exceeding a given level of ground motion at a site, conditioned on a set of event and path characteristics; and a site condition model that describes the characteristics of the soil at each site.

The European project "Seismic Hazard Harmonization in Europe" (SHARE, 2009–2013) has produced a European seismic hazard model (Woessner et al 2015) with three source models (one based on area sources, one that uses fault sources and a third based on distributed seismicity). The three aforementioned models can be used separately to produce a hazard model, although it was recommended by the SHARE consortium that these models should be combined in a logic tree, together with additional logic tree branches to describe the epistemic uncertainty in the GMPEs. The SHARE seismological models are available from the European Facility for Earthquake Hazard and Risk portal (www.efehr.org), and can be used to generate spatially correlated ground-motion fields using the Global Earthquake Model's hazard and risk software, the OpenQuake-engine (Silva et al 2014).

Fig. 8.2 presents the mean hazard map that has been calculated for Tuscany, with the OpenQuake-engine and the SHARE hazard model, in terms of PGA with a 10% probability of exceedance in 50 years. In order to account for site amplification, the Vs30 value of the soil at each location in the exposure model is needed. This is not currently available for the locations of the industrial facilities in the exposure model, and so an estimation of the value of V_{s30} based on a proxy (topography) has been employed[1], as shown in Fig. 8.3.

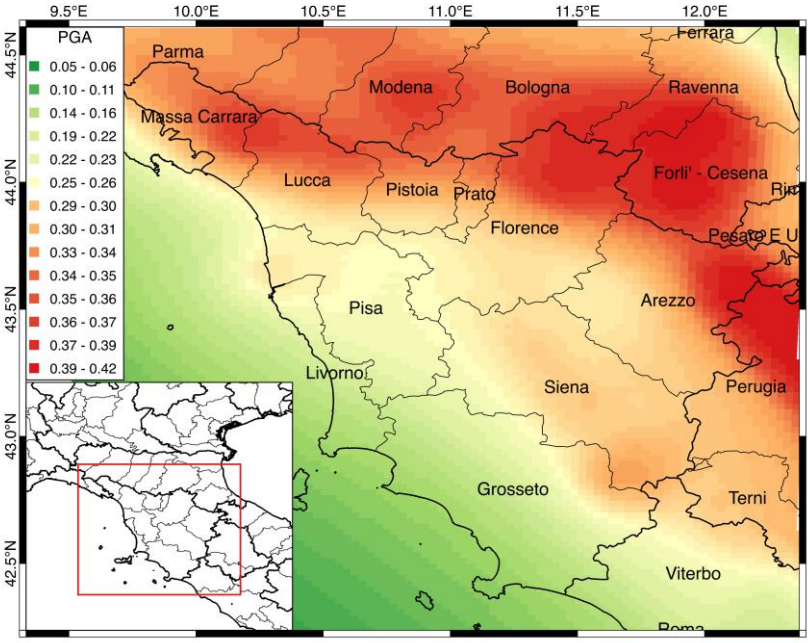

Fig. 8.2 Mean hazard map for Tuscany based on SHARE logic tree with V_{s30} = 800m/s (in terms of PGA with 10% probability of exceedance in 50 years)

[1] http://earthquake.usgs.gov/hazards/apps/vs30/predefined.php

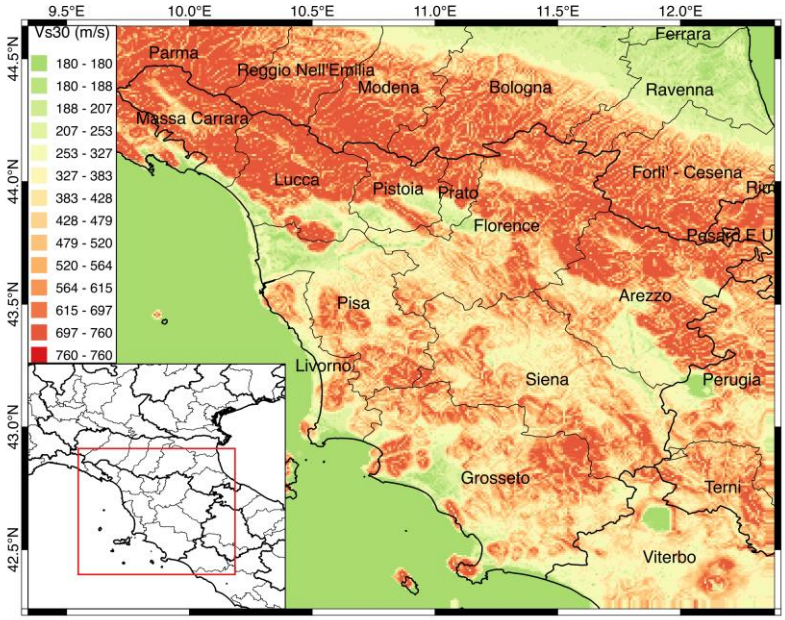

Fig. 8.3 Estimates of site conditions in Tuscany from topographic slope (http://earthquake.usgs.gov/hazards/apps/vs30/predefined.php)

For the component level stress test assessment carried out herein (wherein each industrial facility is considered as an individual component) the annual probability of structural collapse has been taken as the risk measure, and the required objective has been sought by reference to European design norms. An annual structural collapse probability value of 10^{-5} for the boundary A-B and 2.0×10^{-4} for the boundary B-C of the grading system of the STREST methodology.

For the system level assessment, two types of risk metrics have been considered for the stress test:

- Average annual loss;
- Mean annual rate of specific level of loss.

Specific objectives for these risk metrics have not been defined by Regione Toscana, and so hypothetical values have been considered for illustrative purposes of the methodology. It has been decided to use the following objectives for the total average annual loss: the boundary A-B would be less 0.05% of the total exposure value and 0.1% would define boundary B-C. For the second objective, the mean annual rate of a loss due to business interruption equal to 7 times the daily business interruption exposure (i.e. 10 Million Euro) should not be higher than 10^{-4} (i.e. 1 in 10,000 years) for boundary A-B and this would be 30 days for boundary B-C (i.e. 42 Million Euro).

8.2 Phase 2: Assessment phase (ST-L1a / ST-L2b)

A risk-based component level assessment has been undertaken for all 300 industrial facilities in Arezzo using hazard curves (i.e. PGA versus annual probability of exceedance) estimated with the OpenQuake-engine using the SHARE hazard model (Woessner et al 2015), and amplified considering topography-based V_{s30} estimates, together with the complete damage structural fragility functions for each sub-class of structure that were derived in STREST D4.3 (Crowley et al 2015).

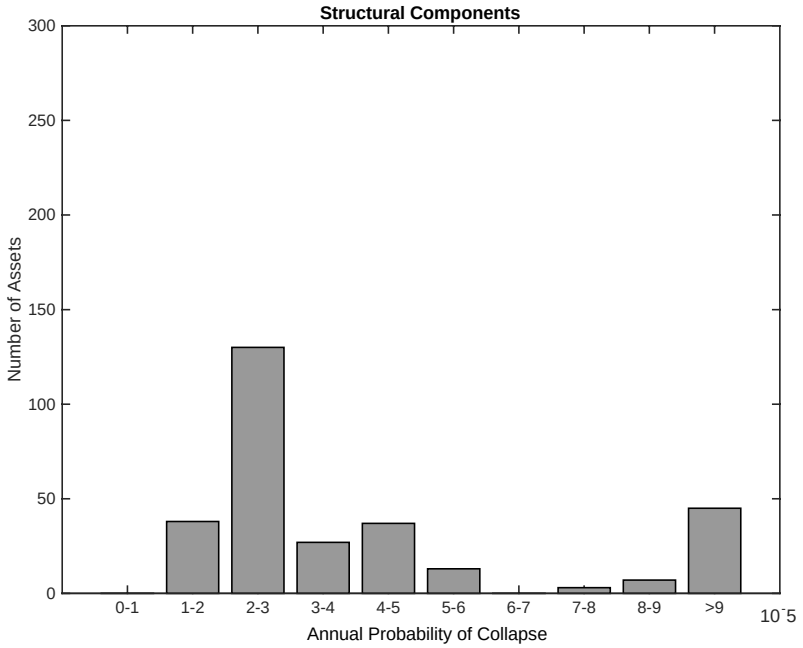

Fig. 8.4 Annual probability of collapse of all industrial buildings in Arezzo

For the system level assessment, vulnerability models have been developed for each sub-class for structural, non-structural, contents and business interruption loss following the methodology and assumptions outlined in STREST D4.3 (Crowley et al 2015). The SHARE logic tree model and the topography-based site conditions have been used to model the seismic hazard. In order to calculate probabilistic seismic risk for a spatially distributed portfolio of assets in Arezzo, the Probabilistic Event-Based Risk calculator from the OpenQuake-engine (Silva et al 2014) has been employed. This calculator is capable of generating loss exceedance curves and risk maps for various return periods based on probabilistic seismic hazard, with an event-based Monte Carlo approach that allows both the spatial correlation of the ground motion residuals and the correlation of the loss uncertainty to be modelled. Loss curves and loss maps can be computed for five different loss types such as: structural components, non-structural components, contents, downtime losses and fatalities. The loss exceedance curves describe the probability of exceedance of different loss levels and the risk maps describe the loss values for a given probability of exceedance, over the specified time period. Additionally, aggregated loss exceedance curves can also be produced using this calculator, which describe the probability of exceedance of different loss levels for all assets in the exposure model.

The total loss results of the probabilistic risk assessment for the portfolio of industrial facilities in Arezzo are shown in Fig. 8.5 in terms of a loss exceedance curve. Similar curves for each component of the loss (structural, non-structural, contents and business-interruption) have also been produced. The loss exceedance curve for each of the branches of the logic tree is shown with a thin line and the mean across all branches is shown with a thick line.

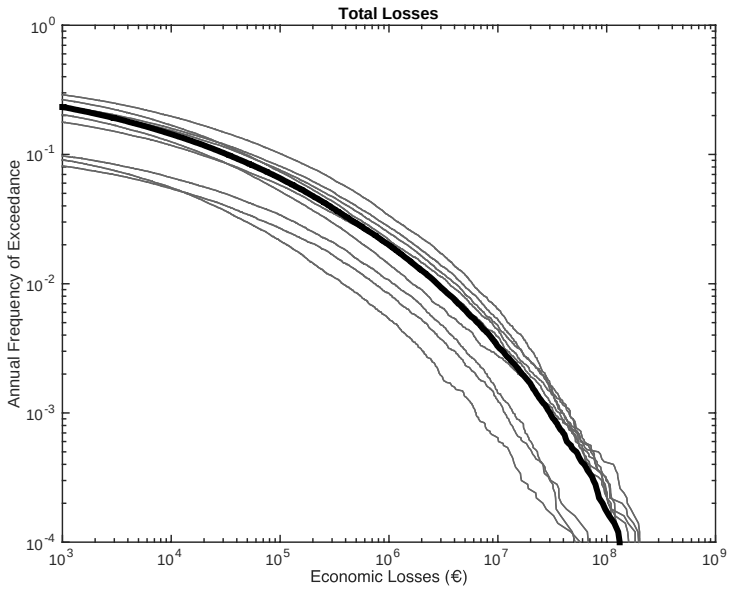

Fig. 8.5 Total loss exceedance curves for all industrial facilities in Arezzo

The average annual losses (AAL) have been calculated from the loss exceedance curves and the results are presented in Table 8.1. This table shows that the largest component of loss is given by business interruption. The values of AAL as well as the mean annual rates of specific loss values will be checked against the risk objectives in the Decision Phase.

Table 8.1 Average annual losses for Arezzo industrial facilities

	Average Annual Losses	Average Annual Loss Ratio (%)[1]
Structural	€ 7,330	0.016
Non-Structural	€ 25,047	0.018
Contents	€ 49,022	0.033
Business Interruption	€ 93,932	0.067
Total Losses	€ 175,330	0.052

[1] Calculated as AAL / exposure value for each component

8.3 Phase 3: Decision phase

This step of the stress test requires a comparison of the results of the risk assessment with the risk objectives, to check whether the industrial facilities pass each level of the Stress Test.

According to the grading system of the component test, 260 facilities are assigned grade B (partly pass) and 40 facilities are assigned grade C (and thus fail the stress test).

The results also show that the A-B system level assessment objective is not met as the total AAL percentage is 0.052%, but the B-C level is met. Hence the grading would be B (partly pass) for this objective. The business interruption loss at a mean annual rate of exceedance of 10^{-4} is 64 Million Euro (which can be translated as an average of 45 days of business interruption), and so the grading would be C (fail) for this objective.

In order to provide guidance on how to mitigate the risk, disaggregation of the results has been carried out. The critical components for each loss, according to the disaggregation of the average annual loss are given in Fig. 8.6. It can be noted that the most critical typologies might depend on the type of loss that is of most concern.

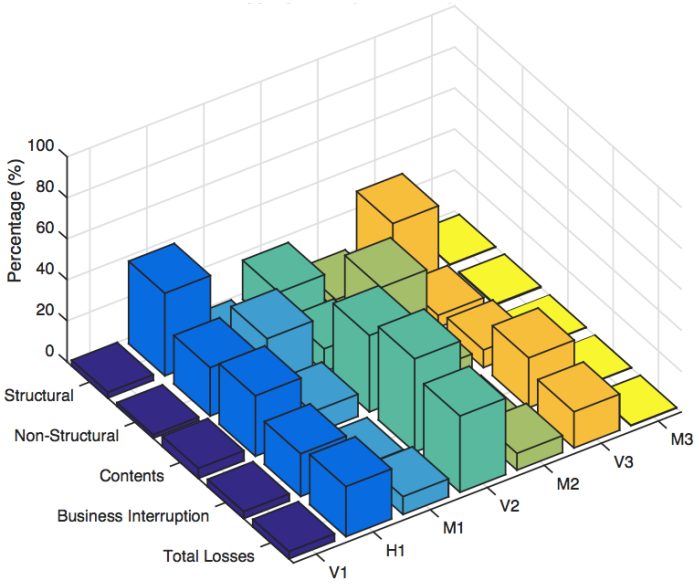

Fig. 8.6 Disaggregation of average annual loss according to building sub-class for each component of loss

In order to understand the indirect impact of the business interruption losses on the region and/or whole country, the customer base of the facilities that are contributing to the average annual business interruption loss can also be presented (a similar calculation could be done also for any value of loss calculated herein). The percentage of each customer base AAL, as a portion of the total AAL, is given in Table 8.2, where it can be seen that 45% of the business interruption AAL is caused by facilities that have a customer base that goes beyond the province of Arezzo, and could thus cause additional indirect losses at a regional, national and international scale (in a decreasing order of importance).

Table 8.2. Percentage of each customer base AAL to the total business interruption AAL

Customer base	Percentage of AAL (for BI) %
Not Determined (ND)	21
Comune (municipality)	8
Province	27
Regional	23
National	18
International	3

There are 40 facilities that fail the component level assessment and should be targeted for structural investigation and potential upgrade. They all belong to the H1 subclass (i.e. pre-code type 1 portal frame with horizontal cladding).

The sub-typologies that contribute most to the total average annual losses are V2 (i.e. pre-code type 2 portal frame with vertical cladding), H1 (i.e. pre-code type 1 portal frame with horizontal cladding) and V3 (i.e. low-code type 2 portal frame with vertical cladding). Hence, in addition to investigating further the H1 sub-class buildings, the V2

and V3 typologies should also be addressed, and the customer base of the facility should also be used as a prioritization tool to identify the facilities to investigate and potentially retrofit first, in order to also reduce the impact of indirect losses from these facilities.

Disaggregation of the hazard (not shown here due to space limitations) for the business interruption loss (which is also the largest contribution to total loss), has identified that a wide range of events contribute to the loss from lower magnitude close events to higher magnitude distance events. This implies that these losses are not just driven by the rare events, and thus mitigation efforts to protect against business interruption should be given high priority. Given that business interruption is directly related to structural and non-structural damage, this can be addressed through the retrofitting activities mentioned above.

8.4 Phase 4: Report phase

The final stage of the test involves reporting the findings, which are summarized in Table 8.3.

Table 8.3. Summary report of the stress test outcomes

Level 1	**Component level – Seismic Hazard**	
	Structural elements of buildings	
Number of components	300	
Target probability of collapse	10^{-5} - $2x10^{-4}$	
Outcome	260 partly pass (grade B) and 40 fail (grade C)	
Level 2b	**System level – Seismic Hazard (PRA)**	
Risk measure	Average Annual Loss (as percentage of total exposure)	1 in 10,000 year business interruption loss
Objectives boundaries	A-B: 0.05% B-C: 0.1%	A-B: 7 days B-C: 30 days
Grade	B	C
Outcome	partly pass	fail
Next stress test objectives	A-B (as above)	B-C (as above)

9. Conclusions and recommendations

In the context of STREST project, an engineering risk-based methodology for stress test critical non-nuclear infrastructures, named ST@STREST, has been developed (see STREST ERR4 Esposito et al 2016). In particular, a multi-level framework has been proposed composed of four main phases and nine steps to be conducted sequentially. First the goals, the method, the time frame, and the total costs of the stress test are defined. Then, the stress test is performed at component and system levels; subsequently, the outcomes are checked and compared to the acceptance criteria. A stress test grade is assigned and the global outcome is determined by employing a grading system proposed herein. According to the outcome the parameters of the following evaluation of stress test are adjusted. Finally, the results are reported and communicated to stakeholders and authorities.

ST@STREST has been applied and tested in six CIs in Europe, namely: a petrochemical plant in Milazzo, Italy (CI-A1), large dams of the Valais region, Switzerland (CI-A2), hydrocarbon pipelines, Turkey (CI-B1), the Gasunie national gas storage and distribution network, Holland (CI-B2), the port infrastructure of Thessaloniki, Greece (CI-B3), and an industrial district in the region of Tuscany, Italy (CI-C1). Different stress test levels were selected according to the characteristics and available resources in each case study. The objective was to demonstrate how the proposed framework is implemented in different classes of CIs exposed to variant hazards, therefore reasonable assumptions or simplifications were made in some steps of the applications. It is noted that the STREST consortium takes no responsibility in the research results provided in this report, as these results should not be considered formal stress tests.

The stress test to the ENI/Kuwait oil refinery and petrochemical plant in Milazzo, showed that the earthquake impact is more important for the atmospheric storage tanks, while the tsunami effect on the atmospheric storage vessels along the shore line is limited. Neither an earthquake nor a tsunami significantly increases the failure frequency of, and hence the risk imposed by, pressurized vessels (like LPG spheres). The stress test to the large dams in the Valais region of Switzerland exposed to multi-hazard effects, considering earthquakes, floods, internal erosion, bottom outlet malfunctions, and hydropower system malfunction concluded that the risk associated with the conceptual dam following the characteristic point of risk approach is acceptable. The stress test to the major hydrocarbon pipelines in Turkey, exposed to seismic hazard, and in particular to permanent fault displacements, indicated that retrofit is potentially needed for the pipes at pipe-fault intersection locations. The stress test to the Gasunie national gas storage and distribution network in Holland, exposed to earthquake and liquefaction effects, showed that soil liquefaction is the dominant failure mechanism. Specific pipe sections, which were identified to be the weakest links in the network, should be checked on their current actual state assessing the need for upgrading, while retrofitting of specific stations might be also necessary. The stress test to the port infrastructures of Thessaloniki subjected to earthquake, tsunami and liquefaction hazards showed a variation in the outcomes depending on the analysis type. Infrastructures where potential upgrade should be considered were indicated. The stress test to the industrial district in the region of Tuscany, exposed to seismic hazard, pointed out the facilities which should be targeted for structural investigation and potential upgrade, and that mitigation efforts to protect against business interruption should be given high priority. Table 9.1 summarizes the results of the six applications in terms of the grading range that is defined in each level and hazard considered.

In the framework of the case studies the objectives boundaries have been set mainly based on judgments, however, formulation of risk acceptance criteria is not a straightforward task. In practice, setting objectives and establishing risk measures is very difficult and strongly dependent on legal, socio-economic and political contexts and they should be defined by the corresponding stakeholders. Nevertheless, the results of the stress test will stimulate stakeholders to take specific measures to upgrade or not

the existing infrastructure such that they will improve their grading in the following stress test cycle.

Table 9.1. Grading range for the six case studies of STREST

Case study	Hazard	Grading range								
		ST-L1a	**ST-L2a**	**ST-L2b**	**ST-L2c**	**ST-L2d**	**ST-L3a**	**ST-L3b**	**ST-L3c**	**ST-L3d**
CI-A1	Earthquake	AA-C	-	AA-C	-	AA-C	-	-	-	-
	Tsunami	AA-C	-	AA-C	-	AA-C	-	-	-	-
CI-A2	Earthquake/ Flood/ Internal erosion/ Outlet malfunction/ Hydropower system malfunction	AA-A	-	AA-A	-	AA-A	-	-	AA-A	AA-A
CI-B1	Earthquake	AA	AA	-	-	-	-	-	-	-
CI-B2	Earthquake/ Liquefaction	AA-A	AA-A	-	-	-	-	-	-	-
CI-B3	Earthquake	C	-	-	-	-	-	-	-	-
	Tsunami	AA-C	-	AA	-	-	-	-	-	-
	Earthquake/ Liquefaction	-	-	B	-	AA-C	-	-	-	AA-C
CI-C1	Earthquake	B-C	-	B-C	-	-	-	-	-	-

References

1. Esposito S, Stojadinovic B, Mignan A, Giardini D, Dolšek M, Babič A, Selva J, Iqbal S, Cotton F, Iervolino I (2016) Reference Report RR4: Guidelines for stress-test design for non-nuclear critical infrastructures and systems: Methodology. STREST project: Harmonized approach to stress tests for critical infrastructures against natural hazards
2. Cornell C, Krawinkler H (2000). Progress and challenges in seismic performance assessment. PEER Center News, 3 (2)
3. Esposito S, Stojadinovic B, Mignan A, Dolšek M, Babič A, Selva J, Iqbal S, Cotton F, Iervolino I (2016) Deliverable D5.1: Report on the proposed engineering risk assessment methodology for stress tests of non-nuclear CIs. STREST project: Harmonized approach to stress tests for critical infrastructures against natural hazards
4. Selva J, Iqbal S, Taroni M, Marzocchi W, Cotton F, Courage W, Abspoel-Bukman L, Miraglia S, Mignan A, Pitilakis K, Argyroudis S, Kakderi K, Pitilakis D, Tsinidis G, Smerzini C (2015). Deliverable D3.1: Report on the effects of epistemic uncertainties on the definition of LP-HC events. STREST project: Harmonized approach to stress tests for critical infrastructures against natural hazards
5. SSHAC (1997). Recommendations for probabilistic seismic hazard analysis: guidance on uncertainty and use of experts (No. U.S. Nuclear Regulatory Commission Report, NUREG/CR-6372), U.S. Nuclear Regulatory Commission Report, NUREG/CR-6372. Washington, D.C.
6. Jonkman SN, Van Gelder PHAJM, Vrijling JK (2003) An overview of quantitative risk measures for loss of life and economic damage. Journal of Hazardous Materials 99(1):1-30
7. Bowles DS, Anderson LR, Evelyn JB, Glover TF, van Dorpe DM (1999) Alamo dam demonstration risk assessment. ASDSO meeting, http://www.engineering.usu.edu/uwrl/www/faculty/DSB/alamo.html
8. Health & Safety Executive (HSE) (1989). Risk criteria for land use planning in the vicinity of major industrial Hazards. HSE Books ISBN 0-11-885491-7
9. MHLUPE (1988). Dutch National Environment Plan. Ministry of Housing Land Use Planning and Environment (MHLUPE), The Hague
10. Paté-Cornell ME (1994) Quantitative safety goals for risk management of industrial facilities. Structural Safety 13, 145–157
11. Whitman RV (1984): Evaluating calculated risk in geotechnical engineering. Journal of Geotechnical Engineer, ASCE 110 (2), 145-188
12. Krausmann E, Cozzani V, Salzano E, Renni E (2011) Industrial accidents triggered by natural hazards: an emerging risk issue. Natural Hazards and Earth System Sciences 11:921–929
13. Salzano E, Basco A, Busini V, Cozzani V, Renni E, Rota R (2013) Public Awareness Promoting New or Emerging Risk: Industrial Accidents Triggered by Natural Hazards. Journal of Risk Research 16:469-485
14. Parsons T, Geist EL (2009) Tsunami probability in the Caribbean region, Pure appl. Geophys. 165: 2089–2116
15. Lorito S, Selva J, Basili R, Romano F, Tiberti MM, Piatanesi A (2015) Probabilistic hazard for seismically-induced tsunamis: accuracy and feasibility of inundation maps, Geophys. J. Int. 200 (1): 574-588

16. Salzano E, Basco A, Karafagka S, Fotopoulou S, Pitilakis K, Anastasiadis A, Matos JP, Schleiss AJ (2015). Deliverable D4.1 Guidelines for performance and consequences assessment of single-site, high-risk, non-nuclear critical infrastructures exposed to multiple natural hazards. STREST project: Harmonized apporach to stress tests for critical infrastructures against natural hazards

17. VROM (2005). Guidelines for quantitative risk assessment. (Purple Book), PGS 3, Ministry of Housing Spatial Planning and the Environment (VROM), The Hague.

18. Salzano E, Iervolino I, Fabbrocino G (2003) Seismic risk of atmospheric storage tanks in the framework of Quantitative Risk Analysis. Journal of Loss Prevention in the Process Industry 16:403-409

19. Campedel M, Cozzani V, Garcia-Agreda A, Salzano E (2008) Extending the Quantitative Assessment of Industrial Risks to Earthquake Effects. Risk Analysis 5:1231-1246

20. Fabbrocino G, Iervolino I, Orlando F, Salzano E (2005) Quantitative risk analysis of oil storage facilities in seismic areas. Journal of Hazardous Materials 12:361-69

21. Salzano E, Garcia-Agreda A, Di Carluccio A, Fabbrocino G (2009) Risk assessment and early warning systems for industrial facilities in seismic zones. Reliab. Eng. Syst. Saf. 94:1577-1584

22. Gunn R, Balissat M, Manso P, Mouvet L, Schleiss AJ (Eds.) (2016) In the 13th International Benchmark Workshop on Numerical Analysis of Dams, in: ICOLD Proceedings. Swiss Committee on Dams, Lausanne, Switzerland.

23. Zenz G, Goldgruber M (Eds.) (2013) In the 12th International Benchmark Workshop on Numerical Analysis of Dams. ICOLD, Graz, Austria

24. Pitilakis K, Argyroudis S, Fotopoulou S, Karafagka S, Anastasiadis A, Pitilakis D, Raptakis D, Riga E, Tsinaris A, Mara K, Selva J, Iqbal S, Volpe M, Tonini R, Romano F, Brizuela B, Piatanesi A, Basili R, Salzano E, Basco A, Schleiss AJ, Matos JP, Akkar S, Cheng Y, Uckan E, Erdik M, Courage W, Reinders J, Crowley H, Rodrigues D (2016). Deliverable D6.1: Integrated report detailing analyses, results and proposed hierarchical set of stress tests for the six CIs. STREST project: Harmonized approach to stress tests for critical infrastructures against natural hazards

25. Mignan A, Wiemer S, Giardini D (2014) The quantification of low-probability–high-consequences events: part I. A generic multi-risk approach. Natural Hazards, 73:1999-2022. doi:10.1007/s11069-014-1178-4

26. Mignan A, Danciu L, Matos JP, Schleiss A (2015). Deliverable D3.5: Report on cascading events and multi-hazard probabilistic scenarios. STREST project: Harmonized approach to stress tests for critical infrastructures against natural hazards

27. Matos JP, Mignan A, Schleiss AJ (2015) Vulnerability of large dams considering hazard interactions: conceptual application of the Generic Multi-Risk framework. In: 13th ICOLD International Benchmark Workshop on Numerical Analysis of Dams. Lausanne, Switzerland, 285-292

28. Froehlich D (2008) Embankment dam breach parameters and their uncertainties. Journal of Hydraulic Engineering 134:1708–1721, doi:10.1061/(ASCE)0733-9429(2008)134:12(1708)

29. Darcourt A (2016) Numerical simulation of dam break flood wave propagation in the Rhone River. From dam breach formation to loss assessment (M.Sc.) École Polytechnique Fédérale de Lausanne (EPFL)

30. Suppasri A, Mas E, Charvet I, Gunasekera R, Imai K, Fukutani Y, Abe Y, Imamura F (2013) Building damage characteristics based on surveyed data and fragility curves

of the 2011 Great East Japan tsunami. Natural Hazards 66:319–341. doi:10.1007/s11069-012-0487-8

31. Eidinger JM, Avila EA (1999) Guidelines for the seismic evaluation and upgrade of water transmission facilities (Vol. 15). ASCE Publications
32. American Lifelines Alliance (ALA) (2001). Seismic Fragility Formulations for Water Systems, Part 1–Guideline, http://www.americanlifelinesalliance.org
33. American Lifeline Alliance (ALA) (2005). Design Guidelines for Seismic Resistant Water Pipeline Installations. Report FEMA, NIBS and ALA 2005/03. G&E Engineering Systems Inc.
34. Cheng Y, Akkar S (2016) Probabilistic permanent fault displacement hazard via Monte Carlo simulation and its consideration for the probabilistic risk assessment of buried continuous steel pipelines. Earthquake Engineering and Structural Dynamics (accepted).
35. McGuire RK (2004) Seismic Hazard and Risk Analysis, Earthquake Engineering Research Institute: Oakland, CA
36. Honegger DG, Wijewickreme D (2013) Seismic risk assessment for oil and gas pipelines. In Handbook of Seismic Risk Analysis and Management of Civil Infrastructure Systems pp.682-715. Elsevier
37. ASCE (2010). Minimum design loads for buildings and other structures, ASCE/SEI 7-10, American Society of Civil Engineers, Reston, VA
38. WINN_TA-NAM (2016). Technical Addendum to the Winningsplan 2016. NAM, April 1st (in Dutch)
39. Dost B, Caccavale M, Van Eck T, Kraaijpoel D (2013). Report on the expected PGV and PGA values for induced earthquakes in the Groningen area, KNMI report, 26pp. (http://bibliotheek.knmi.nl/knmipubDIV/Report_on_the_expected_PGV_and_PGA_values_for_induced_earthquakes.pdf)
40. Akkar S, Sandıkkaya MA, Bommer JJ (2014a) Empirical ground-motion models for point-and extended-source crustal earthquake scenarios in Europe and the Middle East. Bulletin of Earthquake Engineering 12(1):359–387
41. Akkar S, Sandıkkaya MA, Bommer JJ (2014b) Erratum to: Empirical ground-motion models for point- and extended-source crustal earthquake scenarios in Europe and the Middle East. Bulletin of Earthquake Engineering 12(1):389–390
42. Bommer JJ (2013) Proposals for New GMPEs for the Prediction of PGA and PGV in the Groningen Gas Field, NAM internal note, 37pp.
43. Esposito S (2011) Systemic seismic analysis of gas distribution networks. Ph.D. thesis, University of Naples Federico II, Italy, Advisor: I. Iervolino. Available at: http://wpage.unina.it/iuniervo/
44. CPR 18E (1999). Guidelines for quantitative risk assessment. Committee for the Prevention of Disasters (CPR)
45. CAROLA (2010) Program version 1.0.0.51. Associated Technology Pipeline Ltd and Rijksinstituut voor Volksgezondheid en Milieu (www.rivm.nl/milieuportaal/bibliotheek/modellen/carola.jsp)
46. Acton MR, Baldwin TR, Jager EER (2002) Recent Developments in the Design and Application of the PIPESAFE Risk Assessment Package for Gas Transmission Pipelines, ASME International. Proceedings of the International Pipeline Conference (IPC), 29 September – 3 October, Calgary, Canada
47. Esposito S, Stojadinović B (2016b) Deliverable D5.3: Tools and strategies to incorporate stress tests into the long-term planning and life cycle management of

non-nuclear Cis. STREST project: Harmonized approach to stress tests for critical infrastructures against natural hazards

48. Franchin P, Cavalieri F, Pinto PE, Lupoi A, Vanzi I, Gehl P, Kazai B, Weatherill G, Esposito S, Kakderi K (2011). General methodology for systemic seismic vulnerability assessment. Deliverable 2.1 Syner-G Project, http://www.vce.at/SYNER-G/

49. Idriss IM, Boulangier RW (2008) Soil Liquefaction during earthquake, EERI monograph MNO-12 on earthquake engineering. Earthquake Engineering Research Institute, Oakland (CA) USA

50. Miraglia S, Courage W, Meijers P (2015) Fragility functions for pipeline in liquefiable sand: a case study on the Groningen gas-network. In Haukaas T (Ed.) In the 12th International Conference on Applications of Statistics and Probability in Civil Engineering (ICASP12), Vancouver, Canada, July 12-15

51. Lanzano G, Salzano E, Santucci de Magistris F, Fabbrocino G (2013) Seismic vulnerability of gas and liquid buried pipelines. Journal of Loss Prevention in the Process Industries http://dx.doi.org/10.1016/j.jlp.2013.03.010

52. National Institute of Building Sciences, NIBS (2004). Direct physical damage—general building stock. HAZUS-MH Technical manual, Chapter 5. Federal Emergency Management Agency, Washington, D.C.

53. Pitilakis K, Crowley H, Kaynia A (Eds) (2014a). SYNER-G: Typology definition and fragility functions for physical elements at seismic risk. Buildings, lifelines, transportation networks and critical facilities. Geotechnical, Geological and Earthquake Engineering, 27, Springer, Netherlands

54. Anastasiadis A, Raptakis D, Pitilakis K (2001) Thessaloniki's detailed microzoning: subsurface structure as basis for site response analysis, Pure and Applied Geophysics. 158, 2597-2633

55. Aki K (1957) Space and Time Spectra of Stationary Stochastic Waves, with Special Reference to Microtremors. Bull. Earthquake Res. Inst. Tokyo Univ, 25: 415-457

56. UPGRADE (2015). Technical reports with the calculation results of the vulnerability of specific Greek port facilities (in Greek). Deliverable 8.2, Research project: Contemporary Evaluation Methodology of Seismic Vulnerability and Upgrade of Port Facilities, http://excellence.minedu.gov.gr/thales/en/thalesprojects/380174

57. Kappos AJ, Panagiotopoulos C, Panagopoulos G, Panagopoulos El (2003). WP4-Reinforced concrete buildings (Level I and II analysis), RISK-UE: An advanced approach to earthquake risk scenarios with applications to different European towns

58. Kappos AJ, Panagopoulos G, Panagiotopoulos C, Penelis G (2006) A hybrid method for the vulnerability assessment of R/C and URM buildings. Bulletin of Earthquake Engineering 4:391-419

59. SRMLIFE (2007). Development of a global methodology for the vulnerability assessment and risk management of lifelines, infrastructures and critical facilities. Application to the metropolitan area of Thessaloniki. Research project, General Secretariat for Research and Technology, Greece (in greek)

60. Karafagka S, Fotopoulou S, Pitilakis K (2016) Tsunami fragility curves for seaport structures. In 1st International Conference on Natural Hazards & Infrastructure, Chania, Greece

61. Fajfar P, Dolšek M (2012) A practice-oriented estimation of the failure probability of building structures. Earthquake Engng Struct. Dyn, 41 (3): 531–547

62. Lazar N, Dolšek M (2013) Application of the risk-based seismic design procedure to a reinforced concrete frame building. In 4th ECCOMAS Thematic Conference on

Computational Methods in Structural Dynamics and Earthquake Engineering, M. Papadrakakis, V. Papadopoulos, V. Plevris (eds.) Kos Island, Greece

63. Silva V, Crowley H, Bazzuro P (2014) Risk-targeted hazard maps for Europe. In Second European Conference on Earthquake Engineering and Seismology, Istanbul, Turkey

64. Pitilakis K, Franchin P, Khazai B, Wenzel H (Eds) (2014b). SYNER-G: Systemic seismic vulnerability and risk assessment of complex urban, utility, lifeline systems and critical facilities. Methodology and applications. Geotechnical, Geological and Earthquake Engineering, 31, Springer, Netherlands

65. Kakderi K, Fotopoulou S, Argyroudis S, Karafagka S, Pitilakis K, Anastasiadis A, Smerzini C, Selva J, Giannopoulos G, Galbusera L, Courage W, Reinders J, Cheng Y, Akkar S, Erdik M, Uckan E (2015). Deliverable D4.2: Guidelines for performance and consequences assessment of geographically distributed, non-nuclear critical infrastructures exposed to multiple natural hazards. STREST project: Harmonized approach to stress tests for critical infrastructures against natural hazards

66. Selva J (2013) Long-term multi-risk assessment: statistical treatment of interaction among risks. Natural Hazards 67 (2): 701-722

67. Weatherill G, Esposito S, Iervolino I, Franchin P, Cavalieri F (2014). Framework for seismic hazard analysis of spatially distributed systems, in: K. Pitilakis et al (eds). Systemic seismic vulnerability and risk assessment of complex urban, utility, lifeline systems and critical facilities. Methodology and applications. Springer, Netherlands, 57-88

68. Giardini D. et al (2013) Seismic Hazard Harmonization in Europe (SHARE). Online Data Resource, http://portal.share-eu.org:8080/jetspeed/portal/, doi: 10.12686/SED-00000001-SHARE

69. Akkar S, Bommer JJ (2010) Empirical equations for the prediction of PGA, PGV and spectral accelerations in Europe, the Mediterranean and the Middle East. Seismol Res Lett, 81: 195–206

70. Jayaram N, Baker JW (2009) Correlation model of spatially distributed ground motion intensities. Earthquake Engineering and Structural Dynamics, 38 (15): 1687–1708

71. EN 1998-1. Eurocode 8 (2004). Design of structures for earthquake resistance-Part 1: General rules, seismic actions and rules for buildings. CEN, Bruxelles

72. Volpe M, Selva J, Tonini R, Romano F, Brizuela B, Piatanesi A, Basili R, Lorito S, in prep: From regional to site specific SPTHA through inundation simulations: a case study for Milazzo (Italy) and Thessaloniki (Greece)

73. Selva J, Tonini R, Molinari I, Tiberti MM, Romano F, Grezio A, Melini D, Piatanesi A, Basili R, Lorito S (2016a) Quantification of source uncertainties in Seismic Probabilistic Tsunami Hazard Analysis (SPTHA), Geophys. J. Int. doi:10.1093/gji/ggw107

74. Selva J, Tonini R, Romano F, Volpe M, Brizuela B, Piatanesi A, Basili R, Lorito S (2016b) From regional to site specific SPTHA through inundation simulations: a case study for three test sites in Central Mediterranean, EGU General Assembly, Vienna, Austria, Abstract #EGU2016-16988

75. Basili R, Tiberti MM, Kastelic V, Piatanesi A, Selva J, Lorito S (2013) Integrating geologic fault data into tsunami hazard studies, Natural Hazards and Earth System Sciences 13:1025-1050, DOI: 10.5194/nhess-13-1025-2013

76. Molinari I, Tonini R, Piatanesi A, Lorito S, Romano F, Melini D, Gonzalez Vida JM, Macias J, Castro M, de la Asuncion M submitted (2016) Fast evaluation of tsunami

scenarios: uncertainty assessment for a Mediterranean Sea database, submitted to NHESS (under review)

77. Marzocchi W, Taroni M, Selva J (2015) Accounting for epistemic uncertainty in PSHA: logic tree and ensemble modeling. Bulletin of the Seismological Society of America 105 (4), doi: 10.1785/0120140131

78. González Vida JM, Macias J, Castro M, de la Asuncion M, Melini D, Romano F, Tonini R, Lorito S, Piatanesi A, Molinari I (2015). Tsunami-HySEA: a GPU based model for the Italian candidate tsunami service provider, in EGU General Assembly, Vienna, EGU2015-13797

79. Papaioannou C (2004) Seismic hazard scenarios-Probabilistic seismic hazard analysis. SRM-Life Project: Development of a global methodology for the vulnerability assessment and risk management of lifelines, infrastructures and critical facilities. Application to the metropolitan area of Thessaloniki (in greek)

80. Bommer JJ, Acevedo AB (2004) The use of real accelerograms as input to dynamic analysis. Journal of Earthquake Engineering 8(1):43-91 DOI: 10.1080/13632460409350521

81. Smerzini C, Pitilakis K, Hasmemi K, submitted (2016) Evaluation of earthquake ground motion and site effects in the Thessaloniki urban area by 3D finite-fault numerical simulations. Bulletin of Earthquake Engineering

82. Kottke AR, Rathje EM (2008). Technical Manual for Strata. PEER Report 2008/10. University of California, Berkeley

83. Elgamal A, Yang Z, Lu J (2015) Cyclic1D Seismic Ground Response Version 1.4, User's Manual, University of California, San Diego, Department of Structural Engineering

84. Toro GR (1995) Probabilistic models of site velocity profiles for generic and site-specific ground-motion amplification studies. Upton, New York: Brookhaven National Laboratory

85. Krausmann E, Piccinelli R, Ay BÖ, Crowley H, Uckan E, Erdik M, Lanzano G, Salzano E, Iervolino I, Esposito S, Pistolas A, Kakderi K, Pitilakis D, Pitilakis K, Steenbergen R (2014). Deliverable D2.3: Report on lessons learned from recent catastrophic events. STREST project: Harmonized approach to stress tests for critical infrastructures against natural hazards

86. Woessner J, Danciu L, Giardini D, Crowley H, Cotton F, Grunthal G, Valensise G, Arvidsson R, Basili R, Demircioglu M, Hiemar S, Meletti C, Musson R, Rovida A, Sesetyan K, Stucchi M (2015) The 2013 European Seismic Hazard Model - Key Components and Results. Bulletin of Earthquake Engineering, DOI 10.1007/s10518- 015-9795-1

87. Silva V, Crowley H, Pagani M, Pinho R (2014) Development of the OpenQuake engine, the Global Earthquake Model's open-source software for seismic risk assessment. Natural Hazards 72(3): 1409-1427

88. Crowley H, Casotto C, Dolšek M, and Babič A (2015). Deliverable D4.3: Guidelines for performance and consequences assessment of multiple-site, low-risk, high-impact, nonnuclear critical infrastructures (exposed to multiple natural hazards, etc.). STREST project: Harmonized approach to stress tests for critical infrastructures against natural hazards

89. Esposito S, Stojadinović B, Babič A, Dolšek M, Iqbal S, Selva J (2017) Engineering risk-based methodology and grading system for stress testing of critical non-nuclear infrastructures (STREST Project). In 16th World Conference on Earthquake Engineering, Santiago, Chile

List of abbreviations and definitions

ALARP	As Low As Reasonably Practicable
BLEVE	Boiling Liquid Expanding Vapour Explosion
BTC	Baku-T'Bilisi-Ceyhan
CIs	Critical Infrastructures
CL	Connectivity Loss
CPT	Cone Penetration Test
EDP	Engineering Demand Parameter
EPCIP	European Programme for Critical Infrastructure Protection
EPN	Electric Power Network
EQL	Equivalent-Linear
ERR	European Reference Report
ET	Evaluation Team
ET	Event Tree
GMPE	Ground Motion Prediction Equation
GenMR	Generic Multi-Risk
GR	Gutenberg-Richter
ICOLD	International Commission on Large Dams
IM	Intensity Measure
IR	Internal Reviewers
MAF	Mean Annual Frequency
M&R	Measure and Regulation
NL	NonLinear
NTUA	National Technical University of Athens
PFDs	Permanent Fault Displacements
PGA	Peak Ground Acceleration
PGD	Permanent Ground Deformation
PIs	Performance Indicators
PM	Project Manager
PoE	Pool of Experts
PRA	Probabilistic Risk Analysis
PSHA	Probabilistic Seismic Hazard Analysis
QRA	Quantitative Risk Analysis
RC	Reinforced Concrete
SBRA	Scenario-Based Risk Analysis
SDGEE	Soil Dynamics and Geotechnical Earthquake Engineering
SHARE	Seismic Hazard Harmonization in Europe

SPAC	SPatial Autocorrelation Coefficient
SPT	Standard Penetration Test
SPTHA	Seismic Probabilistic Tsunami Hazard Analysis
SR	Serviceability Ratio
ST	Stress Test
ST-L	Stress Test Level
STREST	harmonized approach to stress tests for critical infrastructures against natural hazards
TCaH	Total Cargo Handled (loaded and unloaded) per day
TCoH	Total number of Containers Handled (loaded and unloaded) per day
TEU	Twenty-foot Equivalent Units
TI	Technical Integrator
URM	UnReinforced Masonry

List of figures

Fig. 2.1 Workflow of ST@STREST methodology and interaction among the main actors during the multiple-expert process EU@STREST 5

Fig. 2.2 ST-Levels in the ST@STREST methodology 7

Fig. 2.3 Grading system for the global outcome of stress test 9

Fig. 2.4 Grading system in time domain using scalar risk objectives (top) and limit F-N curves (bottom): a) two different results of the first evaluation of stress test (ST1), b) redefinition of the parameters of the grading system due to Result 1 in ST1, and c) redefinition of the parameters of the grading system due to Result 2 in ST1 10

Fig. 3.1 Overview of population density as used in QRA 13

Fig. 3.2 Grid of potential epicentres around Milazzo considered in the PSHA analysis. Grid points within a 50 km radius from Milazzo are displayed as red dots 14

Fig. 3.3 Hazard curve for Milazzo in terms of MAF of exceedance of PGA, calculated according to the methodology presented 14

Fig. 3.4 Locational risk – Single hazard only. Larger figures are included in Appendix I 18

Fig. 3.5 Location of LPG Spheres (red squares) 19

Fig. 3.6 Locational risk – Hazard combinations 20

Fig. 3.7 The cross-section of the locational risk (red line) in Fig. 3.8 21

Fig. 3.8 Locational risk transect 21

Fig. 3.9 Societal risk without accounting for natural hazards- with and without LPG tanks 22

Fig. 3.10 Societal risk- industrial, earthquake or tsunami induced 22

Fig. 3.11 Societal risk- cumulated risks 23

Fig. 4.1 Dam break wave spreading across a river flood plain and inundating a city. Colour characterizing water depths from dark blue (0 m) to bright red (30 m) 25

Fig. 4.2 Scheme of hazards, elements, system states, and interactions considered in the application of the GenMR framework to large dams. Case of an embankment dam. Adapted from Mignan et al (2015) and presented in Matos et al (2015) 27

Fig. 4.3 Example of a chain of events leading to failure (Pitilakis et al 2016) 28

Fig. 4.4 Inundations calculated for low (left) and high (high) peak discharge/volume breach hydrographs. Adapted from Pitilakis et al (2016) 29

Fig. 4.5 F-N curve based on collapsed or washed away built volume following a dam failure upstream (Pitilakis et al 2016) 30

Fig. 4.6 Most likely damage to 3 or more stories reinforced concrete buildings in the event of a dam failure upstream. Adapted from Pitilakis et al (2016) 31

Fig. 4.7 Return period of buildings collapsing or being washed away as a consequence of dam failures. Adapted from Pitilakis et al (2016) 31

Fig. 4.8 Time to maximum depth 31

Fig. 5.1 Overview of BTC pipeline 33

Fig. 6.1 Selected sub system of the gas distribution network (right) located above main natural gas field (top left) 38

Fig. 6.2 Distribution of pipe diameters (mm) present in the modelled sub network (black lines on background indicate the earthquake zones) 39

Fig. 6.3 Locations of stations in the modelled sub network: source stations (green) demand stations (red) and M&R stations (blue). Pipeline colours and colour bar refer to the pressures ([bar]) in the pipe sections 39

Fig. 6.4 Division of Groningen area in seismic zones (Dost et al 2013) 40

Fig. 6.5 ST-L1a: annual failure frequencies (per km) for the pipe sections 43

Fig. 6.6 ST-L1a: annual failure frequencies for the stations 43

Fig. 6.7 Soil liquefaction fragilities of two soil profiles in the Groningen area (Miraglia et al 2015) 44

Fig. 6.8 Distribution of reliability indices for failure due to soil liquefaction for different pipe sections 44

Fig. 6.9 Calculated pipe fragilities with respect to transient seismic load effects. Different solid lines correspond to different pipe properties. The red dotted line is taken from Lanzano et al (2013) 45

Fig. 6.10 Annual probability of exceedance for network connectivity loss *CL* (top) and network serviceability rate *SR* (bottom) 46

Fig. 6.11 Obtained grading for the individual pipelines (M_{max} = 6; annual rate =30) ... 47

Fig. 6.12 Obtained grading for the stations (M_{max} = 6; annual rate =30) 47

Fig. 6.13 Exceedance frequencies for connectivity loss relative to (indicative) grading boundaries. 48

Fig. 7.1 Flowchart of the ST@STREST framework for the stress test application in the port of Thessaloniki 51

Fig. 7.2 Geographical representation of Thessaloniki's port infrastructures 52

Fig. 7.3 Location of geotechnical tests and geophysical field measurements in port area 52

Fig. 7.4 Site specific hazard curves for ground shaking and tsunami 55

Fig. 7.5 Mean annual frequency (MAF) of exceedance values for the normalized performance loss of the container terminal (TCoH, right) and the bulk cargo terminal (TCaH, left) for the seismic hazard case. The green, blue and red continuous lines correspond to the boundaries between risk grades AA (negligible), A (ALARP), B (possibly unjustifiable risk), and C (intolerable) 57

Fig. 7.6 Mean annual frequency (MAF) of exceedance values for the normalized performance loss of the bulk cargo terminal (TCaH, left) and for the buildings in complete damage state (right) for the tsunami hazard case. The green, blue and red continuous lines correspond to the boundaries between risk grades AA (negligible), A (ALARP), B (possibly unjustifiable risk), and C (intolerable) 58

Fig. 7.7 Median ± standard deviation elastic 5% response spectra at the ground surface for soil profile A using the EQL (left) and NL (right) approaches for the 475 years scenario (top) and the 4975 years scenario I (bottom) 60

Fig. 7.8 Variation of effective confinement (left) and settlement with depth (right) for soil profile A for the 475 years scenario (top) and the 4975 years scenario (bottom) ... 61

Fig. 8.1 Sub-classes of buildings in terms of structural and non-structural elements ... 65

Fig. 8.2 Mean hazard map for Tuscany based on SHARE logic tree with V_{s30} = 800m/s (in terms of PGA with 10% probability of exceedance in 50 years) 66

Fig. 8.3 Estimates of site conditions in Tuscany from topographic slope (http://earthquake.usgs.gov/hazards/apps/vs30/predefined.php) 67

Fig. 8.4 Annual probability of collapse of all industrial buildings in Arezzo 68

Fig. 8.5 Total loss exceedance curves for all industrial facilities in Arezzo 69

Fig. 8.6 Disaggregation of average annual loss according to building sub-class for each component of loss 70

List of tables

Table 2.1 ST-Levels 8
Table 3.1 Scenarios and frequencies for stationary vessels due to natural hazards 16
Table 3.2 Ignition probabilities 16
Table 3.3 Representative substances 17
Table 3.4 BLEVE probability 17
Table 5.1 Aggregated failure probability of BTC pipeline under 2475-year PFD hazard before and after the risk mitigation strategies 36
Table 6.1 Gutenberg-Richter parameters (Dost et al 2013) 40
Table 6.2 Grading boundaries (failure frequencies) for stations and pipe sections 41
Table 6.3 Stress test results for Gasunie-GTS sub-network 49
Table 7.1 Fragility functions used in the risk analyses 53
Table 7.2 Estimated normalized performance loss of the port system for TCaH and TCoH and comparison with risk objectives for the scenario based assessment 62
Table 7.3 Summary report of the stress test outcomes 63
Table 8.1 Average annual losses for Arezzo industrial facilities 69
Table 8.2. Percentage of each customer base AAL to the total business interruption AAL 70
Table 8.3. Summary report of the stress test outcomes 71
Table 9.1. Grading range for the six case studies of STREST 74

Europe Direct is a service to help you find answers to your questions about the European Union.

Freephone number (*)**:**

00 800 6 7 8 9 10 11

(*) The information given is free, as are most calls (though some operators, phone boxes or hotels may charge you).

More information on the European Union is available on the internet (http://europa.eu).

HOW TO OBTAIN EU PUBLICATIONS

Free publications:

- one copy:
  via EU Bookshop (http://bookshop.europa.eu);
- more than one copy or posters/maps:
  from the European Union's representations (http://ec.europa.eu/represent_en.htm);
  from the delegations in non-EU countries (http://eeas.europa.eu/delegations/index_en.htm);
  by contacting the Europe Direct service (http://europa.eu/europedirect/index_en.htm) or
  calling 00 800 6 7 8 9 10 11 (freephone number from anywhere in the EU) (*).

  (*) The information given is free, as are most calls (though some operators, phone boxes or hotels may charge you).

Priced publications:

- via EU Bookshop (http://bookshop.europa.eu).

LB-NA-28341-EN-N

JRC Mission

As the science and knowledge service of the European Commission, the Joint Research Centre's mission is to support EU policies with independent evidence throughout the whole policy cycle.

EU Science Hub
ec.europa.eu/jrc

@EU_ScienceHub

EU Science Hub - Joint Research Centre

Joint Research Centre

EU Science Hub

Publications Office

doi:10.2788/85094

ISBN 978-92-79-64600-3